Advancing Renewable Polymers: Itaconic Acid as a Renewable Source and Modulating Material Properties Through Vitrification

By

Mary Hnatyshyn

A thesis submitted to McGill University in partial fulfillment

of the requirements of the degree of Master of Science

Department of Chemical Engineering

McGill University

Montreal, Canada

February 2025

Abstract

An increasing demand for polymer materials coupled with depleting fossil-fuel reserves necessitates a shift in the polymer industry to sustainably sourced products. Therefore, developing materials from renewable sources that have properties comparable to those of commodity polymers is a critical endeavour. To replace the petroleum derived products that are on the market already, materials from renewable sources must first be developed and their properties matched to industry standards to fulfill the demands of their application.

To address this challenge, a method for incorporating itaconic acid into polymeric materials was developed. This was accomplished by functionalizing bio-derived itaconic acid with a methacrylate group in a four-step synthesis route. Two novel itaconate-based monomers were obtained and subjected to polymerization by various methods of reversible-deactivation radical polymerization. Polymers of target molecular weight and narrow dispersities were achieved in high conversion reactions. The two distinct monomers gave polymers with a range of properties, with glass transition temperatures for the two species being -40 and 14°C. Both displayed strong thermal stability, and tunable rheological properties across the synthesized range of molecular weights (10 000 to 400 000 g/mol). Typically, challenges are faced when attempts are made to polymerize itaconic acid. However, by functionalizing the molecule with a methacrylate group, the polymerization of the itaconate-based monomers could proceed with characteristics typical of methacrylic monomers. This work therefore shows how methacrylate functionalization can be a potential pathway for incorporating bio-sourced itaconic acid into polymeric materials.

In a second study, the material properties of renewably sourced polymers were improved through vitrimer chemistry. By introducing reversible boronic-acid ester exchange chemistry into the polymer matrix, a material that is both cross-linked and recyclable was obtained. This allowed for enhanced tensile strength, hardness, and rubbery rheological behaviour to be observed in the previously gel-like polymers. By incorporating diblock copolymers into the matrix and consequently inducing microphase separation in the material, rheological properties that approached standards typical of commercial materials were achieved. Phase-separated regions of high glass transition temperature within the material increased the tensile strength and improved the creep resistance of the material without impeding the ability to relax stress or self-heal. Further, mechanical and thermal properties were preserved through three rounds of recycling. Overall, this

study demonstrated the ability to modulate and improve the macroscopic properties of renewably sourced polymers by coupling vitrimer chemistry with microphase separation.

In summary, this work presents two strategies for improving renewable polymer materials. First, it demonstrates an alternative method for incorporating biomolecules into polymers. Second, it explores how microstructures in vitrimer networks can enhance the properties of renewable polymers, making them more comparable to petroleum-based materials. Simplifying the integration of biomolecules and optimizing phase separation and cross-linking in vitrimers could further help renewable polymers meet the performance standards needed for wider applications.

Resume

Une demande croissante de matériaux polymères, couplée à l'épuisement des réserves de combustibles fossiles, nécessite un changement dans l'industrie des polymères vers des produits issus de sources durables. Par conséquent, le développement de matériaux provenant de sources renouvelables présentant des propriétés comparables à celles des polymères les plus courants constitue un enjeu crucial. Pour remplacer les produits dérivés du pétrole actuellement sur le marché, il est d'abord nécessaire de développer des matériaux renouvelables dont les propriétés satisfont les normes industrielles afin de répondre aux exigences de leurs applications.

Pour relever ce défi, une méthode d'incorporation de l'acide itaconique dans les matériaux polymères a été développée. Cela a été réalisé en fonctionnalisant de l'acide itaconique biosourcé avec un groupe méthacrylate selon une voie de synthèse en quatre étapes. Deux nouveaux monomères à base d'itaconate ont été obtenus pour ensuite être soumis à des polymérisations par différentes méthodes de polymérisation radicalaire à désactivation réversible. Des polymères possédant la masse moléculaire ciblée et ayant une faible dispersité ont été obtenus avec des taux de conversion élevés. Les deux monomères distincts ont conduit à des polymères présentant une gamme de propriétés comme des températures de transition vitreuse de -40 et de 14 °C. Les deux ont démontré une stabilité thermique élevée et des propriétés rhéologiques modulables sur toute la gamme de masses molaires synthétisées (de 10 000 à 400 000 g/mol).

En général, la polymérisation de l'acide itaconique pose des défis. Cependant, en fonctionnalisant la molécule avec un groupe méthacrylate, la polymérisation des monomères à base d'itaconate a pu se dérouler avec des caractéristiques typiques des monomères méthacryliques. Ce travail démontre ainsi comment la fonctionnalisation méthacrylate peut constituer une voie prometteuse pour incorporer l'acide itaconique biosourcé dans des matériaux polymères.

Dans une deuxième étude, les propriétés des polymères renouvelables ont été améliorées grâce à la chimie des vitrimères. En introduisant une réaction réversible des esters boroniques dans la matrice polymère, un matériau à la fois réticulé et recyclable a été obtenu. Cela a permis d'améliorer la résistance à la traction, la dureté et le comportement rhéologique élastique desdits polymères dont les propriétés étaient semblables à celles d’un gel avant le procédé décrit ci-dessus.

En incorporant des copolymères dibloc dans la matrice et en induisant ainsi une micro-séparation de phase, des propriétés rhéologiques se rapprochant des standards des matériaux commerciaux ont été obtenues. Les régions à température de transition vitreuse élevée ségrégées par phases ont augmenté la résistance à la traction et ont amélioré la résistance au fluage sans toutefois compromettre la capacité du matériau à relaxer les contraintes ou à s'auto-cicatriser. De plus, les propriétés mécaniques et thermiques ont été préservées après trois cycles de recyclage.

Dans l'ensemble, cette étude a démontré la capacité à moduler et améliorer les propriétés macroscopiques des polymères renouvelables en couplant la chimie des vitrimères à la séparation des microphases.

En résumé, ce travail présente deux stratégies pour améliorer les matériaux polymères renouvelables. Premièrement, il démontre une méthode alternative pour incorporer des biomolécules dans les polymères. Deuxièmement, celui-ci explore comment les microstructures des réseaux de vitrimères peuvent améliorer les propriétés des polymères renouvelables, les rendant ainsi plus comparables aux matériaux à base de pétrole. Simplifier l'intégration des biomolécules et optimiser la séparation des phases ainsi que la réticulation dans les vitrimères pourraient contribuer davantage à l’atteinte des normes de performances requises pour un plus grand nombre d’application.

Acknowledgements

I would first like the thank my three supervisors, Dr. Milan Maric, Dr. Richard Leask, and Dr, Jim Nicell. I have greatly appreciated the guidance, advice and time that you three have provided over the past two years. However, I am also extremely grateful for the freedom you have allowed me in pursuing my scientific interests! The opportunity to follow the research paths I found interesting has been a wholly enriching experience. It was not only motivating, but it also allowed for my confidence as a student, researcher, and person to truly grow.

The projects here were made possible due to the funding provided by the Eugenie Ulmer Lamothe Award from McGill University and from the Natural Sciences and Engineering Research Council (NSERC).

I would like to thank the members of the Maric and Leask lab groups, for helping with questions, and providing company in the lab! I would like to thank both the summer students I had the opportunity to work with, Max Laykish and Katya Shchukin, for their hard work and positive attitudes. The opportunity to be a mentor in your projects was enriching, and you both were diligent researchers who made the summer semesters productive and fun.

Thank you also to the staff at McGill in the Departments of Chemical Engineering and Chemistry. I would like to thank Hatem Titi for his help in running the SAXS samples, and Mohini Ramkaran for her time running and analyzing the AFM experiments.

Thank you to my friends in the Department of Chemical Engineering who went through the undergraduate and now graduate programs with me. You made Wong a great place to come to for seven years, and I will hold all our Thomson House memories dear! I would like to express my gratitude for the McGill Cycling Team, for the frequent trips and weekend rides that gave me something to look forward to with excitement. My favourite memories have come from the trips, years spent as roommates, and days on the bike, and I cannot wait for more.

Finally, I am grateful for my family's support and encouragement. I trust you will all read my thesis in full to show how much you truly care.

Table of Contents

List of Figures

List of Tables

Contribution of Authors

This manuscript-based thesis consists of two articles that have been prepared for submission for publication, of which I am the primary author of both.

Mary Hnatyshyn, Hollaran, M., Laykish, M., Nicell, J.A., Leask, R.L., Maric, M. (2024). "Methacrylate Functionalized Itaconates." (Chapter 3).

Mary Hnatyshyn, Asempour, F., Nicell, J.A., Leask, R.L., Maric, M. (2024). "Boronic Ester Vitrimers: Balancing Self-Healing and Creep Through Self-Assembling Block Copolymers." (Chapter 4).

For the first manuscript, I planned the components of the project and performed the experiments. Matthew Halloran planned the synthesis for the functionalization to obtain the monomer. Maxwell Laykish assisted me in the conduct of experiments. I analyzed and interpreted the results and prepared and edited the manuscript. Jim Nicell, Richard Leask, and Milan Maric were responsible for funding acquisition, supervision of the research, and editing of the manuscript.

The second manuscript was prepared with the help of Farhad Asempour. I planned the components, conducted the experiments and lab work, analyzed and interpreted the results, and prepared and edited the manuscript. Farhad Asempour assisted with polymer synthesis, rheological tests, and editing of the manuscript. Jim Nicell, Richard Leask, and Milan Maric were responsible for funding acquisition, supervision of the research, and editing of the manuscript.

Chapter 1: Introduction

1.1 Overview

The increasing demand globally for both robust polymeric materials and sustainable solutions to mitigate the impact that daily routines have on the environment has created growing awareness on the importance of moving from traditional petroleum-based polymers towards renewable alternatives.[1, 2] Polymers derived from fossil fuels, which currently encompass 99% of the polymer market, are significant contributors to the environmental pollution that results in global warming.[3] Annually, 3.3% of greenhouse gas emissions are related to the polymer industry, and it is estimated that 90% of the polymer related greenhouse gases are emitted during the production stage of refining fossil fuels to obtain polymeric materials.[4] Therefore, switching to renewable sources has the potential to significantly decrease the worldwide negative impacts of the polymer industry.

Various routes have been proposed for incorporating more sustainable sources into polymeric materials. Emerging methods may be categorized into three broad groups, with the first being to derive traditional monomers from renewable sources. Using, for example, bioethanol as a feedstock, traditional and well-known monomers such as ethylene can be obtained that is chemically identical to its petroleum-based analog.[5] The second method involves the polymerization of renewably sourced chemicals without their modification, revealing new classes of polymers with distinct properties. Polylactide (PLA) is one such example that has emerged on an industrial scale as a green alternative for food packaging.[6] Its production involves the fermentation of starches to produce lactic acid, which can then produce PLA through polycondensation reactions. A third method used in producing new, renewably sourced polymers involves the functionalization or chemical modification of the renewable compound before polymerization.[7] Feedstock oils that occur naturally in plants, such as limonene, menthol, α-pinene and β-pinene are commercially available terpenes that following functionalization, generate polymers with an increased bio-content.[8]

Employing the second or third method, a plethora of readily available feedstocks can be exploited for use in new polymeric materials with greater renewable content. However, to compete with petroleum derived polymers, the economics of the starting feedstock must be favourable and the material properties of the obtained polymers must be competitive with industry standards.

Advances in biomanufacturing has opened the door to not only new bio-sourced chemicals to act as feedstock materials, but the commercialization of bioreactors, which has made the cost of these materials more feasible.[9] As such, the US Department of Energy has named twelve chemicals as being the top value-added chemicals from biomass which have the potential to beneficially reshape the chemical industry.[10] Itaconic acid (IA) is one of these twelve chemicals, however, since being named, has yet to emerge as a promising alternative in the polymer industry.[11] Previous attempts at generating polymers of itaconic acid have focused on direct polymerization methods, without exploring the opportunity of functionalizing IA before polymerization. As a result of its chemical structure, polymerizing IA directly, either at the site of its unsaturated carbon bond, or by dehydration of its carboxylic acid groups lead to complicated reactions.[12] Thus, functionalization could be a viable route to more readily incorporate IA into polymeric materials.

However, for a renewably sourced alternative to successfully compete with its petroleum-based counterparts, the material properties of the product cannot be compromised. This is where polymerizing sustainable molecules directly, or functionalizing them before polymerization, leads to challenges. Polymerizing new chemical species inherently leads to a distinct polymer with unique thermal, rheological and mechanical behaviour, that may not be suitable for a direct application, and thus requires additives or other copolymers to be made useful.[13, 14] In functionalizing chemical species like IA into a more readily polymerizable form, the resulting monomer may lead to polymers with, for example, high critical entanglement molecular weights and consequently weaker mechanical strength and poorer rheological properties.[15] Nevertheless, methods exist to help overcome these deficiencies. For instance, introducing cross-linking between polymer backbones, copolymerization, employing specific molecular architectures, or including additives can help tune properties to suit the desired application. However, no alternative comes without drawbacks.

In the past two decades, vitrimer networks have emerged as an attractive way to add cross-linking into polymeric materials, reminiscent of a thermoset, without impeding the recyclability of the material.[16-18] This is achieved by designing the cross-links to be reversible using dynamic covalent chemistry, such that the materials flow under pre-designed criteria, allowing for their reprocessing like thermoplastics. A broad range of covalent chemistries have been explored for vitrimers, including amine exchange, imine exchange, boronic acid ester exchange, or disulfide exchange.[17] By incorporating vitrimer chemistry into polymeric materials that may not be as

naturally robust, rheo-mechanical properties can be tuned allowing for bio-sourced polymers to be comparable to benchmarks and further allow for recyclability and durability of the material.[19] Still, with just 1% of the polymers on the market being renewably-sourced,[20] the need to advance the options for bio-sourced polymers remains apparent. The development of new alternatives from promising chemical species and methods to tune and improve their material properties are required so that the diverse applications of polymeric materials may be covered.

1.2 Objectives

The primary objective of this work is an investigation into methods of developing bio-based polymeric materials using renewable sources. This study did not encompass the feasibility of production, use, or end-of-life of the materials, which in designing an appropriate replacement for polymers, are important lifecycle stages that eventually must be accounted for. In particular, the environmental footprint encompassing all stages of the product lifespan, biodegradability, social impact, and use of renewable sources are all of relevance in designing sustainable materials. This work, however, presents an important initial step in exploring the use of renewable sources in plastic formulations. Broader questions encompassing the research were thus:

1. Can renewably sourced materials be incorporated into polymeric materials, with controlled polymerization kinetics, predictable molecular weights, and narrow dispersities?
2. How can the quality of renewable polymeric materials be made more comparable to market standards?

To examine these questions, two research projects were undertaken. First, the functionalization of itaconic acid was completed to investigate if its polymerization can be improved to allow for the realization of an itaconic-acid based polymeric material. A methacrylate group was affixed to the IA species via a four-step synthesis route, and its polymerization kinetics using three methods of reversible deactivation radical polymerization (RDRP) were studied. Secondly, a study on controlling rheo-mechanical behaviour in bio-sourced polymeric materials was conducted. With the intention of improving rheo-mechanical properties of polymers resulting from high molecular weight bio-sourced species, vitrimer chemistry was introduced into the materials. Further tuning of rheological behaviour was studied by inducing microphase separation in the material via the use of advanced polymer architectures.

The scope of the first project included:

1. Synthesis of two novel itaconic acid-based monomers by functionalization with a methacrylate group, which differ in pendant side arms;
2. Investigation of the ease of polymerization and reaction kinetics of functionalized IA via methods of RDRP; and
3. Thermal and rheological testing to understand the material behaviour and potential.

The scope of the second project included:

1. Synthesis of boronic-acid ester exchange vitrimer networks from commercially available bio-sourced monomers, of both homogeneous and microphase separated architectures;
2. Investigation of the mechanical properties imparted by dynamic cross-linking within the network;
3. Comparison of the effect of microphase architecture with respect to their abilities to control the material's rheological properties; and
4. Investigation of the recyclability of the material and retention of properties through reprocessing.

Chapter 2: Literature Review

This chapter provides essential background on key topics relevant to the thesis. It offers an overview of the current state of the literature, contextualizing the contributions of this work within the academic landscape.

2.1 Polymers of Itaconic Acid

2.1.1 Overview of Itaconic Acid

In emerging chemical process design and synthesis pathways, an increasing emphasis is being placed on practices characterized by "green chemistry".[21] Implementing renewable feedstocks is a key parameter in green chemistry, as the field is characterized by minimizing or eliminating the use of hazardous substances.[22] Intrinsic to this is using non-depletable starting materials. Depletable materials pertain to those derived from fossil fuels or obtained through mining or drilling operations,[23] whereas renewable feedstocks are most commonly from agricultural products. While the motivation behind choosing alternatives for fossil-fuel-derived starting materials is predominantly to mitigate harm against human and environmental health, it also offers the benefit of revealing new chemical building blocks with unique features.[24] Looking towards different sources for platform materials reveals many compounds over and above those which can be obtained from fossil fuels, thereby opening the door to a wide range of new materials. The economic feasibility of using these chemicals as starting materials has also improved, as moving away from petroleum feedstocks has seen the industrialization of alternative production methods.[25]

One chemical which is emerging as a renewable feedstock and is being produced on an industrial scale is itaconic acid (IA). IA is a naturally occurring unsaturated dicarboxylic acid, with structural similarities to petroleum-based acrylic and methacrylic acids, thus leading to its increasing substitution for these two compounds.[26] All three compounds are shown below in Figure 2.1.

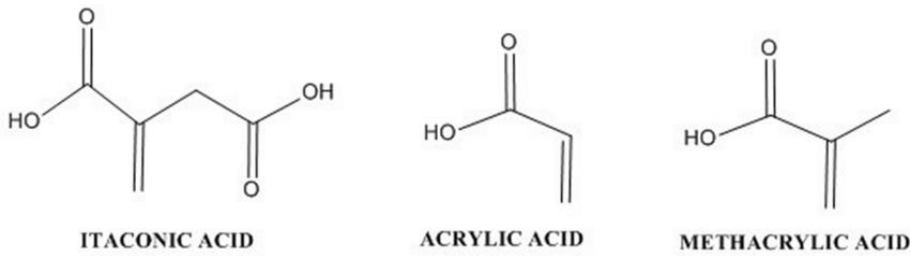

Figure 2.1. Structural comparison of itaconic acid and petroleum-based counterparts.[27]

Itaconic acid is produced during fermentation of select microorganisms. For example, it is currently being produced industrially using the fungus *Aspergillus terreus*, favoured for its daily production capacity of 86g/L.[28] The generation of IA is through the citric acid cycle intermediate cis-aconitate, so can be produced from *Aspergillus terreus* when growing on sugars including glucose, classifying it as a renewable chemical feedstock. However, while using pure glucose or sucrose as the growth substrate is the current practice, it also increases the cost of production.[29] Alternative methods including the use of agricultural residues from wheatgrass, cassava, sago and corn have been reported as effective in IA production, and if implemented on an industrial scale, could reduce manufacturing costs.[30, 31]

Global production of IA in 2020 was estimated at 80,000 tons,[11] encompassing a market valued at 98.4 million USD in 2021.[32] The compound annual growth rate between 2022 and 2027 is expected to be 6.5%, as the applications for the use of itaconic acid are extensive, including as coatings for paper, metal and concrete, in polymers, and biofuels, to cosmetic additives and textile modification.[32] The increasing demand for IA, for its renewability and broad range of applications means it can be a promising, inexpensive starting material suitable for use in green synthesis pathways.

The potential for IA to contribute to a more sustainable chemical industry was highlighted in 2004 when it was listed as one of the "Top-12 Platform Chemicals" in a report commissioned by the US Department of Energy summarizing renewable feedstocks.[10] However, IA was removed from this list in 2010, due to comparatively little progress in its research relative to other compounds such as bioethanol.[33] Contributing to this fall in ranking are the difficulties which are faced when attempting to polymerize IA.

While IA has been scouted as a candidate feedstock for a more sustainable chemical industry, its relevance still depends on many factors. Industrialization of its synthesis via fungi has increased

its level of production, but using agricultural residues in place of glucose or sucrose will allow for its production costs to become more comparable to petroleum-based feedstocks. It is imperative to note that while IA is in principle accessible from renewable sources, the products obtained from it are not necessarily "green", as using renewable feedstocks is just one of 12 principles defining "green chemistry".[22]

2.1.2 Polymerization

Using renewable feedstocks in the polymer industry, much like the rest of the chemical industry, has the potential to reduce the carbon emissions of this sector, which emits 925 Mt of CO_2 annually.[34] Moving away from non-renewable resources, while improving sustainability, can also help to align the sector with consumers and businesses who are increasingly seeking sustainable options. Generating more options for sustainable polymeric materials is critical, as no one renewably sourced material is likely to be able to encompass all applications. Due to its structural similarities with acrylates and methacrylates, IA has received considerable attention since as early as the 1950's.[35] In these early studies, free radical polymerization of the unsaturated double bond failed to yield high molecular weight polymers and proceeded sluggishly.[36] However, advancements in polymerization methods (specifically the development of reversible-deactivation radical polymerization techniques) have improved upon these preliminary results, and the increasing relevance of IA as a chemical feedstock indicates that it should be revisited as a potential renewably sourced building block for the polymer industry. The polymerization of IA at its unsaturated double bond is depicted in Figure 2.2 below.

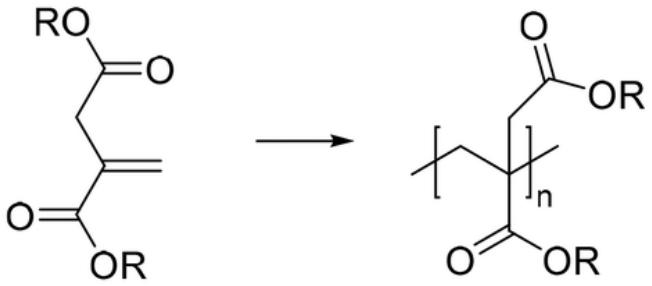

Figure 2.2. Polymerization of itaconic acid (IA) at its double bond.[24]

The polymerization rates of acrylates, methacrylates, and IAs are in a ratio of 1000:100:1, demonstrating the extremely slow behaviour of IAs relative to popular counterparts.[37] It is hypothesized that this slow rate of polymerization is due to the deprotonation of the double bonded

carbon in itaconic acid forming a resonance stabilized radical, delaying the propagation step in chain growth.[12] Using low pH environments below 3.8 encourages increasing rates, as does increasing the pressure of the system, with some reports increasing the pressure to as high as 4900 bar, but in both cases, the obtained molecular weights remain low.[38, 39] Even under these more favourable acidic conditions, the homopolymerization of IA achieves just 35% conversion after 68 hours of reaction under free radical polymerization at 50°C.[35]

More recently, reversible deactivation radical polymerization (RDRP) has been used with IA and its derivatives with better success. RDRP techniques include nitroxide-mediated polymerization (NMP), atom transfer radical polymerization (ATRP), and reversible addition and fragmentation chain transfer polymerization (RAFT). In RDRP, polymerization is controlled by a group which reacts reversibly (e.g., termination or chain transfer) with the free radical. These reversible reactions moderate the kinetics of the polymerization, where the radical is capped into its dormant form, effectively lowering the concentration of free radicals in the reaction media. As a result, polymer chains are less likely to undergo premature termination, and the resulting polymers have lower dispersities compared to polymers obtained by free radical polymerization.[40] RDRP also allows more controlled polymeric architectures to be achieved, with block copolymers, for example, becoming a possibility by injecting a second batch of monomer sequentially onto the macroinitiator species capped with the reversible groups.

In previous reports, RDRP methods have been fine-tuned to find conditions for homopolymerizing itaconic acid derivatives with more favourable outcomes.[12] ATRP of dibutyl itaconate achieved 23-31% conversions and molecular weights of 4 900 – 7 500 g/mol, under optimized conditions employing a CuBr/ PMDETA catalyst.[41] RAFT polymerization of dibutyl itaconate achieved ~70% conversion and molecular weights of ~40 000 g/mol using optimized chain transfer agents. However, to reach these molecular weights, the reaction was required to run for lengthy periods of ~150 hours.[42] In most RDRP studies, copolymers of itaconic acid and additional compounds are employed to allow for greater molecular weights and conversions.

An alternative route to polymerizing IA is step-growth polycondensation reactions to produce polyesters, as depicted in Figure 2.3.

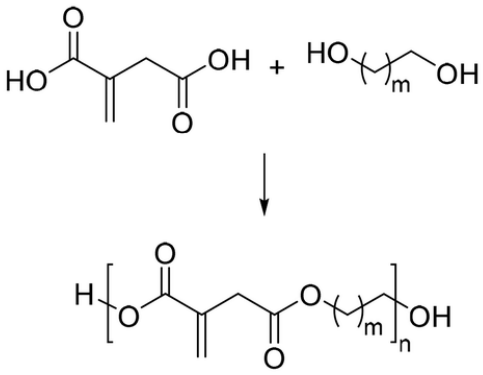

Figure 2.3. Polycondensation polymerization of IA to form polyesters.[24]

Similarly, ring-opening addition condensation polymerization, as shown in Figure 2.4, can be used to generate polyesters of IA.

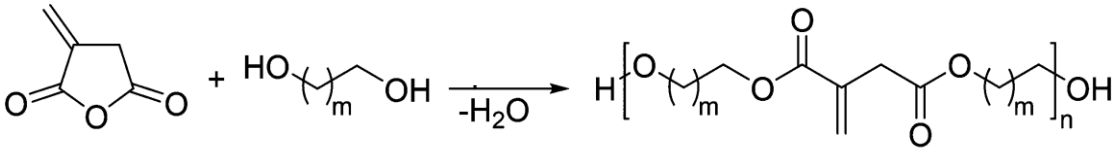

Figure 2.4. Ring opening polymerization of IA to form polyesters.[24]

In reports regarding the synthesis of IA containing polyesters, the double bond in the backbone has allowed for interesting material properties to be obtained. Inducing crosslinking can allow for hydrogel microspheres to be obtained for applications in drug delivery, to produce shape memory materials, as well as make elastomers and thermally cured coatings.[43-45] However, challenges common to these studies were a reduction in final molecular weight and slower rates of reaction when the itaconic acid content was increased. Additionally, while the double bond allowed for interesting features to be observed in the final material, it also resulted in crosslinking and gelling of the reaction mixture when high conversions were sought.[46] Enzymatic reactions have been used to obtain IA containing polyesters, but long reaction times of 94 hours were necessary to achieve a relatively modest molecular weight of 11 900 g/mol.[47]

Incorporating IA into polyesters has been shown to be of benefit, as the unsaturated double bond allows for interesting modifications giving complexity to the final material. For example, the double bond has been exploited to introduce UV-initiated cross-linking into polyesters based off IA.[48] IA can be a useful, renewably sourced tool for incorporating these desirable features in a

broad range of industries. However, the extent to which it can be incorporated into the final material is limited. High IA content in polyesters lead to crosslinking and reduced reaction extents, so it has been used primarily as an additive to achieve desired properties, rather than as the component making up the bulk of the polymer.

2.1.3 Functionalization Prior to Polymerization

Functionalization with an acrylate or methacrylate group has been applied previously to a broad scope of molecules, allowing for polymerizable monomers with applications in biomaterials, coatings, UV-curable resins, drug-delivery systems, and standard everyday polymer applications.[8] In the final polymer, the acrylate or methacrylate group creates the main backbone, with the group that was functionalized serving as the pendant arm. This allows for the starting molecule to be carried into the material. As such, polymer scientists have employed this method to carry desired properties into their final material, from specific material properties, or functional groups, to bio-content.

The ability to bring specific functional groups into polymers by functionalizing the base molecule has been exploited for a range of applications. Glycidyl methacrylate originates from the base chemical glycidol, which due to its epoxy group, enables the final polymer to take part in crosslinking and further reactions, being particularly desirable for use in coatings, adhesives, and medical materials.[49-51] Methacrylated ethylene glycol enables the realization of a biocompatible and water-soluble polymers, with purpose in hydrogels, drug delivery systems, and contact lenses.[52] In these cases, the choice of group being carried into the final material via the methacrylate backbone allows for tunable material properties, to fit the purpose of the application. While bringing desirable chemical or mechanical properties into materials has prompted the development of functionalization techniques, making the synthesis routes well reported, applying this method with the purpose of increasing the polymer's bio-content is becoming more popular.[8]

Lignin, chitosan, and plant cellulose have all been employed in synthesis schemes with the purpose of generating methacrylic monomers for polymerization.[53, 54] Functionalization typically requires an esterification reaction, with methacrylic anhydride or methacryloyl chloride reacting with the molecule to be functionalized (typically with the hydroxyl forms). Currently, methacrylic anhydride and methacryloyl chloride are commercially available, coming from petroleum derived sources. Due to this, the resulting monomers are not entirely bio-derived but offer an improved

bio-content compared to conventional polymers. Following functionalization, the resulting monomers can be polymerized by conventional RDRP schemes due to their methacrylic structure. As such, applying methacrylate functionalization to IA could provide a route to incorporate its bio-content into polymeric materials more readily.

2.2 Tuning Properties by Vitrimer Networks

2.2.1 Entanglement Molecular Weight

Polymer macromolecules with a long carbon backbone present unique rheological and mechanical properties, in part due to the interactions arising between chains.[55] The ability for the backbones to interpenetrate and create a distinctive topology of entanglements has implications on their mobility and relaxation, both in melts, solutions, and as solids.[56] Large degrees of interactions, such as knotting of the polymer backbones, coils, and loops restrict movement within the network, behaving as physical cross-links holding the materials structure in place.[57] Whereas rubbers including neoprene gain elastic properties from permanent chemical cross-links in the matrix, high degrees of entanglement in polymer matrices impart rubbery qualities due to the physical cross-links.[58]

The mechanical properties of polymer materials are highly dependent on the absence or presence of entanglements. In polymers with a high glass transition temperature, macroscopic properties go from brittle to tough as entanglements become more significant, while in low glass transition temperature polymers, introducing entanglements changes the material from gel-like to rubbery type.[59] This allows it to experience large deformations and give an elastic response. In most applications, the properties of the entangled materials are more desirable than their disentangled analogs.[55] For entanglements to arise in networks, the polymer backbones must be of sufficient length to be able to wrap around each other. The ability to coil and loop is also dependant on the side arms off the carbon backbone, and therefore the molecular weight that will cause entanglements to exist within the polymer is unique to each polymer species.[60] This point, termed the critical entanglement molecular weight, M_c, is typically in the range of 1 000 to 20 000 g/mol for polymer materials encountered on the market. Polyethylene and polystyrene, for example, have M_c values of 1 150 and 26 000 g/mol, respectively.[61, 62] Typically, as the molecular weight of the monomer used to generate the polymer increases, so does the resulting polymer's M_c. The presence

of large pendant arms off the polymer backbone add bulk to the polymer, preventing the chain from looping and coiling, and subsequently impeding entanglements.

Functionalizing chemical species to produce novel monomers inherently leads to monomers of substantial molecular weight, due to the combination of starting species. This in turn causes the M_c of the resulting polymers to be high, and the material properties at conventional molecular weights to be disappointing.[63] Simply increasing the molecular weight of the polymers to be above the M_c threshold is also not necessarily practical. Targeting larger molecular weights in the synthesis can be difficult in conventional radical polymerization due to the fast termination of the system, and processing of larger macromolecules is challenging due to the increased viscosity of the molten state.[64] Therefore, when functionalizing a renewable chemical species with the intention of carrying bio-content into the final polymeric material, there exists a new challenge which is being able to obtain the same macroscopic properties of conventional petroleum polymers caused by entanglements.

2.2.2 Vitrimer Networks

Vitrimer networks were first introduced by Liebler in 2011, describing a new class of polymer materials bridging thermosets and thermoplastics.[16] Specifically, they are polymer networks cross-linked by dynamic covalent bonding that therefore maintain a cross-linked matrix but can flow and be reprocessed under certain stimuli.[18] The cross-links in the network can undergo exchange reactions without the depolymerization of the polymer itself, allowing for rearrangements in the network while preserving the mechanical integrity. Where this becomes a significant advantage is in developing reprocessable and recyclable materials. Thermosetting materials, including traditional rubbers, are composed of a permanently cross-linked matrix.[65] While this forms a rigid and robust network with strong mechanical properties, its environmental sustainability is limited, motivating the development of vitrimer networks with dynamic cross-links.

However, associative dynamic covalent chemistry can also be applied to improve the properties of bio-sourced materials. Instead of being limited to producing reprocessable replacements for traditional thermosets, the concept can have many beneficial implications. While chain entanglements mimic permanent chemical bonds and impart elastic behaviour, introducing covalent bonding into materials can mimic chain entanglements when the polymers have large M_c values, producing desirable macroscopic properties. This is particularly useful when trying to

impart improved material properties into bio-sourced materials, as it does not impede the environmental considerations of the material. For example, Yang *et al.* introduced reversible transesterification bonding into bio-based soybean oil networks, resulting in vitrimers with tensile strength exceeding 16 MPa, that were fully reprocessable at 180°C without catalysts.[66] In addition, softwood kraft lignin was shown by Moreno *et al.* to effectively produce partially bio-based vitrimers with polyethylene glycol divinyl ether, with the benefit of the lignin requiring no processing before vitrification. Varying the lignin content allowed for a range of mechanical properties to be realized, and mechanical properties were retained upwards of 90% compared to the virgin material through recycling.[67]

Dynamic chemistry can strengthen and impart desirable qualities to polymeric materials, and it has been shown that designing networks at the microscopic level can be used to attain targeted macroscopic properties. For example, employing different types of associative chemistry allows for exchange to be triggered by different stimuli. Transesterification reactions cause the bonding in the network to respond to changes in temperature, whereas disulfide exchange is stimulated by light or heat, imine exchange is responsive to pH changes, and boronic acid ester exchange is driven by moisture.[18] Selecting the mode of cross-linking allows for the reprocessing to be achieved by the respective method, and the extent of cross-linking has proven to alter the macroscopic material responses. By varying the ratio of cross-linking within epoxy vitrimers, it has been shown that the tensile strength of the resulting material could cover two orders of magnitude (0.18 to 25 MPa) with the same epoxy prepolymers being used as the starting material.[68] In designing materials with their environmental impact in mind, combining vitrimer chemistry with bio-sourced monomers can allow for required material properties to be achieved through reversible cross-linking, and compensate for any property shortcomings arising from the use of bio-based alternatives.

2.2.3 Methods to Control Creep

Despite the early optimism of vitrimer networks as being a replacement for thermosetting materials, their associative dynamic bonding lends itself to poor creep resistance.[69] Network rearrangements allowed by the ongoing reformation of bonds in the material, which give the benefit of self-healing, reprocessability, and constant cross-linking density (lending itself to mechanical strength), also exchange when exposed to prolonged stresses. The creeping behaviour

termed “cold flow” has limited the application of vitrimers for load-bearing and long-term structural uses.[70] Methods to try and minimize this downfall are being explored, to allow vitrimers to contend on the commercial market as a viable alternative to thermosets.

Enhancing mechanical stability can be completed by increasing the amount of cross-linking in the material, as this reduces the chain mobility in the network, slowing the rearrangement of bonding within the material.[71, 72] Torkelson also explored using a small fraction of permanent bonding within the material to reduce creep. In this study, the extent of permanent links was minor enough as to not impede reprocessing but could reduce creep by 71% compared to the network lacking the permanent bonding.[73] Since vitrimer creep tends to worsen with increased temperature, due to the increased mobility of the polymer backbones, including a high glass transition temperature monomer into the polymer material has been shown to limit the creep at moderate temperatures. Fillers, such as metal complexes that engage with imine bonds, were shown to effectively supress creep, enhance mechanical properties, and solvent and acid resistance, without preventing recyclability.[74]

Inducing microphase separation, by blending incompatible polymers, or by using block copolymers in the network, has also emerged as a successful method for improving creep resistance.[75] In this strategy, it is hypothesized that self-assembly into highly ordered topologies causes localization of the cross-linking, resulting in regions of high cross-link density that restrict strand diffusion. Sumerlin and Lessard’s initial work in combining block copolymers with vitrimers investigated a system of AB type block copolymers, in which both blocks had glass transition temperatures below the service temperature.[76] In this sense, the stability of the system came from the regions of high cross-linking restricting deformation. Ishibashi *et al.* studied a similar AB system, with two low T_g components. This work agreed with previous studies that the block topology was effective in resisting creep behaviour at high temperatures relative to statistical counterparts, but noted the block topology was causing an increase of network defects such as loops and dangling ends.[77] In using low T_g components, the block lacking cross-linking acts as a region of network mobility, which can have the drawback of allowing greater deformation under applied stresses. Despite this, block vitrimer systems of a high T_g and a low T_g component are less frequently reported.

Fang *et al.* reported a series of triblock ABA vitrimers with glassy A regions, highlighting the potential of including a hard region in the block vitrimers.[78] In this work, the cross-linking of the soft phase also allowed tuning of the macroscopic properties, with the ability to minimize the necking that is observed in traditional thermoplastic elastomers, potentially making them suitable for higher stress applications.[78] Incorporating hard blocks can limit creep behaviour even further at the service temperature, as the structure is held in the hard blocks due to the high T_g and held in the soft regions due to cross-linking. Just as in thermoplastic elastomers, using this network architecture could allow for a combination of plastic and elastic properties at service temperatures, such as rubbery behaviour.

Efforts have been successful in determining strategies to reduce the creeping nature of vitrimers. However, they are yet to be completely comparable to traditional thermosets, and thus, ongoing studies into improving creep control are being made.

Chapter 3: Methacrylate Functionalization of Itaconic Acid for Improved Polymerization

3.1 Preface

Chapter 3 consist of a manuscript that details a novel synthetic route to obtain a new family of itaconic acid-based methacrylic monomers, by a four-step synthesis route. After thorough characterization of the intermediates was completed, kinetic studies of the monomer's polymerization by three methods of reversible deactivation radical polymerization (RDRP) ensued. A series of homopolymers was synthesized by reversible addition-fragmentation chain transfer polymerization (RAFT) for two novel monomers, targeting a range of molecular weights (10 000 to 400 000 g/mol). The ability of RAFT to control the polymerization across the target molecular weights was examined. The polymer's thermal behaviour was assessed, as was the rheological behaviour of one analog. A series of block copolymers was made, showing the ability of the itaconate-based methacrylate to be polymerized into more advanced architectures.

The objective of this chapter encompasses the first objective of the thesis (see Chapter 1), being an investigation into methods of including renewable sources into polymeric materials. Specifically, an alternate method to incorporate itaconic acid into polymeric materials which overcomes the well-documented difficulties of its polymerization was pursued. The article demonstrates an effective synthesis route to obtain the targeted monomers and confirms that using methods of RDRP is effective in producing polymers of defined molecular weight and architecture, with tunable rheological properties and good thermal stability.

Note that this manuscript has been prepared for submission to the journal *Polymer Chemistry*. As per the journal's formatting requirements, the Supporting Information, including experimental methods, are excluded from the main body of the article and are provided in Appendix A.

3.2 Abstract

Itaconic acid (IA) is a renewable molecule with increasing industrial availability. However, IA-based polymers have been limited by low molecular weights and conversions. In this work, we report the synthesis of two novel methacrylate-functionalized itaconic acid monomers. Using

various reversible-deactivation radical polymerization methods, we achieved well-defined polymers with high conversions (≥98%) in moderate reaction times (i.e., 70 minutes by atom transfer radical polymerization at temperatures ~80°C). Homopolymers of these two monomers exhibited a range of properties, with glass transition temperatures (T_g) ranging from -40°C for heptyl-functionalized moieties to 14°C for benzyl-functionalized moieties. Consistent reaction kinetics enabled the synthesis of pre-designed AB-type diblock copolymers, demonstrating the potential of the heptyl-functionalized derivative as a soft block in phase-separated materials. The favorable reaction kinetics of these methacrylate-functionalized itaconic acid monomers make this approach a promising pathway for incorporating renewable content into polymeric materials.

3.3 Introduction

In emerging chemical synthesis pathways and polymer innovations alike, the relevance of using renewable feedstocks is overwhelmingly apparent. Since the publication of the twelve principles of green chemistry in 1998 by Anastas and Warner,[1] growth has been observed in research publications and patents which reference the concept.[2, 3] An essential aspect of this field is using renewable feedstocks instead of those from fossil fuels or mining. While this is motivated largely by the desire to mitigate the carbon emissions accompanying the extraction of these depletable resources, it also offers the benefit of revealing new chemical building blocks with unique features.[4] The economic feasibility of using these alternative chemical starting materials has also seen improvements, as moving away from petroleum feedstocks has led to the industrialization of production methods for these alternative chemicals.[5]

Itaconic acid (IA) is a naturally occurring chemical whose production via the citric acid cycle intermediate cis-aconitate has been commercialized, using the fungus *Aspergillus terreus* in bioreactors.[6] The potential for IA to contribute to a more sustainable chemical industry was highlighted in 2004, when it was listed as one of the "Top-12 Platform Chemicals" in a report commissioned by the US Department of Energy summarizing renewable feedstocks.[7] However, IA was removed from this list in 2010, due to comparatively little progress in its research relative to other compounds such as bioethanol.[8] Contributing to this are the difficulties faced when attempting to polymerize IA.

The aspects of IA which make it an exciting chemical feedstock, namely its dicarboxylic acid structure with a naturally occurring unsaturated group, have also been the features that impede its

use in the polymer industry. Early attempts of polymerization at the double bond using free radical polymerization (FRP) proceeded sluggishly to give low molecular weight polymers, hypothesized to be caused by the carboxylic acid stabilizing the propagating radical via resonance.[9, 10] While advancements in methods of reversible deactivation radical polymerization (RDRP) have brought greater success to the polymerization of IA and its derivatives than FRP, fine tuning of reaction conditions have still resulted in slow reactions yielding low molecular weights and suboptimal conversion.[11]

Looking towards polycondensation reactions of the carboxylic acids to produce polyesters is not more promising. In these polyesters, the unsaturated double bond can be cross-linked to yield unique materials such as hydrogel microspheres, UV cured coatings[12] or shape memory materials,[13] however, attempting to reach high conversions often leads to the double bond inducing gelling in the reaction mixture.[14] A reduction in final molecular weight of these polymers is also typical when attempts to increase IA content are made.

Recently, various other renewable and bio-sourced molecules have successfully been incorporated into novel polymeric materials via functionalization. From plant oil triglycerides, Yuan *et al.* demonstrated a method of obtaining a series of methacrylate monomers, imino ether monomers and cyclic norbornene monomers from which polymers with varying mechanical properties could be realized.[15] The methacrylate and acrylate functionalization of various terpene feedstocks by Atkinson *et al.* presented a pathway from terpene waste streams to well-defined ABA triblock copolymers with promising qualities for application as pressure-sensitive adhesives and thermoplastic elastomers.[16, 17] Lignin-derived vanillin,[18] lactic acid,[19] gum rosin,[20] and abietic acid are several other examples of renewable feedstocks which have been functionalized with a methacrylate group to give polymeric materials with an increased green content. However, until now, this method has yet to be attempted on itaconic acid.

In the present study, we extend the strategy of methacrylate functionalization to derivatives of IA, to overcome the previous pitfalls of IA polymerizations. A sequential hydroboration-oxidation and esterification reaction pathway transforms the unsaturated double bond on the itaconate backbone, that when applied to various itaconate derivate starting materials, presents the opportunity to realize a series of novel itaconate methacrylate monomers. Here, we describe the synthesis, characterization, and polymerization of two novel, itaconic acid-based methacrylate

monomers: diheptyl itaconyl methacrylate (DHIAMA) and dibenzyl itaconyl methacrylate (DBIAMA). Methods of reversible deactivation radical polymerization (RDRP) are used to obtain homopolymers of both, validating the easy incorporation of IA into polymers via this strategy. Initial screening of the homopolymers showed p(DHIAMA) to have a low glass transition (-40 °C), with p(DBIAMA) having a T_g of 14°C. Adjusting the molecular weight of p(DHIAMA) showed the potential to tune the polymer's rheological properties, and an initial investigation into the suitability of p(DHIAMA) to serve in specialized materials was conducted by polymerizing p(DHIAMA) with p(MMA) into targeted diblock architectures, obtaining hard-soft AB polymers.

3.4 Results and Discussion

3.4.1 Monomer Synthesis

The presence of an unsaturated double bond in the backbone of IA was successfully exploited to functionalize this renewable feedstock with a methacrylate group. An overview of the synthesis scheme is shown in Figure 3.1, and detailed methods for the synthesis are provided in the Supporting Information (Appendix A, Section A1.9). As a first step in the synthetic pathway, the carboxylic acid groups of IA are functionalized by an esterification reaction, allowing for a range of distinct monomers to be obtained by varying the choice of alcohol used in this step. The synthesis was completed independently using both heptanol and benzyl alcohol in the first step, serving as the functional arms branching off from the itaconic acid core. These two groups were chosen to explore the potential of tuning the final polymeric properties of our itaconic acid-based monomer due to the flexible saturated carbon chains of heptanol contrasted to the rigid nature of benzene ring. In both cases, the proposed pathway could be carried out successfully, as confirmed by ^{1}H NMR of the intermediates and final monomers (see Supporting Information, Appendix A, Section A1.9).

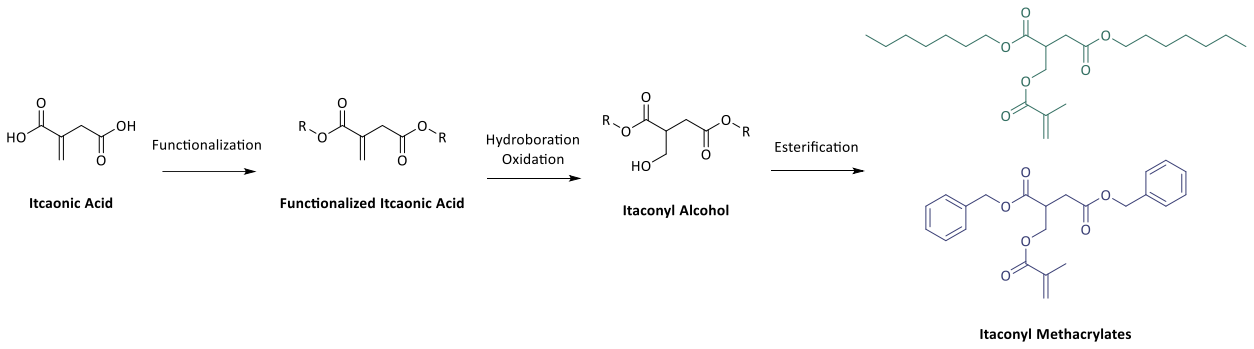

Figure 3.1. Schematic overview for obtaining methacrylate monomers of IA derivatives.

3.4.2 Polymerization by Methods of Reversible Deactivation Radical Polymerization

To demonstrate ubiquity of the obtained methacrylate monomers, DHIAMA was subjected to polymerization by the three most common methods of reversible deactivation radical polymerization using conventional reaction conditions. Kinetic plots displaying the reaction results from the three employed methods are shown in Figure 3.2.

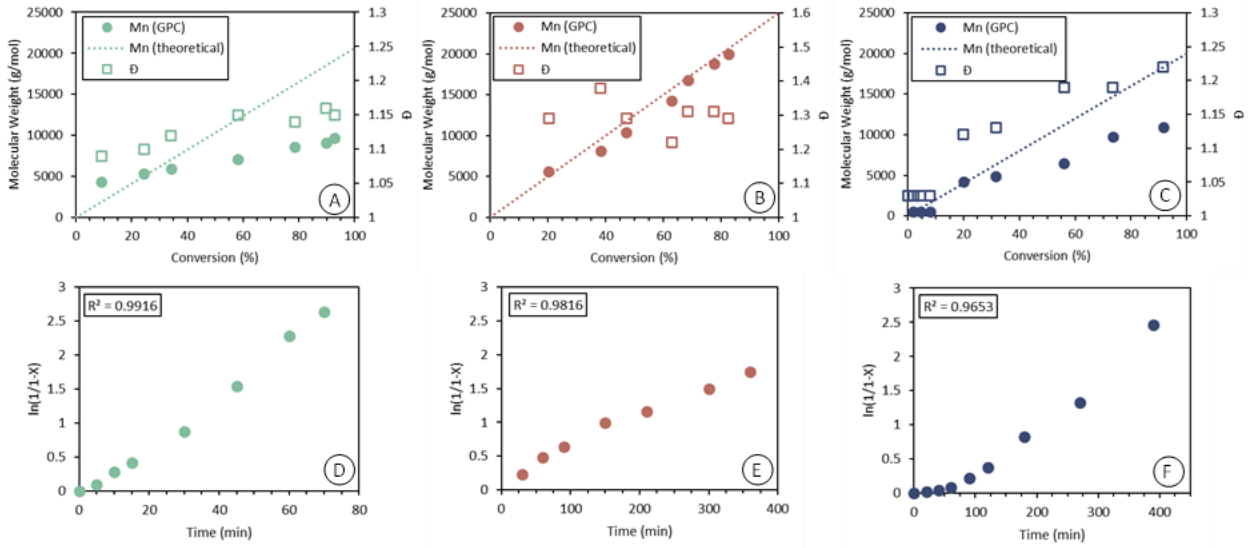

Figure 3.2. RDRP reaction kinetics for DHIAMA: Molecular weight and dispersity (*Đ*) throughout polymerization by: (A) ATRP; (B) NMP; and (C) RAFT. Linearized monomer conversion during polymerization is shown by: (D) ATRP; (E) NMP; and (F) RAFT.

Nitroxide Mediated Polymerization: The obtained diheptyl functionalized monomer was subjected to polymerization by NMP as described in the Supporting Information (Appendix A,

Section A1.10). To ensure control of the reaction, as methacrylate homopolymers tend to generate high dispersity polymers from NMP methods ($Đ$ = 1.5 - 4),[21] DHIAMA was copolymerized with small amounts of styrene in the initial monomer mixture ($f_{ST,0}$ = 0.1).[22] Previous studies incorporating itaconic acid, specifically dibutyl itaconate, into polymeric materials via NMP required styrene as a copolymer as well, and found increasing dibutyl itaconate content above 20 mol% led to drastic plateauing of the molecular weight as reaction conversion increased.[23] It was hypothesized to be partially due to itaconates having a high tendency to partake in chain-transfer reactions.[9, 24] In this study by Kardan *et al.* utilizing BlocBuilder as the SG1, the reaction conversions decreased with itaconate content, led to dispersities >1.5, and obtained low molecular weight polymers (M_n= 2 600 g/mol).[23]

Kinetic plots in Figure 3.2 of monomer conversion (X) expressed as ln[1/1-X] against time show strong linear dependency with reaction time, indicating the reaction progressed as a controlled radical polymerization. From samples obtained for GPC throughout the reaction, the molecular weight and dispersity of the polymer could be monitored throughout the reaction. A consistent increase in molecular weight was observed up to DHIAMA conversions of 83%, which coupled with low dispersities for NMP ($Đ$ < 1.4) suggest a mechanism analogous to an active chain end and successful living polymerization.

Atom Transfer Radical Polymerization: DHIAMA was tested under traditional ATRP conditions (Appendix A, Section A1.11 of the Supporting Information details the methods used) to assess the ubiquity of DHIAMA, given the challenges of itaconate polymerization across known techniques. Specifically, for ATRP, the deprotonation of itaconic acid during chain growth causes coordination complexes to form between conventional copper catalysts and the deprotonated itaconic acid, leading to catalyst deactivation and the cessation of polymerization.[25] Using cyclic itaconimides prevents this unfavorable interaction,[26] as does using itaconate derivatives,[24] but homopolymers in literature made by these methods tend towards high dispersities (> 1.5), and low conversions (< 40%), respectively.[27, 28]

Affixing a methacrylate group to itaconic acid has eliminated these challenges. The pseudo first-order dependance of monomer conversion with reaction time is shown in Figure 3.2, after an induction period, indicate that the commonly used and commercially available Cu(I)Br, EbiB, and PMDETA system effectively controls polymerization. This, along with narrow molecular weight

distributions ($Đ$ < 1.2), and an increasing molecular weight across the conversion of 93% support the application of ATRP for DHIAMA polymerization.

Reversible Addition Fragmentation Chain-Transfer Polymerization: Studies have extended RAFT to the polymerization of itaconates and itaconimides with improved conversions and polymer characteristics (40 000 g/mol, 70% conversion) relative to other RDRP methods, however, long reaction times are required (>150 hours)[29] and the dispersities are higher than typical for RAFT ($Đ$ = 1.70).[30] Here, 2-cyano-2-propyl dodecyl trithiocarbonate was selected as the RAFT chain transfer agent, due to its commercial availability and known ability to effectively polymerize methacrylates.[31] Detailed methods of the synthesis are provided in the Supporting Information (Appendix A, Section A1.12). As with other RDRP methods, kinetic plots show linear (as ln[1/(1-X)]) dependance of conversion with time (see Figure 3.2), and narrow molecular weight distributions are paired with a steady increase in molecular weight with conversion.

It should be noted that the molecular weight determined by gel permeation chromatography calibrated using narrow molecular weight distribution p(MMA) standards deviates from the theoretical molecular weight determined by the monomer conversion at the reaction time, due to not knowing the Mark-Houwink coefficients for this novel polymer. However, it appears this deviation is not as severe for the NMP reaction, which could be caused by a portion of the nitroxide initiator failing to be activated in the reaction. In all three reversible deactivation radical methods, monomodal GPC traces and dispersities below 1.3 indicate the polymerizations proceeded by controlled radical mechanisms,[31] confirming the universality of DHIAMA to a range of polymerization methods.

RAFT was selected as the preferred method for the preparation of a series of homopolymers for both DHIAMA and DBIAMA, due to its simplicity and ability to produce polymers exhibiting low dispersities. This was conducted with the intent of determining if the reaction could be controlled across a range of molecular weights, with target molecular weights ranging from 10 000 g/mol to 400 000 g/mol. The polymerization of the series resulted in polymers with low dispersities and M_n values near those targeted, as determined by gel permeation chromatography equipped with a light scattering detector. Table 3.1 and 3.2 show the molecular weight results of the DHIAMA and DBIAMA series of homopolymers, respectively. From the polymer series, the *dn/dc* value relating the sample concentration to the RI detector output of the GPC could be determined

as 0.066 ± 0.004 for p(DHIAMA) and 0.127 ± 0.006 for p(DBIAMA). Knowing the *dn/dc* allows for the exact molecular weight of the homopolymer samples to be known in future GPC samples run, and the consistency between *dn/dc* values in the polymer series indicates good sample preparation and reliable molecular weight results. In all cases, the polymerization reaction was carried out as detailed in the methods (Appendix A, Section A1.12).

Table 3.1. Molecular weight results for the series of p(DHIAMA) homopolymers by RAFT.

Polymer	Target M_n (g/mol)	Conversion (%)[a]	M_n (g/mol)[b]	$Đ^c$	*dn/dc*[d]
H1	10 000	98	8600	1.07	RIdetector[e]
H2	17 000	89	15 700	1.07	0.074
H3	20 000	99	28 700	1.07	0.067
H4	30 000	97	37 000	1.07	0.068
H5	35 000	95	39 000	1.05	0.064
H6	40 000	95	64 900	1.12	0.059
H7	100 000	95	93 900	1.09	0.063
H8	200 000	97	148 900	1.13	0.063
H9	400 000	94	198 200	1.60	0.069

[a]Calculated from the integrals of monomer peaks in NMR; [b,c,d]Determined from GPC LS detector of final dried samples; [e]H1 was analyzed using the GPC RI detector due to inaccuracies of LS detector at low molecular weights.

Table 3.2. Molecular weight results for the series of p(DBIAMA) homopolymers by RAFT.

Polymer	Target M_n (g/mol)	Conversion (%)[a]	M_n (g/mol)[b]	$Đ^c$	dn/dc[d]
B1	10 000	97	15 400	1.15	0.127
B2	15 000	94	22 400	1.16	0.126
B3	20 000	99	30 700	1.11	0.135
B4	30 000	99	45 900	1.14	0.122
B5	60 000	99	88 000	1.13	0.118
B6	100 000	91	105 200	1.27	0.126
B7	200 000	87	136 000	1.40	0.136

[a]Calculated from the integrals of monomer peaks in NMR; [b,c,d]Determined from GPC LS detector of final dried samples.

The RAFT polymerizations of DHIAMA consistently produced satisfactory results, across a range of molecular weights. High conversions (> 89%) were achieved in the standard polymerization time of 7 hours, and narrow monomodal GPC traces were obtained (not higher than 1.13) from most of the polymers. The exception comes from H9, where extremely high molecular weights were targeted. Although the GPC trace still gave a single peak, the obtained polymer had a greater dispersity (1.60), indicating the reaction was not as controlled as the others. This result is not surprising as the RAFT polymerization of methacrylic monomers is known to be less successful when targeting high molecular weight polymers.[32]

The RAFT polymerization of DBIAMA, using the same conditions, gave defined polymers but of a higher dispersity than the DHIAMA polymers. Monomer conversion expressed in terms of ln[1/(1-X)] exhibited linear dependance with reaction time, and no significant plateauing of the molecular weight was observed with conversion. Example kinetic plots for the polymerization of p(DBIAMA) are provided in the Supporting Information (Appendix A, Figure A11 and A12). While this series of polymerizations exhibited somewhat broader molecular weight distributions, at conventional molecular weights the obtained polymers still produced $Đ$ <1.3 and monomodal GPC traces. Slight shouldering was observed in reactions targeting the highest M_ns, which coupled with the jump in dispersity may indicate branching occurred. Both the increased reaction speed and the possibility of branching are thought to be caused by the electron-dense benzyl side chains. This trend has been noted previously by other groups, where benzyl containing monomers display larger propagation rates than saturated alternatives.[33, 34] The most recent IUPAC benchmark values give the propagation rate of benzyl methacrylate being nearly double that of methyl methacrylate, for example.[35]

3.4.3 Thermal Properties

The influence of the selected side chain on the thermal properties of the polymer were evaluated via thermal gravimetric analysis (TGA) and differential scanning calorimetry (DSC). Both p(DHIAMA) and p(DBIAMA) were determined to have excellent thermal stability under standard processing temperatures, with the onset of 10 wt% decomposition occurring at 262°C and 256°C for p(DHIAMA) and p(DBIAMA), respectively. A clear two-step decomposition pattern is displayed by both p(DHIAMA) and p(DBIAMA), with about 80% of the weight being decomposed in the first stage (Figure A13 and A14). This proportion of weight loss corresponds

well to the pendant chain branching off the backbone that is joined by the itaconate core. Decomposition of the methacrylate-resembling backbone follows, with the onset of 10 wt%, relative to the starting mass, of the second decomposition occurring at 398°C and 387°C for p(DHIAMA), and p(DBIAMA), respectively.

Thermal transitions of polymers, as assessed by DSC, are influenced via several structural factors. The mobility of the polymer's backbone, intermolecular forces, the presence and architecture of pendant groups, and cross-linking between chains all influence the T_g, as well as crystalline and melting temperatures (T_c and T_m, respectively). DSC traces for both p(DHIAMA) and p(DBIAMA) lacked T_m and T_c transitions, indicating amorphous polymers (Figure 3.3). We then probed how the differing pendant arms of p(DHIAMA) compared to p(DBIAMA), as well as the molecular weight, would influence the glassy transition of the polymers. According to the Flory-Fox equation for monodisperse polymers,[36]

$$T_g = T_{g,\infty} - \frac{K}{M_n} \tag{3.1}$$

the glass transition temperature increases with the molecular weight, M_n, until the deviation away from the glass transition temperature at an infinite polymer chain length, $T_{g,\infty}$, becomes minimal (at infinite molecular weight, there is no free volume associated with any chain ends). Assessing the T_gs of the p(DHIAMA) and p(DBIAMA) series revealed this molecular weight dependance of the glassy transition, and Figure 3.3 shows the experimental glass transition temperature data contrasted with the model fitting for both polymer sets. By fitting the experimental data to the Flory-Fox equation, the $T_{g,\infty}$ of p(DHIAMA) and p(DBIAMA) was evaluated to be -40.4°C, and 13.9°C, respectively.

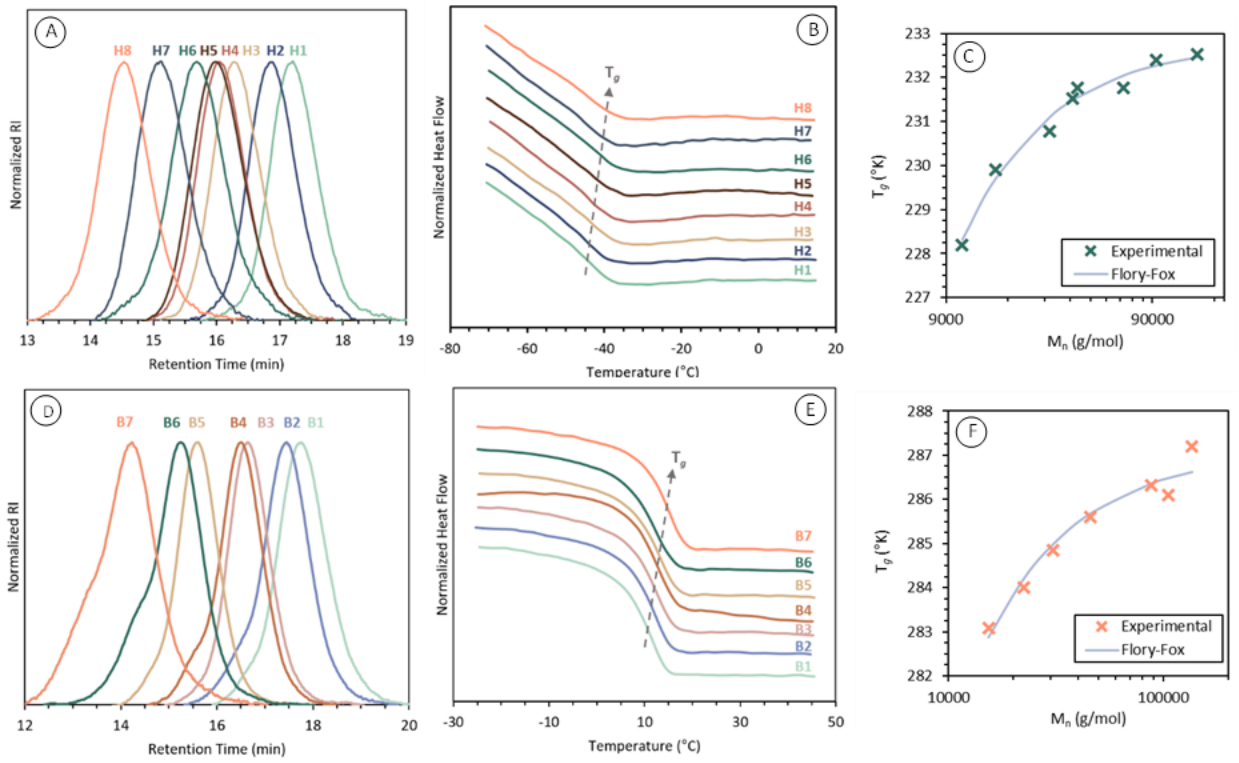

Figure 3.3. (A) Gel permeation chromatography traces of p(DHIAMA) homopolymer series; (B) Differential scanning calorimetry traces of p(DHIAMA) homopolymer series; (C) Flory-Fox model for p(DHIAMA) series; (D) Gel permeation chromatography traces of p(DBIAMA) homopolymer series; (E) Differential scanning calorimetry traces of p(DBIAMA) homopolymer series; (F) Flory-Fox model for p(DBIAMA) series.

While the inclusion of heptyl side arms produced a soft material with a low T_g, substituting these arms for benzyl groups did not have the ability to increase the glass transition as substantially as anticipated. While the pendant benzyl arms offer some rigidity, preserving most of the backbone composed from itaconic acid and a methacrylate group indicates the range of accessible glass transition temperatures is limited. With a transition temperature near ambient conditions, the applications for this benzyl derivative may be less broad than the heptyl alternative, however, it offered a preliminary screening on the extent to which the final polymer's properties depend on the functional group used in the first step of the monomer's synthesis. With a glass transition temperature well below ambient conditions, the heptyl derivative is deemed suitable for a range of soft-polymer applications including rubber toughening,[37] flexible electronics, sensors,

thermoplastic elastomers, or shape memory materials.[38] It was therefore selected for further assessment.

3.4.4 Homopolymer Rheological Properties

Using the series of p(DHIAMA) homopolymers, frequency sweeps and viscosity measurements were completed to gauge their dependance on molecular weight, as shown in Figure 3.4 for H5, H7 and H9. As expected, the viscosity increases with molecular weight, and the range of shearing rates resulting in the zero-shear viscosity plateau becomes smaller. To estimate the molecular weight of entanglement, the zero-shear viscosities were plotted against the number average molecular weight of the polymer samples (Appendix A, Figure A16). However, the zero-shear viscosities exhibited a linear dependance with molecular weight, indicating the critical molecular weight has likely not been obtained in our sample series. As DHIAMA is a highly bulky monomer, it is possible the critical molecular weight is greater than H7, as polymethyl methacrylate alone has a M_c of 20 kg/mol,[39] and lauryl methacrylate, a monomer half the molecular weight of DHIAMA, gives polymers with a critical molecular weight of 225 kg/mol.[40, 41]

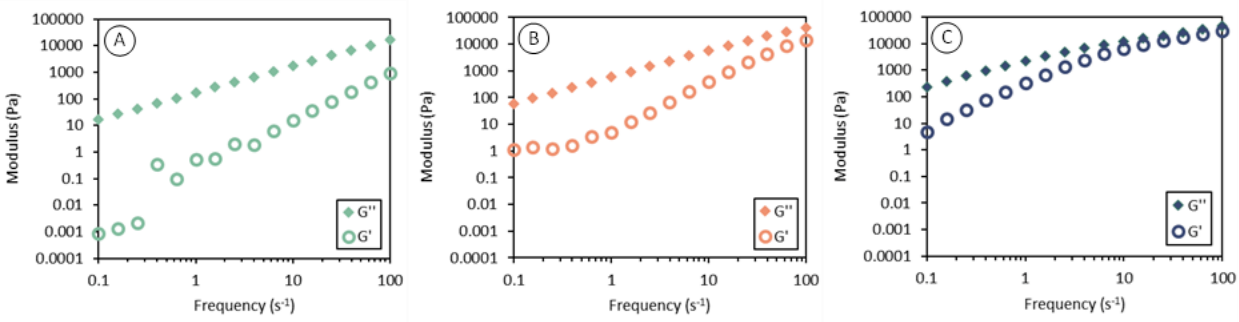

Figure 3.4. Frequency sweeps using a fixed strain of 0.1% for: (A) H5; (B) H7; and (C) H9.

Across the molecular weights (39 kg/mol to 198 kg/mol) and the tested frequencies (0.01 to 100 rad/s), the loss modulus was dominant, indicating the polymer's tendency to flow even at ambient conditions. The strong dependency of the elastic modulus on the frequency further highlights this fluid behavior of the tested samples, with no rubbery plateau region appearing in the sweep range. Despite the common fluid-like characteristic of the DHIAMA-based polymers, adjusting the molecular weight does allow for the value of the modulus to be tuned. As the molecular weight increased from 39 kg/mol to 198 kg/mol, an order of magnitude increase was observed for the loss modulus, with the storage modulus at low frequencies increasing several

orders of magnitude. Although the chains of the largest 198 kg/mol sample are not completely entangled, as hypothesized from the viscosity measurements, more chain-to-chain interactions due to the larger size are evidently imparting more structure and elasticity. It should be noted that the rheological tests were completed at ambient conditions, as the storage modulus of even the largest sample was below the detection threshold of the instrument when testing was done at conventional processing temperatures of 170°C.

3.4.5 Block Copolymer Synthesis

In many value-added applications including those listed previously, defined and advanced polymer architectures are required, which can be realized through methods of reversible deactivation radical polymerization. To test the potential of DHIAMA in obtaining targeted architectures, a series of diblock copolymers were synthesized via RAFT. As the copolymer, methyl methacrylate was selected due to its commercial availability, and its high glass transition temperature, which is expected to contrast against the softer p(DHIAMA). The potential of block copolymers is not fully obtained when microphase separation between the blocks does not occur, and so the monomer-monomer interaction parameter was determined (Supporting Information, Appendix A, Section A3.1), and used to estimate the segregation strength of the system when designing the block-copolymers.

For a monodisperse and symmetric block copolymer, the Flory-Huggins enthalpic interaction parameter, χ , can be used to help understand the phase separation behavior. The Flory-Huggins enthalpic parameter can be estimated using Equation 3.2,[42] as follows:

$$\chi = \frac{\bar{V}}{RT}(\delta_{DHIAMA} - \delta_{MMA})^2 \tag{3.2}$$

where: $\bar{V}$ is the average molar volume approximated by $\bar{V} = \sqrt{V_{DHIAMA}V_{MMA}}$; δ is the solubility parameter and is determined for DHIAMA by group contribution theory; R is the universal gas constant; and T is the temperature of the system. Then, the enthalpic parameter is used with the total degree of polymerization, N, to estimate the segregation strength. For a symmetric and monodisperse diblock polymer, it is estimated that microphase separation will occur when (χN) exceeds a value of 10.5.[43] Detailed calculations can be found in the Supporting Information for the segregation strength of the system (Appendix A, Sections A3.1 and A3.2). A series of diblock

polymer, varying in DHIAMA content, were designed with (χN) > 10.5 to study the phase-behavior across a range of compositions, and exhibit DHIAMA's ability to produce polymers of a targeted design. A macro-RAFT initiator was synthesized by the polymerization of methyl methacrylate, and then re-initiated in the presence of DHIAMA in extensions targeting DHIAMA molar compositions of 0.20 to 0.75 (Methods are detailed in the Supporting Information, Appendix A, Section A1.13 and kinetic results in Section A3.3). Table 3.3 details the molecular weight results of the macro-RAFT initiator and diblock polymer series.

Table 3.3. Polymerization results of the p(MMA-*b*-DHIAMA) diblock series.

Polymer	Macro-RAFT M_n[a] (g/mol)	Macro-RAFT Đ[b]	Block Two Target M_n (g/mol)	Block Two Conversion[c] (%)	M_n, GPC[d] (g/mol)	M_n, NMR[e] (g/mol)	Đ[f]
MbH1	10 000	1.12	10 500	91	19 600	21 500	1.14
MbH2	10 000	1.12	24 000	91	26 800	36 700	1.15
MbH3	10 000	1.12	85 000	90	52 200	115 800	1.29
MbH4	10 000	1.12	118 000	98	65 900	162 800	1.38

[a,b,d,f]Measured by GPC using p(MMA) standards; [c]Calculated using the integrals of monomer peaks in NMR; [e]Calculated from the NMR of the dried sample knowing p(MMA) polymer peak represented 10000 g/mol.

In the chain extension reactions, DHIAMA was shown to be added onto the macro-RAFT initiator in a controlled manner, achieving molecular weights close to those targeted for the extension. The absence of shoulders in the GPC traces (Figure 3.5) indicates the successful re-initiation of the macro-RAFT agent across the series. In the case of MbH1 and MbH2, low $Đ$ < 1.15 indicates there was a controlled addition of the DHIAMA, resulting in a well-defined block copolymer. Targeting higher molecular weights for MhB3 and MhB4 resulted in increased $Đ$, which is again likely due to the reported observations about RAFT being less controlled in methacrylate polymerizations targeting high molecular weights.[32] As was the case in the homopolymerizations, DHIAMA exhibited high conversions in the diblock reactions, and its ease of polymerization under moderate conditions shows its potential for use as a soft block in block copolymer applications (i.e., thermoplastic elastomers).

3.4.6 Block Copolymer Phase Separation

After obtaining the series of diblock copolymers, it was desired to know if phase separation was achieved across the compositions. While the χN values were estimated to be above 10.5 by over an order of magnitude (Supporting Information, Appendix A, Section A3.2), the applicability of exceeding this value to achieve phase separation in the asymmetric diblock polymers of this study is unknown, as the minimum χN value was developed specifically for symmetric diblock polymers.[43] Thus, more concrete evidence was sought to verify the existence of microdomains. Differential scanning calorimetry was completed for the polymers, with all the traces shown in the Supporting Information (Figure A22). For polymers MbH1 and MbH2, two T_gs can be observed, supporting that the p(DHIAMA) regions have separated from the p(MMA) regions. However, due to the minimal MMA content in MhB3 and MhB4, the presence of a second T_g is not discernable. The absence of p(MMA)'s T_g alone is not substantial enough to say the block copolymers formed a miscible system, for if that were the case, there would be one observed T_g. This one transition temperature would be the weight average of the two polymers respective T_gs, but for both MhB3 and MhB4, the single transition temperature is still near the value of DHIAMA's glass transition temperature.

To substantiate the findings from DSC, small angle x-ray scattering (SAXS) experiments were completed on solvent cast films of the diblock copolymers. Shown in Figure 3.5, the SAXS patterns indicate microphase separation exists for all the polymers in the series. From the scattering profiles, the interdomain spacing, d, can be calculated using Equation 3.3,[44] as follows:

$$d = \frac{2\pi}{q^*} \tag{3.3}$$

where; q^* is the position of the first scattering peak from the spectra. The interdomain spacing was seen to be smallest for MbH1, with a value of 17.1 nm, and increased correspondingly with the polymers increasing molecular weights and DHIAMA content (See Table 3.4). MbH4 resulted in the largest interdomain space of 28.3 nm and gave scattering peaks at $\sqrt{3}q^*$ and $\sqrt{12}q^*$, indicative of spherical inclusions. Although this sample had the greatest molecular weight, and thus the influence from degree of polymerization was the most substantial to support its microphase separation, the results are still encouraging as it is composed of just 6 wt% MMA. Its SAXS profile that indicates two regimes is encouraging in that the system will readily phase separate even when

one regime is significantly smaller. This is a particularly useful characteristic for applications such as thermoplastic elastomers requiring small hard regions anchored in an elastic matrix.

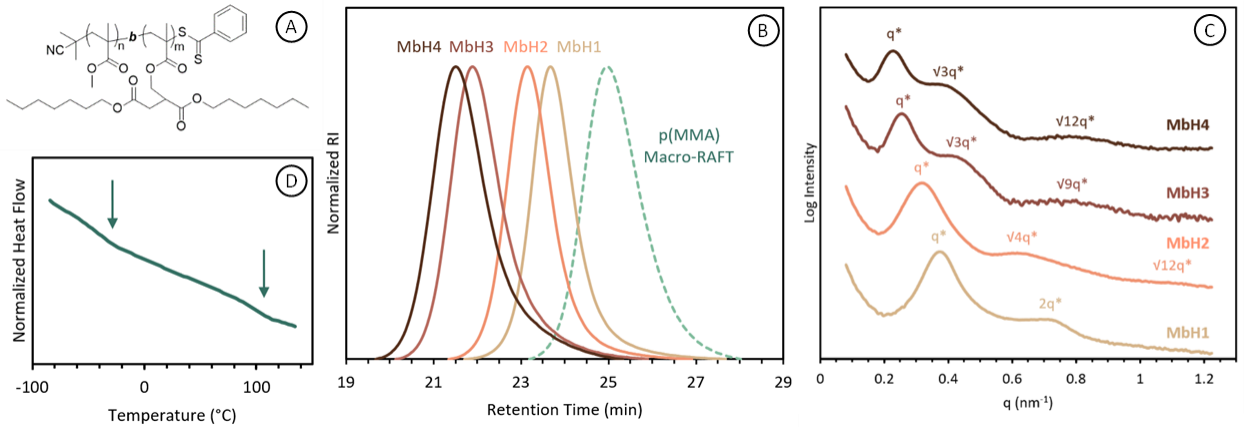

Figure 3.5. Diblock copolymer characterization: (A) Schematic of p(MMA-*b*-DHIAMA) polymer; (B) Gel-permeation chromatography traces of macro-RAFT agent and final p(MMA-*b*-DHIAMA) diblock polymers; (C) SAXS curves of the p(MMA-*b*-DHIAMA) series indicating the presence of microdomains; (D) Differential scanning calorimetry trace of MbH1 presenting two T_gs.

The SAXS tells of microphase separation, but the microstructure of the regions is less apparent, and they lack long-range order. The absence of every characteristic peak, and distinct long-range order may be attributed to fast evaporation of the solvent during casting, as well as a lack of chain uniformity as observed with the $Đ$ exceeding 1.3 for the largest block copolymer.[45] At best, tentative microstructures can be assigned using the broad SAXS peaks compounded with knowledge of the copolymer composition, shown in Table 3.4. MbH1 displays a peak at *2q* and may correspond to a lamellar morphology given its weight composition near parity. MbH2, being 73% DHIAMA by weight, could be expected to follow a gyroid or cylindrical morphology, with p(MMA) cylinders surrounded by a DHIAMA matrix. It exhibits SAXS peaks at $\sqrt{4}q^*$ and $\sqrt{12}q^*$, aligning with the characteristic peaks of hexagonally packed cylinders. Finally, MbH3 shows peaks at $\sqrt{3}q^*$ and $\sqrt{10}q^*$ supporting the presence of unordered spherical patterns.[44]

Table 3.4. Composition and morphology of p(MMA-*b*-DHIAMA) diblock series.

Polymer	F_{DHIAMA}[a]	Wt% DHIAMA[b]	Interdomain spacing[c] (nm)	Microstructure
MbH1	0.22	0.54	17.1	Lamella
MbH2	0.39	0.73	19.9	Hexagonal
MbH3	0.72	0.91	25.1	Not well ordered spherical
MbH4	0.79	0.94	28.3	Not well ordered spherical

[a,b]Calculated from the dried sample's NMR using the integrals of the polymer peaks; [c]Calculated from the principial peak q* of SAXS results.

3.4.7 Block Copolymer Rheological Properties

To allow for reasonable comparison in rheological properties between block copolymers of varying p(DHIAMA) content, the molecular weight of the polymers must be comparable. An additional block copolymer (MbH5), with decreased p(DHIAMA) content but the same molecular weight as MhB4, was therefore synthesized to ensure fair comparability between rheological properties and that of pure p(DHIAMA). Figure 3.6 shows the SAXS results of MbH5 as well as of H9. The presence of scattering peaks in MbH5 at $\sqrt{6}q^*$ and $\sqrt{14}q^*$ gives indication a gyroid-like structure may exist, whereas the absence of any scattering peaks in H9 confirms the homopolymer exists as one homogenous phase. Table 3.5 shows the composition of the block copolymers used in rheological analysis.

Table 3.5. Molecular weight and composition of p(MMA-*b*-DHIAMA) diblock polymers for rheological assessment.

Polymer	Macro-RAFT M_n[a] (g/mol)	Macro-RAFT Đ[b]	M_n, GPC RI[c] (g/mol)	M_n, NMR[d] (g/mol)	Đ[e]	F_{DHIAMA}[f]	Wt% DHIAMA[g]
H9	--	--	81 700	198 200[h]	1.39	1.00	1.00
MbH4	10 000	1.12	65 900	162 800	1.38	0.79	0.94
MbH5	32 200	1.15	61 000	160 000	1.46	0.492	0.80

[a,b,c,e]Determined by RI detector of GPC; [d,f,g]Calculated from the dried sample's NMR using the integrals of the polymer peaks and known p(MMA) block weight; [h]Determined by the LS detector of GPC.

Frequency sweeps conducted on the three samples reveal the significant impact microphase separated hard inclusions have on the rheological behavior. p(DHIAMA) was shown previously to have tunable rheological properties, to an extent, just by altering molecular weight. However, due to the hypothesized high entanglement weight, the molecular weights of the synthesized series all gave flowing and soft viscoelastic materials. This soft characteristic, when paired with a hard segment in diblock copolymer architectures, allows for elastic behavior to be realized. p(DHIAMA) shows no intersection of the viscous and elastic moduli in the tested frequency range of 0.1 to 100 s^{-1}, with the loss modulus dominating, indicating it is structurally relaxed. With a p(MMA) block composing 6 wt% of the final polymer, this behavior changes drastically as can be seen in Figure 3.6. Hard inclusions acting as anchors within the soft p(DHIAMA) matrix resist the shearing, giving the block copolymer MhB4 an elastic modulus 300 times greater than the pure p(DHIAMA) at 25°C and 0.1 s^{-1}. This increase is even more substantial moving to MhB5, where the p(MMA) block composes 14 wt% of the matrix, and the elastic modulus is over 6500 greater than H9 at the previously mentioned conditions.

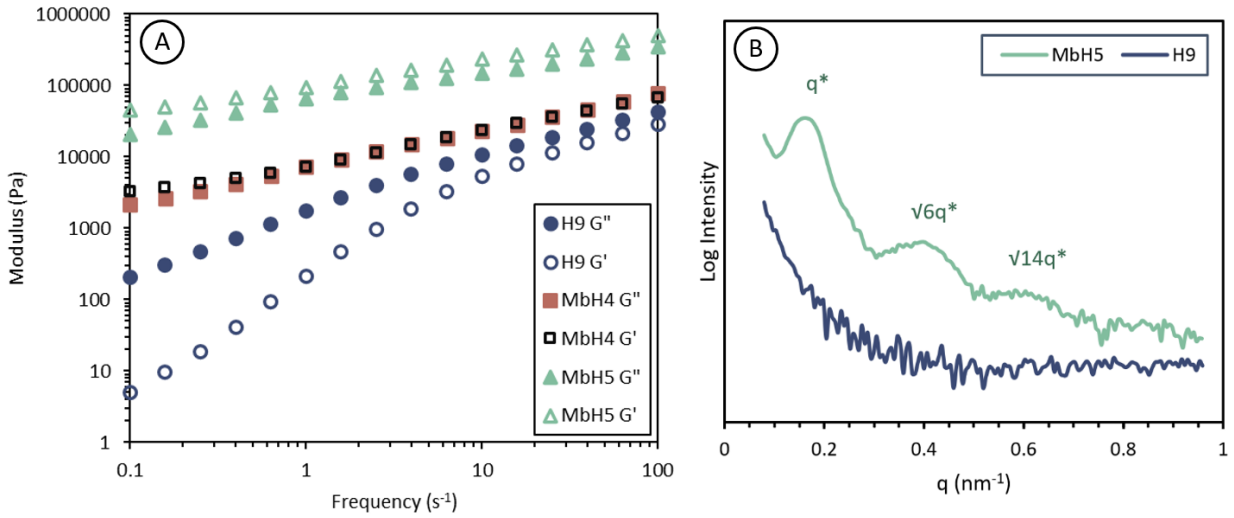

Figure 3.6. (A) Frequency sweep results using a fixed 0.1% strain for diblock p(MMA-*b*-DHIAMA) contrasted with p(DHIAMA) homopolymer; (B) SAXS results of MbH5 and H9 showing refraction in the diblock system and lack of microdomains in the homopolymer.

With the ability to produce block-copolymers of pre-designed architectures, a range of microphase structures can be accessed. In turn, this allows for the flowing behavior of p(DHIAMA) to be controlled by imparting hard regions with a high T_g, giving way to elastic behavior. Observing the ratio of elastic versus loss moduli of the three polymers across the tested frequency range indicates how different the materials behave, as MbH5 is fully dominated by elastic behavior across the range, whereas H9 is dominated strongly by loss. Further, the dominance of loss at low frequency ranges in H9 is several orders of magnitude greater than the dominance at high frequencies. This ratio varies less across the frequency range for MbH5. These differences can be exploited, with a range of properties achievable by varying the content of p(MMA) in the diblock copolymer. This is exhibited by MbH4, where the elastic and loss modulus displayed a crossover point at which they were equal. Thus, in the current study, varying the molecular weight of the p(DHIAMA) homopolymer allowed for the magnitude of the elastic and loss modulus to be altered, with further tuning of their ratio achieved by including a phase-separated hard block.

3.5 Conclusion

Hydroboration-oxidation of itaconic acid derivatives, followed by esterification allowed for the synthesis of a new set of itaconate-based methacrylates to be realized, which avoids the pitfalls typically experienced when polymerizing itaconic acid. Two novel monomers, heptyl arm containing DHIAMA and benzyl arm containing DBIAMA, were synthesized. Various methods of RDRP were used in DHIAMA polymerizations with high monomer conversion, to produce polymers of target molecular weight and narrow dispersity. A range of p(DHIAMA) and p(DBIAMA) polymers were obtained by RAFT in a controlled manner; however, larger molecular weights saw a broadening of dispersity. Changes to the side arms in the first step of the synthesis offers the ability to alter the final polymer's behavior, with the glass transition temperatures of p(DHIAMA) and p(DBIAMA) being -40 and 14°C, respectively.

Adjusting the molecular weight of p(DHIAMA) polymers gave the ability to tune the rheological properties, which were characterized as being loss-dominant due to the low glass transition temperature and hypothesized high entanglement molecular weight of the polymer. Designing phase-separated diblock copolymers where p(MMA) acted as a macro-RAFT agent in chain extensions saw the easy polymerization of DHIAMA able to be utilized, to reliably obtain pre-designed polymers. Phase separation of these diblocks was confirmed by SAXS to give various microphase morphologies, which in turn allowed for elastic-dominant rheological properties to be realized.

3.6 References

(1) Paul Anastas, N. E., Green chemistry: Principles and practice. *Royal Society of Chemistry* **2010,** *39*, 301-312.

(2) Constable, D. J. C., What do patents tell us about the implementation of green and sustainable chemistry? *ACS Sustainable Chemistry & Engineering* **2020,** *8* (39), 14657-14667.

(3) Valderrama, C.; Huamán, H.; Valencia-Arias, A.; Vasquez-Coronado, M.; Cardona-Acevedo, S.; Delgado-Caramutti, J., Trends in green chemistry research between 2012 and 2022: Current trends and research agenda. *Sustainability* **2023,** *15*, 13946.

(4) Robert, T.; Friebel, S., Itaconic acid – A versatile building block for renewable polyesters with enhanced functionality. *Green Chemistry* **2016,** *18* (10), 2922-2934.

(5) De Carvalho, J.; Magalhaes, A.; Soccol, C., Biobased itaconic acid market and research trends - Is it really a promising chemical? *Chimica oggi* **2018,** *36*, 56.

(6) Kirimura, K.; Honda, Y.; Hattori, T., Gluconic and Itaconic Acids. In *Comprehensive Biotechnology (Second Edition)*, Moo-Young, M., Ed. Academic Press: Burlington, 2011; pp 143-147.
(7) Werpy, T.; Peterson, G. *Top Value Added Chemicals from Biomass*; U.S. Department of Energy: 2004.
(8) Jain, S.; Kumar, S., A comprehensive review of bioethanol production from diverse feedstocks: Current advancements and economic perspectives. *Energy* **2024,** *296*, 131130.
(9) S. Nagai, T. U., K. Yoshida, Studies on polymerizations and polymers of itaconic acid derivatives. *Kobunshi Kagaku* **1958,** *15*, 550--554.
(10) Marvel, C. S.; Shepherd, T. H., Polymerization reactions of itaconic acid and some of its derivatives. *The Journal of Organic Chemistry* **1959,** *24* (5), 599-605.
(11) Lea Sollka, K. L., Progress in the free and controlled radical homo- and co-polymerization of itaconic acid derivatives: Toward functional polymers with controlled molar mass distribution and architecture. *Macromolecular Rapid Communications* **2021,** *42* (4).
(12) Dai, J.; Ma, S.; Liu, X.; Han, L.; Wu, Y.; Dai, X.; Zhu, J., Synthesis of bio-based unsaturated polyester resins and their application in waterborne UV-curable coatings. *Progress in Organic Coatings* **2015,** *78*, 49-54.
(13) Guo, B.; Chen, Y.; Lei, Y.; Zhang, L.; Zhou, W. Y.; Rabie, A. B. M.; Zhao, J., Biobased poly(propylene sebacate) as shape memory polymer with tunable switching temperature for potential biomedical applications. *Biomacromolecules* **2011,** *12* (4), 1312-1321.
(14) J. Retuert, M. Y.-P., F. Martínez, M. Jeria Soluble itaconic acid–ethylene glycol polyesters. *Bulletin of the Chemical Society of Japan* **1993,** *66* (6), 1707-1708.
(15) Yuan, L.; Wang, Z.; Trenor, N. M.; Tang, C., Robust amidation transformation of plant oils into fatty derivatives for sustainable monomers and polymers. *Macromolecules* **2015,** *48* (5), 1320-1328.
(16) Sainz, M. F.; Souto, J. A.; Regentova, D.; Johansson, M. K. G.; Timhagen, S. T.; Irvine, D. J.; Buijsen, P.; Koning, C. E.; Stockman, R. A.; Howdle, S. M., A facile and green route to terpene derived acrylate and methacrylate monomers and simple free radical polymerisation to yield new renewable polymers and coatings. *Polymer Chemistry* **2016,** *7* (16), 2882-2887.
(17) Atkinson, R. L.; Monaghan, O. R.; Elsmore, M. T.; Topham, P. D.; Toolan, D. T. W.; Derry, M. J.; Taresco, V.; Stockman, R. A.; De Focatiis, D. S. A.; Irvine, D. J.; Howdle, S. M., RAFT polymerisation of renewable terpene (meth)acrylates and the convergent synthesis of methacrylate–acrylate–methacrylate triblock copolymers. *Polymer Chemistry* **2021,** *12* (21), 3177-3189.
(18) Fache, M.; Boutevin, B.; Caillol, S., Vanillin, a key-intermediate of biobased polymers. *European Polymer Journal* **2015,** *68*, 488-502.
(19) Purushothaman, M.; Krishnan, P. S. G.; Nayak, S. K., Poly(alkyl lactate acrylate)s having tunable hydrophilicity. *Journal of Applied Polymer Science* **2014,** *131* (21).
(20) Zheng, Y.; Yao, K.; Lee, J.; Chandler, D.; Wang, J.; Wang, C.; Chu, F.; Tang, C., Well-defined renewable polymers derived from gum rosin. *Macromolecules* **2010,** *43* (14), 5922-5924.
(21) Moad, G.; Anderson, A. G.; Ercole, F.; Johnson, C. H. J.; Krstina, J.; Moad, C. L.; Rizzardo, E.; Spurling, T. H.; Thang, S. H., Controlled-growth free-radical polymerization of methacrylate esters: Reversible chain transfer versus reversible termination. *ACS Symposium Series* **1998,** *685*, 332-360.

(22) Zaremski, M. Y.; Plutalova, A. V.; Lachinov, M. B.; Golubev, V. B., A concept for quasiliving nitroxide-mediated radical copolymerization. *Macromolecules* **2000,** *33* (12), 4365-4372.
(23) Kardan, S.; Garcia Valdez, O.; Métafiot, A.; Maric, M., Nitroxide-mediated copolymerization of itaconate esters with styrene. *Processes* **2019,** *7* (5).
(24) Hirano, T.; Takeyoshi, R.; Seno, M.; Sato, T., Chain-transfer reaction in the radical polymerization of Di-n-butyl itaconate at high temperatures. *Journal of Polymer Science Part A: Polymer Chemistry* **2002,** *40*, 2415-2426.
(25) Sankhe, A. Y.; Husson, S. M.; Kilbey, S. M., Effect of catalyst deactivation on polymerization of electrolytes by surface-confined atom transfer radical polymerization in aqueous solutions. *Macromolecules* **2006,** *39* (4), 1376-1383.
(26) Okada, S.; Matyjaszewski, K., Synthesis of bio-based poly(N-phenylitaconimide) by atom transfer radical polymerization. *Journal of Polymer Science Part A: Polymer Chemistry* **2015,** *53* (6), 822-827.
(27) Fernández-García, M.; Fernández-Sanz, M.; de la Fuente, J. L.; Madruga, E. L., Atom-transfer radical polymerization of dimethyl itaconate. *Macromolecular Chemistry and Physics* **2001,** *202* (7), 1213-1218.
(28) Szablan, Z.; Toy, A. A.; Terrenoire, A.; Davis, T. P.; Stenzel, M. H.; Müller, A. H. E.; Barner-Kowollik, C., Living free-radical polymerization of sterically hindered monomers: Improving the understanding of 1,1-disubstituted monomer systems. *Journal of Polymer Science Part A: Polymer Chemistry* **2006,** *44* (11), 3692-3710.
(29) Satoh, K.; Lee, D.-H.; Nagai, K.; Kamigaito, M., Precision synthesis of bio-based acrylic thermoplastic elastomer by raft polymerization of itaconic acid derivatives. *Macromolecular Rapid Communications* **2014,** *35* (2), 161-167.
(30) Szablan, Z.; Toy, A. A.; Davis, T. P.; Hao, X.; Stenzel, M. H.; Barner-Kowollik, C., Reversible addition fragmentation chain transfer polymerization of sterically hindered monomers: Toward well-defined rod/coil architectures. *Journal of Polymer Science Part A: Polymer Chemistry* **2004,** *42* (10), 2432-2443.
(31) Perrier, S., 50th anniversary perspective: RAFT polymerization—a user guide. *Macromolecules* **2017,** *50* (19), 7433-7447.
(32) Truong, N. P.; Jones, G. R.; Bradford, K. G. E.; Konkolewicz, D.; Anastasaki, A., A comparison of RAFT and ATRP methods for controlled radical polymerization. *Nature Reviews Chemistry* **2021,** *5* (12), 859-869.
(33) Beuermann, S.; Buback, M.; Davis, T. P.; García, N.; Gilbert, R. G.; Hutchinson, R. A.; Kajiwara, A.; Kamachi, M.; Lacík, I.; Russell, G. T., Critically evaluated rate coefficients for free-radical polymerization, 4. *Macromolecular Chemistry and Physics* **2003,** *204* (10), 1338-1350.
(34) Yokota, K.; Kondo, A., A rotating sector determination of the propagation rate constant for benzyl methacrylate in its radical polymerization. *Die Makromolekulare Chemie* **1973,** *171* (1), 113-122.
(35) Beuermann, S.; Harrisson, S.; Hutchinson, R. A.; Junkers, T.; Russell, G. T., Update and critical reanalysis of IUPAC benchmark propagation rate coefficient data. *Polymer Chemistry* **2022,** *13* (13), 1891-1900.
(36) Fox, T. G., Jr.; Flory, P. J., Second-order transition temperatures and related properties of polystyrene. I. influence of molecular weight. *Journal of Applied Physics* **1950,** *21* (6), 581-591.

(37) Wang, J.; Zhang, X.; Jiang, L.; Qiao, J., Advances in toughened polymer materials by structured rubber particles. *Progress in Polymer Science* **2019,** *98*, 101160.
(38) Li, L.; Han, L.; Hu, H.; Zhang, R., A review on polymers and their composites for flexible electronics. *Materials Advances* **2023,** *4* (3), 726-746.
(39) Choi, J.; Kim, W.; Kim, D.; Kim, S.; Chae, J.; Choi, S. Q.; Kim, F. S.; Kim, T.-S.; Kim, B. J., Importance of critical molecular weight of semicrystalline n-type polymers for mechanically robust, efficient electroactive thin films. *Chemistry of Materials* **2019,** *31* (9), 3163-3173.
(40) Huang, G.; Wu, N.; Wang, X.; Zhang, G.; Qiu, L., Role of molecular weight in the mechanical properties and charge transport of conjugated polymers containing siloxane side chains. *Macromolecular Rapid Communications* **2022,** *43* (17), 2200149.
(41) Chatterjee, D. P.; Mandal, B. M., Triblock thermoplastic elastomers with poly(lauryl methacrylate) as the center block and poly(methyl methacrylate) or poly(tert-butyl methacrylate) as end nlocks. Morphology and thermomechanical properties. *Macromolecules* **2006,** *39* (26), 9192-9200.
(42) Bates, F. S.; Fredrickson, G. H., Block copolymer thermodynamics: Theory and experiment. *Annual Review of Physical Chemistry* **1990,** *41* (Volume 41), 525-557.
(43) Leibler, L., Theory of microphase separation in block copolymers. *Macromolecules* **1980,** *13*.
(44) Hamley, I. W.; Castelletto, V., Small-angle scattering of block copolymers: In the melt, solution and crystal states. *Progress in Polymer Science* **2004,** *29* (9), 909-948.
(45) Kim, G.; Libera, M., Morphological development in solvent-cast polystyrene−polybutadiene−polystyrene (sbs) triblock copolymer thin films. *Macromolecules* **1998,** *31* (8), 2569-2577.

Chapter 4: Boronic Ester Vitrimers: Balancing Self-Healing and Creep Through Self-Assembling Block Copolymers

4.1 Preface

After the successful synthesis of itaconate-based methacrylate monomers and their polymerization, efforts were then made to find a suitable application. While the low T_g of p(DHIAMA) lends itself to the potential for rubber toughening or plasticizing brittle polymers, initial blending experiments revealed little compatibility between p(DHIAMA) and materials which would require plasticization. Other uses for low T_g polymers, such as rubbery elastics were then considered. However, this is when the hypothesized high critical molecular weight of entanglement of p(DHIAMA) became problematic. Using p(DHIAMA) without modification would not lead to macroscopic properties acceptable for practical use. Considerations were then taken for developing a material with useful properties, without impeding the environmental considerations.

While cross-linking the soft p(DHIAMA) material could allow for more desirable elastic properties, this would prevent it from being reprocessable, and not align with the goals of developing better alternatives to what is already available. So, to impart structure, and mimic the chain entanglements of rubbery elastic materials, associative dynamic covalent chemistry was selected to give vitrimeric and bio-based networks. Adding reversible cross-linking into the material was hypothesized to be able to produce mechanical behaviours that would not only exceed the non-cross-linked material, but by varying the extent of cross-linking could allow for a wide degree of tunability, making DHIAMA applicable to many applications.

C13-methacrylate (C13MA) is a commercially available, renewably sourced monomer, that has a T_g comparable to p(DHIAMA). Furthermore, it also has a high M_c that makes its properties at conventional molecular weights unsatisfactory. C13MA was selected as a substitute for DHIAMA in this next study on how to improve the macroscopic behaviour of low T_g, bio-based monomers with high M_c values. This substitution was made due to the lab materials and time required for the synthesis of DHIAMA, making it challenging to scale up its production to be used in projects investigating mechanical properties. Boronic acid ester exchange was selected for cross-linking, since it is catalyst-free, and has low activation energies for viscous flow, meaning it

allows for easy reprocessing. Finally, the creeping behaviour of vitrimers had to be addressed if the final material properties were to be comparable to industrial benchmarks. Cross-linking block copolymers was therefore selected, with the purpose of comparing the inclusion of AB type hard-soft copolymers in soft cross-linked networks, to networks lacking microphase separation.

By completing this second study, as outlined in Chapter 1, insight was to be gained on how bio-based monomers such as DHIAMA, which if synthesized by functionalization and therefore have poor mechanical properties due to high M_c values, can be incorporated in materials with better, and tunable, mechanical and rheological properties. As such, this chapter details the synthesis of four vitrimeric networks, cross-linked by boronic acid ester exchange chemistry. Comparisons are made between two block-copolymer containing networks which display a distinct microphase separated topology, and two networks that lack microphase separation due to being composed of statistical polymers and small molecules. Phase separation was confirmed by atomic force microscopy for prepolymers, and small angle X-ray scattering for the final networks. Mechanical properties were assessed via tensile tests, through two rounds of reprocessing, to confirm the retention of properties during recycling. Thermal behaviour was characterized, and the ability to self-heal both fractured interfaces and surface scratches was examined. Rheological behaviour and nanoindentation tests exemplified the difference in viscoelastic properties of the block containing networks as compared to the homogenous networks.

This chapter consists of a manuscript that is to be submitted for publication in the *Journal of Polymer Science*. As per journal guidelines, the materials and methods can be found in the Supporting Information for the Chapter 4, provided in Appendix B.

4.2 Abstract

Vitrimers offer notable advantages, such as enhanced recyclability and self-healing, but their susceptibility to creep under sustained stress remains a limitation to their widescale adoption. Here, we incorporated hard-soft AB block copolymers into dynamic networks to improve creep resistance and hardness while sustaining self-healing properties. Nitroxide mediated polymerization (NMP) was used to synthesize prepolymers containing boronic acid functionality of either statistical [poly(alkyl methacrylate-*co*-vinyl boronic acid)] or AB diblock [poly(methyl methacrylate-*co*-acrylonitrile)-*block*-poly(alkyl methacrylate-*co*-vinyl boronic acid)]. These prepolymers, along with a small-molecule diboronic ester cross-linker, were blended individually

with a statistical, 2,3-diol-functional prepolymer to form 4 different boronic ester networks: N1 (statistical/ statistical), N2 (statistical/ diblock), N3 (statistical/ diblock), and N4 (statistical/ small molecule cross-linker). Small-angle X-ray scattering (SAXS) confirmed spherical poly(methyl methcarylate) (PMMA) microdomains in blocky N2 and N3. Mechanical tests showed improved tensile strength and hardness in N2 and N3 compared to the homogeneous blend of N1. While small-molecule cross-linked N4 had the highest toughness, N3 exhibited the greatest hardness due to higher PMMA content. Notably, microphase separation in N2 and N3 enhanced their creep resistance and recovery. Stress relaxation tests revealed slower relaxation in the blocky networks, but stress was still fully recovered with characteristic relaxation times less than 33 seconds. All the networks retained their mechanical properties through recycling by hot pressing at 115°C and exhibited bulk self-healing at ambient conditions. These results highlight the potential of incorporating small amounts (<10 wt%) of phase-separated microdomains in vitrimer networks to enhance their rheo-mechanical properties.

4.3 Introduction

The ever-increasing production of polymers worldwide underscores their extensive use in modern life. Annual polymer production is projected to triple by 2060, up from 460 million tonnes in 2019.[1] To mitigate the impacts of global warming and plastic waste pollution, it is imperative to transition from petroleum-based feedstocks to renewable bio-based alternatives and recyclable polymers with circular life cycles.

Polymers are traditionally divided into thermosets and thermoplastics, with the former characterized by a network of permanent cross-links. The cross-linked structure in thermosets provides excellent thermomechanical properties but limits their ability to be reprocessed and recycled. These limitations represent significant environmental and economic challenges.

Recently, covalent adaptable networks (CANs) have bridged the gap between thermosets and thermoplastics, utilizing dynamic covalent bonds to cross-link polymer backbones. Vitrimers are a subset of CANs featuring associative dynamic bond exchanges. The emergence of CANs including vitrimers have unlocked the potential for materials possessing both robust mechanical properties with the ease of reprocessing. Systems using dynamic covalent bonds including Diels-Alder adducts, disulfides, imines and boronic acid esters allowing bond exchange to be triggered by various external stimuli, such as light, heat, or moisture.[2, 3] The exchanges of covalent bonds

allow for self-healing, good stress relaxation, weldability, reprocessability and recyclability.[4, 5] The tunability offered by different dynamic bond chemistries enables CANs and vitrimers to be applied to various feedstocks, presenting significant opportunities for developing sustainable polymers. For example, upcycling of post-consumer waste plastics can be achieved by the introduction of dynamic covalent bonds.[6, 7] Another promising avenue involves applying dynamic cross-linking chemistries to bio-based feedstocks, making them more industrially relevant by enhancing their thermo-mechanical properties to levels comparable with traditional fossil-based alternatives.[8]

Vitrification has been applied to numerous bio-sourced precursors, including derivatives of lignin, saccharides, furans, fatty acids, terpenes, and natural rubber, resulting in promising elastomeric vitrimers.[9] For example, Li *et al.* used epoxidized soybean oil with natural glycyrrhizic acid to develop fully biobased and recyclable vitrimers.[10] These vitrimers showed excellent thermal stability (> 300°C), good welding, repairing, and shape memory, and could be chemically degraded. Averous *et al.* also developed a fully biobased vitrimer, using bio-based furan dialdehyde with a combination of amines.[11] There, the material could be completely depolymerized to recover its constituent building blocks, due to the use of cross-linking transimination reactions.

More recently, our group developed a series of vinylogous urethane vitrimers of poly(β-myrcene).[12] We reported that poor mechanical properties of brush-like terpene elastomers could be improved and highly tuned through vitrification. Three rounds of reprocessing in this study showed retained mechanical properties, which could be varied by over an order of magnitude due to variations in cross-linking density and modulations of glass transition (T_g). In addition, bio-based vitrimeric rubbers exhibited stimuli responsive properties including reprogrammable shape memory effects.[12]

Despite the many advantages of vitrimers, including improved recyclability and self-healing, they also present a significant pitfall: high susceptibility to creep. The exchange of covalent bonds results in lower dimensional stability of vitrimers compared to traditional thermosetting materials on long time scales. Recent efforts have explored various methods to enhance creep resistance in vitrimers. For example, introducing a dual network system, which combines dynamic covalent cross-links with a very small fraction of non-reversible static ones (< 5%) has proven effective in reducing creep without hampering recyclability, but does suppress stress-relaxation.[13, 14]

Inducing microphase-separation within the material has also been shown to reduce creep. Specifically, Lessard *et al.* demonstrated that diblock copolymers of AB structure, even when both blocks were made of soft, low T_g polymers, improved creep resistance and creep recovery when compared to their statistical analogs.[15] The tuning of soft-soft AB diblock vitrimers was also demonstrated by Ishibashi *et al.,* where viscoelastic behavior was shown to be influenced by both the morphology of the phase separation and cross-linking density.[16] Implementing the use of a hard block in conjunction with a cross-linkable soft block, Weerathaworn *et al.* explored how chain architecture can unleash a breadth of mechanical properties.[17] Specifically, AB, ABA, and BAB, led to hard, tough, and elastomeric materials respectively, with A representing the hard regime. In all cases, cross-linking of block-copolymers causes anchoring of the materials shape to be observed, due to the existence of phase-separated regimes stabilizing the structure thus mitigating the vulnerability to creep.[17] Recently, studies on the rheo-mechanical properties of bio-based imine vitrimers of AB hard-soft diblock copolymers with cross-links limited to the hard section found that microphase separation drastically enhances surface hardness and creep resistance while reducing the tensile properties.[14] The reduction in tensile properties was attributed to the low entanglements in the soft block.

Until now, however, few studies have employed block copolymer vitrimers using boronic acid ester exchange as the dynamic cross-linking method. Furthermore, previous research on boronic acid-based vitrimers has primarily focused on small molecules as cross-linking agents, while the use of polymer-polymer cross-links directly within the polymer backbone remains unexplored. Wang *et al.* demonstrated that the macro-cross-linker approach leads to superior mechanical properties by preventing formation of network defects and cross-linking loops.[18]

In designing this study, we aimed to demonstrate the potential for vitrimer chemistry to improve and tune the characteristics of polymers derived from renewable feedstocks, which on their own lack the properties to compete with commodity polymers. C13-methacrylate (C13MA), a vegetable oil derived long chain alkyl methacrylate with a bio-renewable carbon content of 76% was used in the polymers to serve as a soft block comprising the bulk of the material.[19] Due to its long pendant chain (causing a low T_g) and high entanglement molecular weight (M_e), it lacks the robustness and elastic properties that are required for it to be useful in most applications.

For the dynamic exchange mechanism, boronic acid ester exchange was selected due to being well characterized and non-toxic. Boronic acid ester exchange has been used previously in biomedical and biotechnological applications such as hydrogels[20] and glucose sensors[21], and displays rapid exchange kinetics that can be exploited for materials capable of self-healing under ambient conditions.[22, 23] It also does not require catalysts for the establishment of bonding, and vitrimers based from boronic-acid ester exchange can be blended mechanically, eliminating the need for solvents.[24, 25] The reprocessibility of the materials in the study was examined, by comparing mechanical and thermal attributes of the initial material with reprocessed material.

Here, vitrimers cross-linked by three methods are to be compared. The first is a blend of statistical polymers where cross-linking is within the polymer backbones. The second is a blend of statistical polymers cross-linked by a small molecule. The final system is a blend containing diblock copolymers and statistical polymers. Figure 4.1 shows examples of the blending mechanism and resulting homogeneous or phase-separated networks.

We also created two versions of the block-statistical polymer blend with different block copolymer content to explore tunability. Phase separation in the block-copolymer containing systems was confirmed, prior to assessing the rheo-mechanical, thermal, and self-healing properties. We found that using block-copolymers in vitrimers cross-linked by polymer-polymer interactions was effective in improving both creep resistance, and creep recovery, without impeding the ability to self-heal under ambient conditions, or relax stress.

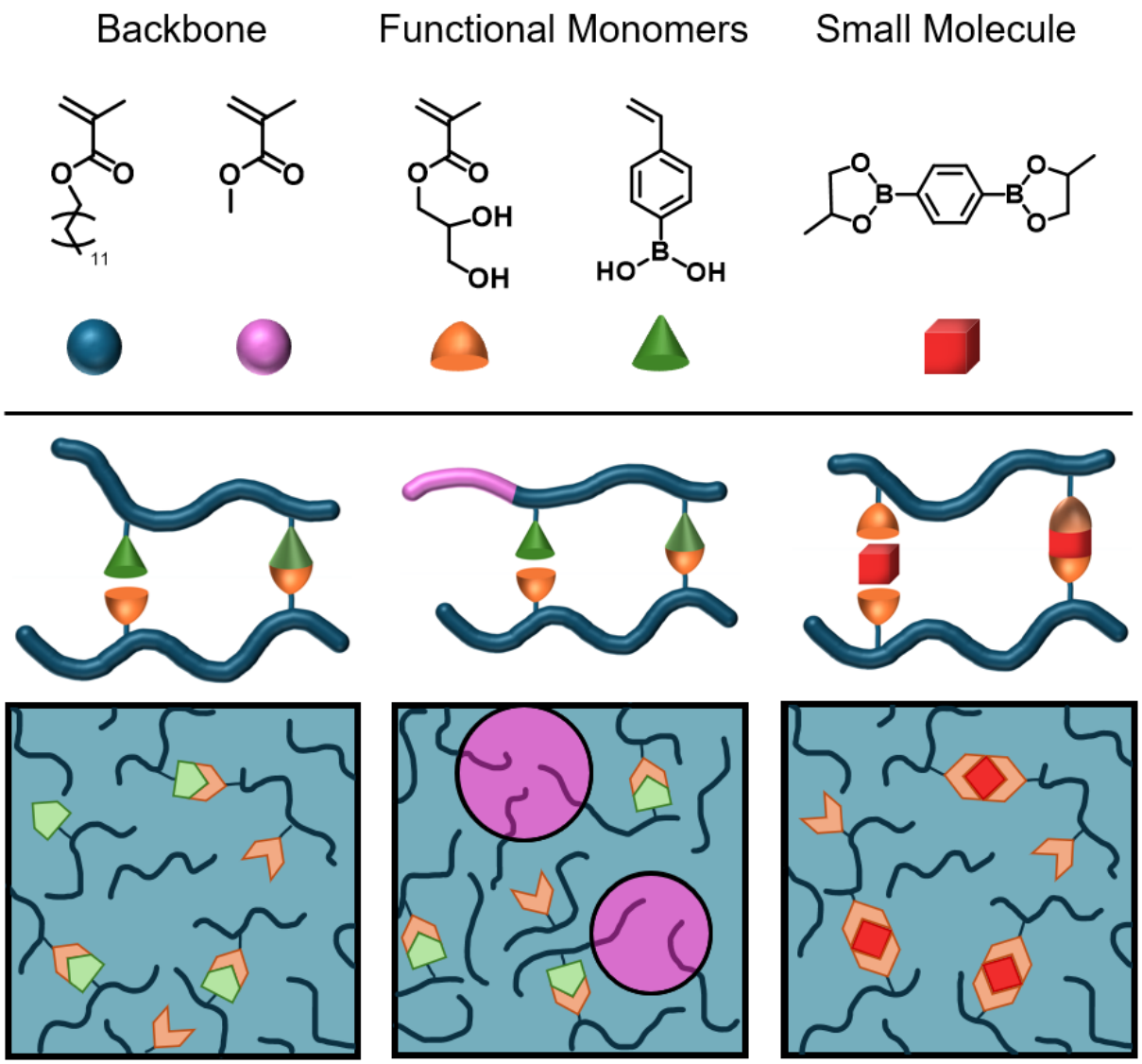

Figure 4.1. Components, blending methods and resulting networks.

4.4 Results and Discussion

4.4.1 Synthesis and Characteristics of Prepolymers

Nitroxide mediated polymerization (NMP), a form of reversible deactivation radical polymerization (RDRP) was used for the prepolymer synthesis, with SG1-based BlocBuilder alkoxyamine serving as both initiator and nitroxide source. NMP ensured targeted molecular weights (M_n) could be realized with a relatively low dispersity ($Đ$), and that block-copolymers could be obtained. NMP also avoids the use of sulfur containing chain transfer agents and toxic metallic ligands, as is the case for reversible addition fragmentation chain transfer (RAFT)

polymerization and atom transfer radical polymerization (ATRP), respectively. Avoiding these components thus simplifies the post-polymerization processing, as both the sulfur chain transfer agents and metallic ligands must be removed from polymers synthesized via these methods before further manipulation into the desired function.[26]

Figure 4.2 illustrates the molecular structure of the 3 prepolymers synthesized and Table 4.1 summarizes their molecular characteristics (Note: In the nomenclature used, “P” refers to prepolymer, “S” or “B” the molecular architectures of either statistical or block, and “GM” or “VP” the functional monomer contained in the polymer being either GMMA or VPBA, respectively). P1-S-GM is a statistical terpolymer of C13MA, styrene and diol functional glycerol monomethacrylate (GMMA). A low concentration, initially 10 mol% of styrene was used as a controlling comonomer for SG1-based NMP.[27] P2-S-VP is a statistical copolymer of C13MA with functional 4-vinylphenylboronic acid (VPBA). Previously Savelyeva *et al*. showed VPBA can effectively control the polymerization of methacrylates using BlocBuilder.[28] Finally, P3-B-VP is a diblock copolymer of poly(methyl methacrylate-*co*-acrylonitrile)-*block*-poly(C13MA-*co*-VPBA). Acrylonitrile was used as the controlling comonomer of the first block to increase the polarity and ensure microphase separation. This architecture will induce hard-soft microphase separated regions within the network after cross-linking, allowing their influence on macroscopic properties to be studied.

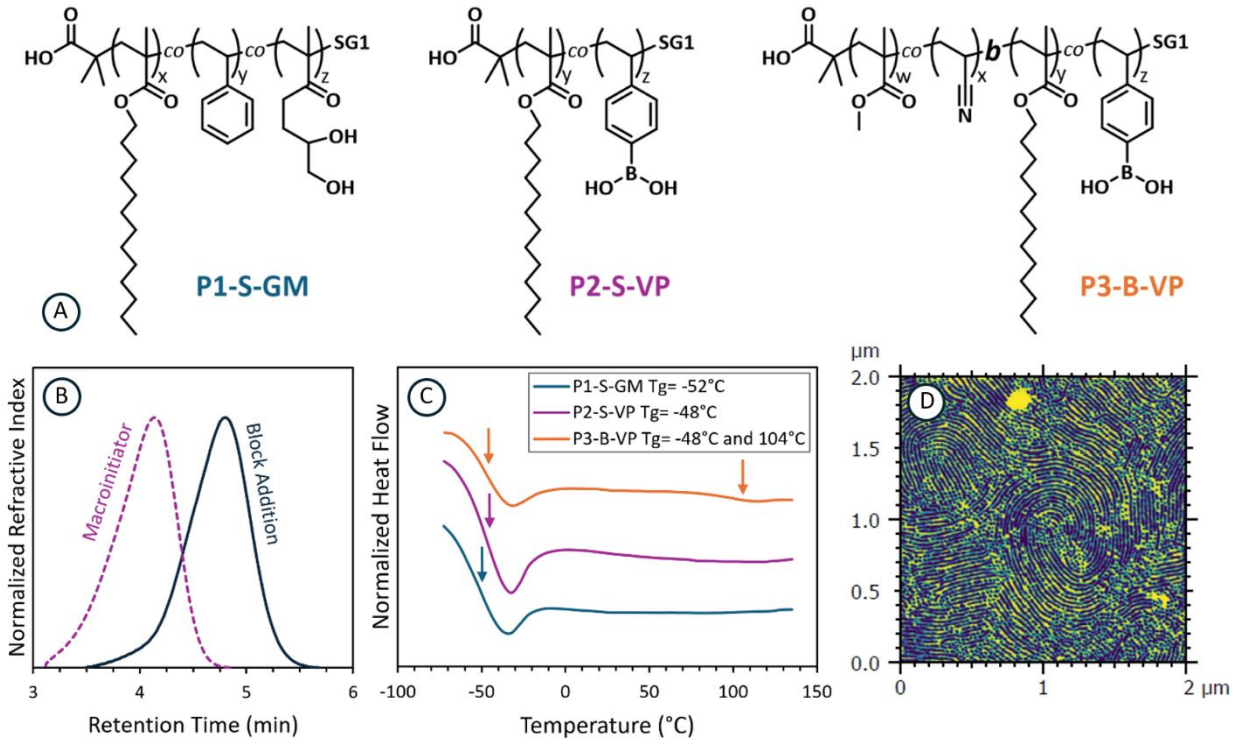

Figure 4.2. Prepolymer characteristics: (A) Schematic of the three prepolymers synthesized by NMP; (B) GPC traces of the first block and block addition of P3-B-VP showing a distinct molecular weight increase from the second block addition; (C) DSC traces of the three prepolymers with their glass transition temperatures indicated by arrows: two T_gs are observed for P3-B-VP due to microphase separation; (D) AFM imaging in the phase channel of P3-B-VP showing microphase separation.

Table 4.1. Molecular weight, dispersity, glass transition temperature and composition of the prepolymers.

Prepolymer	M_n[a] (g/mol)	$Đ$[b]	T_g[c] (°C)	F_{C13MA}[d]	F_{MMA}[d]	F_{GMMA}[d]	F_{VPBA}[d]	$F_{Styrene}$[d]
P1-S-GM	20 800	1.40	-52	0.75	0	0.14	0	0.11
P2-S-VP	19 100	1.50	-48	0.89	0	0	0.11	0
P3-B-VP	37 700	1.53	-48 & 104	0.54	0.40	0	0.06	0

[a,b] Determined by GPC compared to PMMA standards; [c] Determined by DSC; [d] Calculated from ^{1}H NMR of the purified prepolymers.

The synthesis of the GMMA containing prepolymer P1-S-GM as well as the VPBA containing prepolymers P2-S-VP and P3-B-VP followed the procedures detailed in the Supporting Information (Appendix B, Section B2). C13MA was the main component comprising 80 to 90 mol% of the statistical prepolymers. C13MA was selected to increase the bio-content of the final vitrimers and demonstrate how the mechanical properties of its polymers can be tuned by vitrification.

Sampling during the polymer synthesis was done to monitor the composition and reaction kinetics by ^{1}H NMR and GPC analysis. Pseudo-first order kinetics of monomer conversion with time showed a linear dependance, and a steady increase of M_n with conversion (see Supporting Information, Appendix B, Figure B2, B6 and B10) indicate the living characteristic behavior of the controlled radical polymerization.[26] Final polymer compositions were determined by ^{1}H NMR (Appendix B, Figure B3, B7 and B12), and indicate the incorporation of functional groups was near the designed concentration. The GPC traces of P3-B-VP (Figure 4.2) show a clear monomodal shift towards higher M_n values, from 8.1 kg/mol for the first PMMA-rich block to 37.7 kg/mol for the diblock, with $Đ$ of 1.53 indicating a successful chain extension.

Following the synthesis and purification of the prepolymers, P3-B-VP displayed very distinct macroscopic properties compared to the statistical prepolymers. Notably, all prepolymers contained over 75 wt% C13MA; however, P3-B-VP was mechanically firmer at ambient conditions, forming rigid flakes. In contrast, P2-S-VP was a firm gel, exhibiting greater stiffness than P1-S-GM, which exhibited more elastic behavior. Given that P2-S-VP has the highest C13MA content, we hypothesize that the interactions between the VPBA groups in its backbone contribute significantly to the rigidity of the material. Images of the prepolymers, demonstrating their varying properties, are provided in the Supporting Information (Appendix B, Figure B4, B8 and B13).

The thermal stability and transitions of the prepolymers were investigated by thermal gravimetric analysis (TGA) and differential scanning calorimetry (DSC), respectively. P1-S-GM had the lowest onset of 10 wt% degradation among the prepolymers with $T_{onset10wt\%}$ of 202°C while the VPBA-based prepolymers exhibited $T_{onset10wt\%}$ of 243°C and 228°C for P2-S-VP and P3-B-VP, respectively. The slightly higher thermal stability of the VPBA-based prepolymers can be attributed to the strong VPBA-VPBA interactions. All prepolymers displayed relatively good thermal stability under conventional processing temperatures. A low T_g was observed for the three

prepolymers (ranging from -52 to -46°C), due to their high C13MA content, with P3-B-VP showing a second T_g at 105°C corresponding to the PMMA block in its structure. The presence of two T_gs gives strong indication that P3-B-VP exists with two separate microphase domains, and the DSC trace is shown in Figure 4.2.

Microphase separation in the P3-B-VP diblock prepolymer was further examined using atomic force microscopy (AFM), as illustrated in Figure 4.2. The AFM image of a solvent-cast film of the prepolymer, obtained in tapping mode and displayed in the phase channel, reveals clear evidence of self-assembly, showcasing distinct patterns consistent with either a cylindrical or lamellar morphology. Given that the prepolymer comprises 20% PMMA by weight, the phase separation observed in the AFM images suggests that the micro-domains are likely cylindrical in shape.

4.4.2 Synthesis of small molecule cross-linker

The small molecule cross-linker synthesis details are provided in the Supporting Information (Section B2.5). The capping of benzene 1,4-diboronic acid (BDB), for use in the small-molecule cross-linked network was completed to allow BDB to be soluble during solvent blending. Successful capping was confirmed by ^{1}H NMR.

4.4.3 Network Formation and Characteristics

To form the vitrimers, the diol-containing prepolymer, P1-S-GM, was blended with boronic acid-containing prepolymers P2-S-VP, P3-B-VP, and BDB, resulting in 4 different vitrimeric networks of N1 to N4 with distinct molecular architectures. Table 4.2 details the exact compositions of each network.

Table 4.2. Network characteristics: microstructure, prepolymers, glass transition temperature and composition of the four networks.

Network	Prepolymer 1	Prepolymer 2 / or XLinker	VPBA:GMMA ratio	Feature	T_g (°C) [a]	*wt%* C13MA [b]	*wt%* MMA [b]	*wt%* GMMA [b]	*wt%* VPBA [b]	*wt%* Styrene [b]
N1	P1-S-GM	P2-S-VP	0.50	Statistical	-50	88.5	—	6.2	2.4	2.9
N2	P1-S-GM	P3-B-VP	0.25	Block	-51	82.0	6.4	7.0	1.4	3.3
N3	P1-S-GM	P3-B-VP	0.50	Block	-50	79.8	10.3	5.3	2.1	2.5
N4	P2-S-GM	BDB	0.90	Small-Molecule	-51	80.6	—	9.0	6.2[c]	4.2

[a]Apparent glass transition determined by DSC; [b]Calculated from the composition of prepolymers; [c] wt% of BDB cross-linker.

Network N1 is composed of two statistical prepolymers, forming a homogeneous phase with cross-linking between polymer backbones. Networks N2 and N3 combine the prepolymer P1-S-GM with the block copolymer P3-B-VP, leading to small phase-separated hard domains of PMMA within a cross-linked soft matrix of mostly C13MA. The key difference between N2 and N3 is that N3 contains a higher proportion of P3-B-VP, which increases the cross-linking density and PMMA content. N4, on the other hand, uses P1-S-GM and a small-molecule cross-linker (BDB) to create its homogeneous structure. All networks exhibit a stoichiometric imbalance between GMMA and VPBA, allowing for associative exchange, with GMMA in excess to facilitate this process.[29, 30] The weight fractions of GMMA across the networks remain comparable, such that different cross-link stoichiometries can correspond to different cross-linking density, ensuring consistent evaluation.

The detailed procedure of network formation is provided in the Supporting Information (Appendix B, Section B3.1). The networks were formed by dissolving the prepolymers in approximately 100 wt/v% tetrahydrofuran (THF) and mixing them at appropriate ratios. The constituents rapidly gelled upon blending, as illustrated by the example image of network N4 in Figure 4.3.[23, 31] Subsequently, the networks were vacuum-dried and then subjected to hot pressing to shape the vitrimers into dogbone specimens for tensile testing and disks for rheometry (detailed methods are in the Supporting Information, Appendix B, Section B1.2.8). We hypothesized that hot pressing not only aids in the removal of residual solvent but also promotes further reactions between the two components.

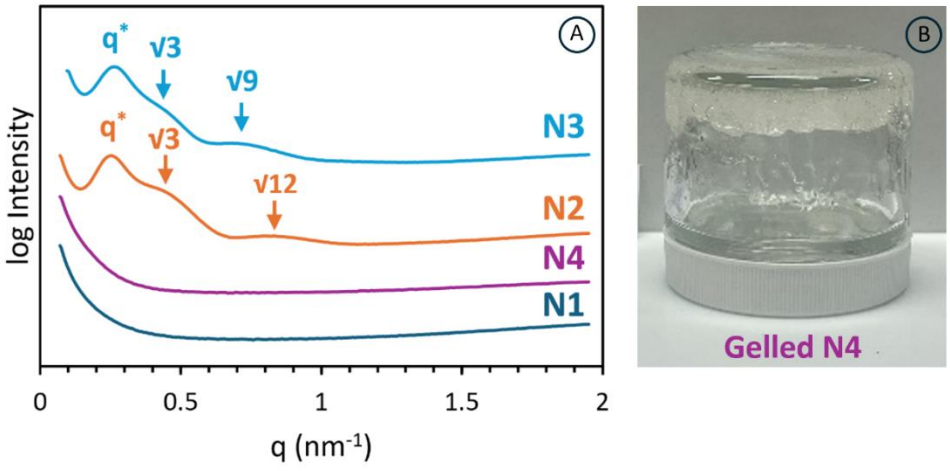

Figure 4.3. (A) SAXS curves of the four networks; distinct scattering peaks are seen in block-containing networks; (B) Rapid gelation was observed in the cross-linking procedure of N4.

To verify network formation beyond the observed rapid gelation, Attenuated Total Reflectance Fourier Transform Infrared Spectroscopy (ATR-FTIR) spectra were compared, shown in the Supporting Information (Figure B20). Networks showed a reduction in -OH stretching at 3200 cm^{-1} (VPBA)[32] and 3500 cm^{-1} (GMMA),[33] when compared to the spectra of the prepolymers, confirming bond formation. Signals were not fully eliminated due to the intentional stoichiometric imbalance that leaves some hydroxyl groups of GMMA unbound.

As a result of the associative nature of cross-linking bonds in vitrimers, the cross-linking density within them remains constant despite the dynamic character of the bonds.[5] Consequently, ideal vitrimers will not dissolve when they are introduced to non-reactive solvents, but rather swell, enabling the gel content and swelling ratio to be determined.[4] To estimate gel content and swelling ratios, samples were immersed in toluene for 48 hours, confirming that a cross-linked system had been established in networks N1 through N3. N2, having the lowest cross-linking density (VPBA:GMMA = 0.25), exhibited the highest swelling ratio, with N1 and N3 producing more comparable swelling ratios due to their identical cross-linking density (VPBA:GMMA = 0.5).

The gel content, however, was less influenced by cross-linking stoichiometry and more by PMMA content. Increasing PMMA content from N1, N2 to N3 caused gel contents of 67.4 ± 12.4%, 84.5 ± 2.7%, and 89.9 ± 2.2% to be observed for the networks, respectively. This may be attributed to the microphase separation forcing the soft, functional regions of the polymer chains to aggregate together in a smaller space, encouraging not only the occurrence of cross-linking, but also forming regions of high cross-linked density within the network, anchoring the polymers together.[34, 35]

Contradicting the observed gelation during synthesis, a reduction in FTIR -OH stretching signal, and significantly improved mechanical robustness after cross-linking of P1-S-GM with the small molecule BDB, N4 dissolved after 48 hours in toluene. This may be attributed to 1,2-propanediol, resulting from the cross-linking reaction of BDB with VPBA during the synthesis of the vitrimer, remaining in the network and cleaving the boronic acid cross-linking.

4.4.4 Network microphase characterization

The microscopic architecture of the networks was investigated using small-angle X-ray scattering (SAXS). The resulting SAXS patterns (Figure 4.3) reveal that the inclusion of block copolymers in N2 and N3 introduced a distinct microstructure, while the absence of scattering

peaks in N1 and N4 suggests that the statistical polymers used in these systems formed homogeneous networks. From the principle scattering peaks, q^*, the domain spacing, d, was calculated using the formula $d = \frac{2\pi}{q^*}$.[36] For N2 and N3, domain spacing was 25.0 nm and 26.7 nm, respectively. These results align with the increased amount of PMMA in N3 compared to N2 causing a larger domain spacing. Subsequent scattering peaks for N2 appeared at $\sqrt{3}q^*$ and $\sqrt{12}q^*$, while for N3, they occurred at $\sqrt{3}q^*$ and $\sqrt{9}q^*$. Given the microphase regions account for 6 wt% of N2 and 10 wt% of N3, the scattering patterns correspond to spherical microphase structures lacking long-range order.[37] Factors such as polymer dispersity, cross-linking variability, and conducting SAXS on bulk samples may have contributed to the absence of a more well-defined microphase pattern.[38] Nonetheless, the presence of multiple peaks supports the existence of non-homogeneous microphase architectures in block copolymer based N2 and N3.

4.4.5 Network Mechanical Properties

After confirming network formation and the microphase-separated structures in N2 and N3, uniaxial tensile testing was performed at room temperature. The tensile properties were influenced by both cross-linking density and the presence of PMMA regions, and the results are shown in Figure 4.4.

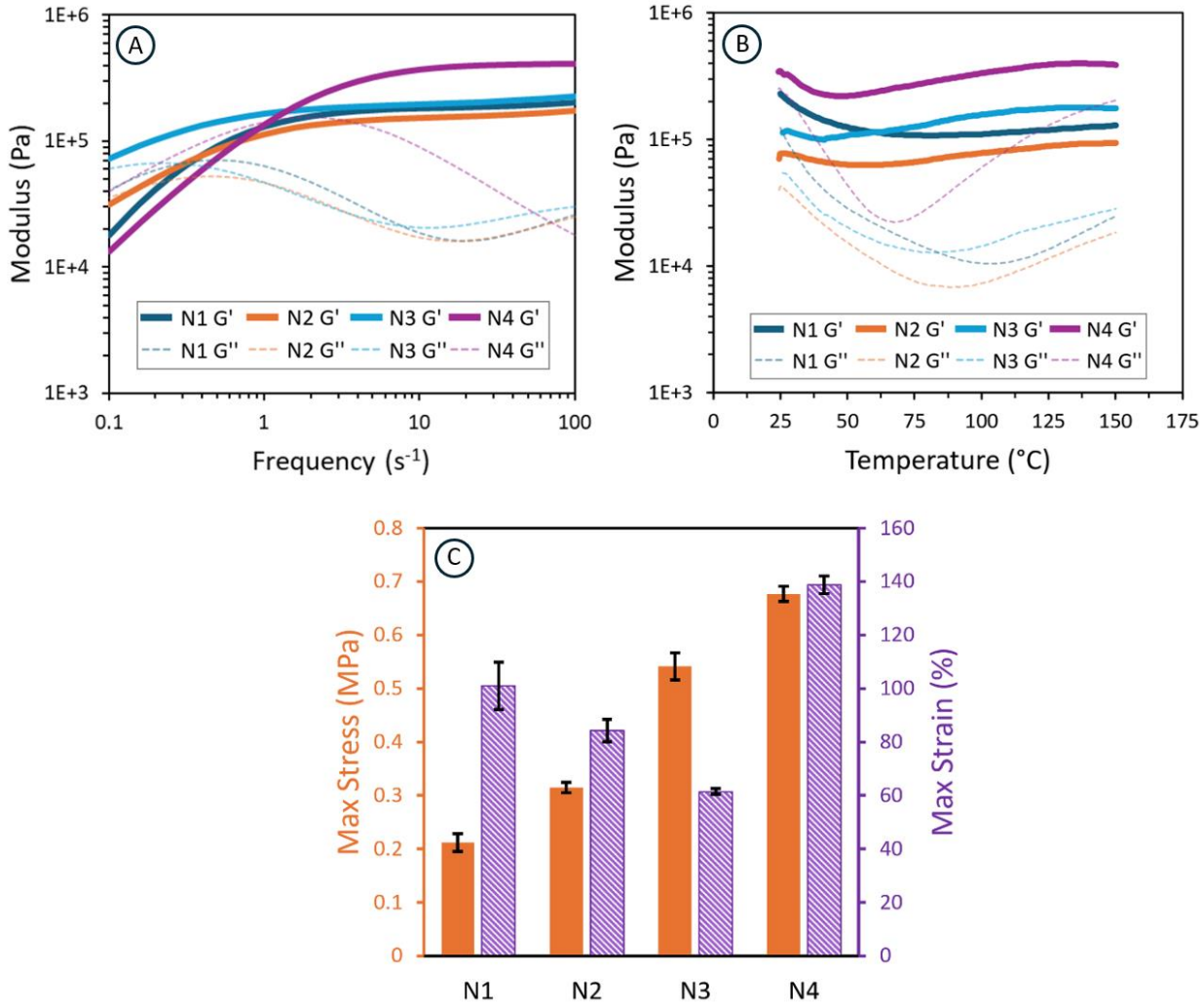

Figure 4.4. Network properties: (A) Frequency sweep of the networks at 130°C; (B) DMTA results of elastic and loss moduli from 25°C to 150°C under a shear strain of 0.5%; (C) Mechanical properties obtained through uniaxial tensile testing.

We first examined the influence of incorporating a PMMA block while keeping the cross-linking density constant by comparing N1 (composed of P1-S-GM with P2-S-VP) and N3 (P1-S-GM with P3-B-VP). Although N1 and N3 had similar cross-linking, N3 achieved a maximum stress at break of 0.54 ± 0.05 MPa—more than double N1's 0.21 ± 0.03 MPa—demonstrating the reinforcing effect of the 10 wt% PMMA block. Subsequently, we compared N2 with N3 as both were made of the same prepolymers but N2 had 6.4 wt% PMMA and half the cross-linking relative to N3. Interestingly, N2 exhibited ~60% lower stress of 0.34 ± 0.2 MPa and higher strain at break of 84.3 ± 8.4 %. Comparing N1 to block copolymer-based N2 and N3, the incorporation of PMMA

systematically increased the maximum stress at break and reduced the networks ability to deform. This trend shows the high tunability of the diblock copolymer approach. However, the network made of the BDB small molecule cross-linker, N4, exhibited considerably different tensile properties by having the highest stress and strain break of 0.68 ± 0.03 MPa and 138.8 ± 6.6 %, respectively. The high toughness in N4 can be attributed to its higher cross-linking density.

To assess network hardness, an indenter with a Berkovitch tip was used to generate force-displacement curves. The average hardness results from nine indentation tests for each vitrimer are presented in Figure 4.5. N1, the statistical polymer-polymer network, possessed the lowest hardness while block-copolymer based N3 exhibited the highest hardness. Interestingly, although N4's higher cross-linking provided the greatest tensile strength, N3's PMMA microphase separated block resulted in the highest hardness from indentation testing.

Next, the mechanical reprocessability of the vitrimers was examined. Regardless of cross-linking mechanism, all networks showed excellent preservation of their mechanical properties through three cycles of hot pressing and tensile testing. Following the first round of tensile testing (R×0), N1 and N2 samples were subsequently cut up into small pieces, then repressed into new tensile bars for retesting. Completing this process twice revealed no statistically significant differences in either maximum tolerable stress or maximum strain achieved compared to the R×0 processed tensile bars. The detailed results of tensile tests are provided in Supporting Information (Table B7). Furthermore, the samples preserved good optical clarity during the reprocessing. Initially, all networks exhibited a striking transparent appearance, with only slight yellowing occurring after three cycles of processing and tensile testing, shown by images of N2 in Figure 4.5.

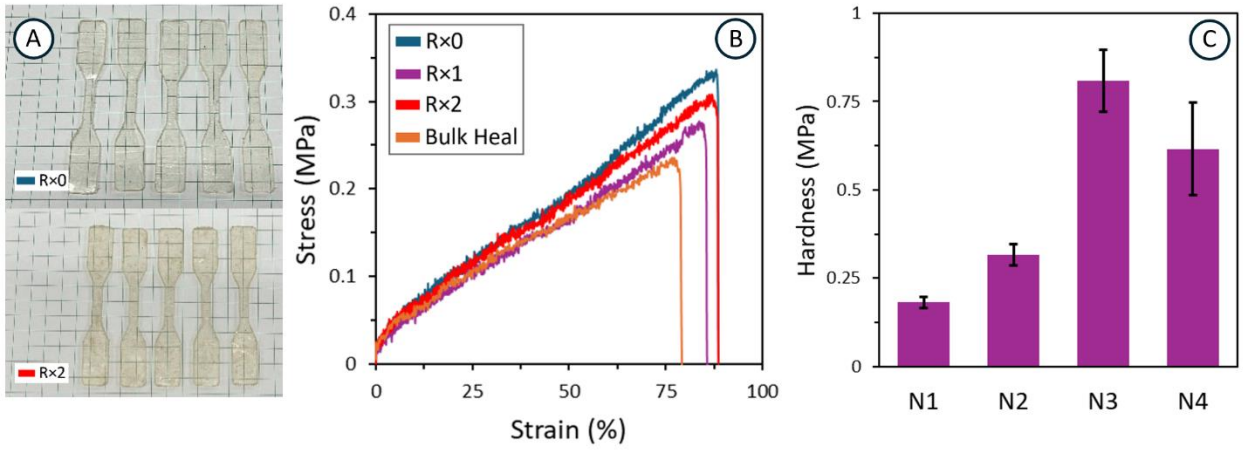

Figure 4.5. Recycling and hardness: (A) Tensile bars of N2 after the initial shaping (R×0), and after the second re-shaping (R×2); (B) Stress-strain plots from uniaxial tensile testing for N2 across three rounds of processing and after having healed in bulk; (C) Hardness modulus of the networks as determined from nanoindentation experiments.

4.4.6 Thermal Properties

The networks thermal transitions and stability were analyzed using DSC and TGA, respectively, with the results provided in the Supporting Information (Figure B17 for DSC and Figure B18 for TGA). Samples from both freshly solvent-mixed networks and twice-processed networks were analyzed to verify the retention of thermal properties during reprocessing under heat. DSC traces showed all four networks had similar T_gs ranging from -51.8 to -50.5°C, and that this transition was unaffected from reprocessing. Thermal decomposition, measured as the onset of 10 wt% loss, varied based on the prepolymers used. Due to thermal stability differences between prepolymers, the resulting networks showed decomposition temperatures aligned with the contributions from their constituents. In N4, where just P1-S-GM is cross-linked via BDB small molecule, the 10 wt% loss decomposition temperature increased from 202°C for the prepolymer to 220°C after the network formation, giving indication that incorporating boronic ester chemistry into the polymers does not negatively affect the thermal stability of the material. Table B3 provides the TGA of the unprocessed, and twice reprocessed networks and their onset temperature of 10 wt% decomposition. Some slight increase in the $T_{onset10wt\%}$ was observed, indicating some thermal decomposition of the networks which were more prominent in blocky samples. An additional isothermal TGA experiment on N2 showed a minimal 2.75 wt% decrease over three hours at

150°C, which can be attributed to moisture loss in the first 30 minutes (Figure B19). This result confirms that the networks can withstand standard processing temperatures without significant degradation.

4.4.7 Network Rheological Properties

The rheological behavior of the networks was first assessed through strain sweep tests to examine the linear viscoelastic region (LVR), as shown in the Supplementary Information (Appendix B, Figure B22). Figure 4.4 shows the elastic (G′) and loss (G″) modulus traces from dynamic mechanical thermal analysis (DMTA). Across the temperature range of 25 to 150°C, the networks exhibited a dominant elastic moduli (G′ > G″) corroborating the elastic nature of the vitrimers. The observed rubbery plateau also confirmed the formation of cross-linked structures in all cases. The magnitude of the elastic modulus increased with cross-link density in the networks.

In addition, frequency sweep tests were conducted at 50, 90, and 130°C (Figure 4.4 and Supplementary Information, Appendix B, Figure B23). These revealed the distinct dynamics which exist between the networks. Notably, the homogeneous networks, N1 and N4, showed a significant decrease in their elastic modulus at low frequencies (<1 s^{-1}) as we conducted the frequency sweep tests at higher temperatures. Between the tests at 50 and 130°C, the elastic modulus of N1 and N4 dropped seven-fold, and four-fold, respectively. This decline reflects increased polymer chain mobility and faster associative bond exchange in their cross-linking at higher temperatures and longer time scales. In contrast, the block-copolymer networks, N2 and N3, showed much lower declines in elastic modulus over the same temperature range at low frequencies (<1 s^{-1}), revealing a more stable elastic behavior from 50 to 130°C. Even with the test at 130°C being conducted above the T_g of the PMMA domains, adding chain mobility, the microphase separation evidently helped retain elastic behaviour.

The recyclability of vitrimer networks stems from associative covalent bond exchanges that enable continuous cross-link reformation. This also allows the networks to relax internal stress, and the speed at which stress can be relieved gives indication of their ease of processability. Fast stress relaxation can come from both rapid dynamic exchange and fewer cross-links.[39] We conducted stress relaxation tests to examine how the microphase separated PMMA domains and BDB small cross-linker would influence the networks flow behaviour. Following the Kohlrausch–Williams–Watts equation model, stress relaxation in vitrimers can be described by a stretched

exponential (Supporting Information Equation B4) with parameters τ* (characteristic relaxation time) and β (relaxation deviation factor away from an ideal Maxwellian model).[13] The extreme cases occur when β is equal to one and zero, representing an ideal single Maxwellian element and a complex multiple relaxation mode, respectively.[16] The homogeneous statistical-based networks, N1 and N4, displayed β values from 0.70 to 0.87. In contrast, the block-copolymer-based networks, N2 and N3, had lower β values of 0.57 to 0.65 and 0.51 to 0.59, respectively. This indicates a higher deviation from the ideal Maxwell model, suggesting a more complex relaxation mechanism due to the phase-separated microstructure. Notably, increasing the loading of microphase-separated PMMA in N2 and N3 led to greater deviations from the Maxwellian single element model.

Regardless, across the samples, stress relaxation was rapid. τ* varied between 1.0 and 33.1 s across the four networks. The fast and complete stress relaxation is manifested in networks that are composed of fast exchanging bonds, lending to easy reprocessing. Despite having the highest cross-link density, N4 displayed the smallest τ* values. With cross-linking existing via small molecule interactions, the movement of polymer chains in the network is not required for the stress to be relaxed, but instead can be achieved by the rearrangement of the small molecules. This agrees with Wang *et al.*, who showed polymer-polymer cross-linking leads to slower relaxation times compared to polymer-small molecule interactions.[39] Comparing N1 and N3, which have similar degrees of cross-linking, incorporating PMMA domains restricts strand movement in the network, leading to higher τ* values. All the characteristic relaxation times and β values can be found in the Supporting Information (Appendix B, Table B4).

The activation energy for viscous flow was then estimated by fitting the characteristic relaxation time with an Arrhenius-type model (Equation B5) as suggested by Leibler *et al*.[40] The small-molecule bound N4 displayed the lowest activation energy for viscous flow (E_a = 48 kJ/mol), with the PMMA domains and increased cross-linking of N3 requiring the highest activation energy of 56 kJ/mol.

Network dynamics that result in favourable relaxation times, low activation energies for viscous flows, and easy reprocessing, are also what lead to an important disadvantage of vitrimers: their susceptibility to creep. We performed creep tests to examine the impact of microphase structure on the vitrimers dimensional stability. Increased cross-link density from N1 to N4

improved creep resistance, but both exhibited limited recovery. As it was observed by the temperature dependance of the elastic modulus in the frequency sweeps, increasing the temperature allows for faster cross-linking exchanges. This manifested in the creep resistance experiments: creep in N1 and N4 increased more than fourfold between 90°C and 130°C with shear strain rising from 5% to 19% for N1, and from 2% to 8% for N4. Results from creep tests are shown in Figure 4.6 and Figure B26 (Supporting Information, Appendix B).

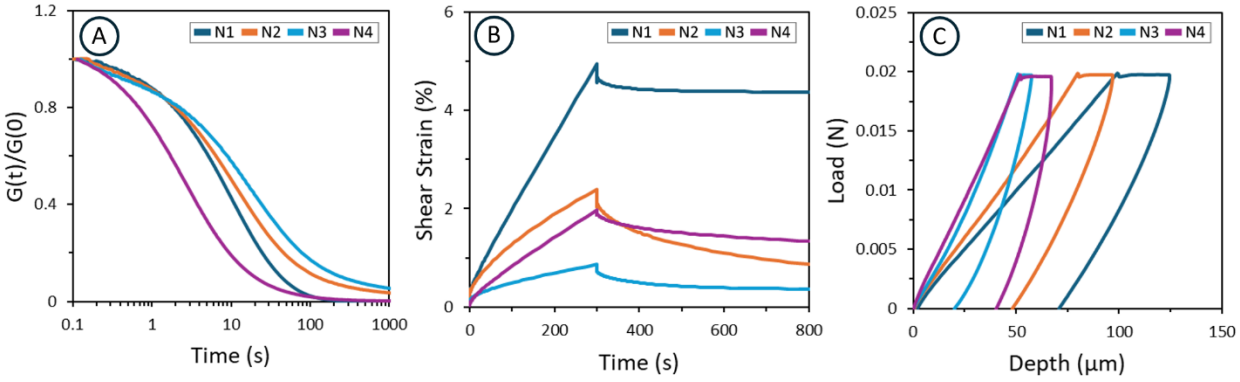

Figure 4.6. Creep resistance: (A) Normalized stress relaxation of the networks at 90°C; (B) Creep recovery curves at 90°C; (C) Load-displacement (depth) curves of the networks as obtained from indentation using a Berkovitch tip.

In contrast, creep resistance significantly improved with the incorporation of PMMA-based block copolymers, as seen in N3, which shared N1's cross-link density but exhibited a maximum shear strain of only 1 % at 90°C and 2 % at 130°C. This lower and less temperature-sensitive creep in N3 is attributed to the microphase separation between PMMA and the cross-linked C13MA domains, which effectively anchor the network and restricts strand movement even above PMMA's T_g. This is consistent with the finding of Asempour *et al.*, and the phenomena reported by Summerlin *et al.*, where AB block-copolymers cross-linked by small molecules were shown to have superior creep resistance compared to their statistical analogs above the T_g of the system.[14, 15] Again, this trend was verified by Fang in vitrimers composed of ABA type polymers.[41]

Creep recovery was also observed in the block-containing networks. While the homogeneous networks N1 and N4 displayed minimal recovery and higher temperature sensitivity, N2 and N3 achieved significant recovery (recovering at a minimum, 54.2% of shear strain; see Supporting Information, Appendix B, Table B6 for creep recovery values). The creep data collected through rheology aligns with the load-displacement behaviour obtained through indentation tests, shown

in Figure 4.6. Indentation showed N1 had the highest displacement depth, while N3 had the lowest. Microphase separation simultaneously improved creep resistance, and creep recovery.

4.4.8 Self-Healing Attributes

We continued by examining the ability of the networks to self-heal both in bulk and surface scratches, as illustrated in Figure 4.7. Recently, Jiang *et al.* showed that up to 40% of tensile strength could be recovered in poly(styrene-*b*-isoprene-*b*-styrene) triblock based vitrimers using boronic acid cross-linkers, with healing conducted at 100°C.[25] In the work here, three tensile bars of each network were tested for their bulk self-healing properties. Each sample had already undergone three rounds of reprocessing, was hot-pressed into tensile bars, and then cut at their midpoint using a scalpel. Afterwards, the two halves were manually placed together, and left under ambient conditions at 22°C and approximately 60% relative humidity for 100 hours. A Kimwipes® box was placed on top of the tensile bars to hold them in place and maintain contact between the two pieces. All four networks demonstrated healing at their cut interface. While seams remained visible in N2 through N4, N1 completely repaired the cut, resulting in a smooth surface, as shown in Figure B27 (Supporting Information, Appendix B). To test the weld strength, weights were clipped onto the bars; each network held at least 15 grams without failure, as shown in Figure 4.7. Tensile testing on the healed bars showed N3, containing the most phase-separated PMMA loading, had the lowest recovery but still regained 56 ± 17 % of its original tensile strength and 58 ± 18% of its strain. Interestingly, for N1, healing exceeded initial performance, reaching 143 ± 25% of its original maximum stress and 122 ± 24% of its strain, likely due to pressure-induced polymer chain alignment from the Kimwipes® box that was placed on top.[42, 43] While network architecture influenced healing efficiency, it did not prevent bulk recovery in any network. Our approach of polymer-polymer cross-linking along with incorporation of as little as 10 wt% PMMA microphase separated domains drastically could enhance the rheo-mechanical properties without halting self-healing. To our best knowledge, this is among the first reports showing room temperature self-healing of block copolymer-based networks.

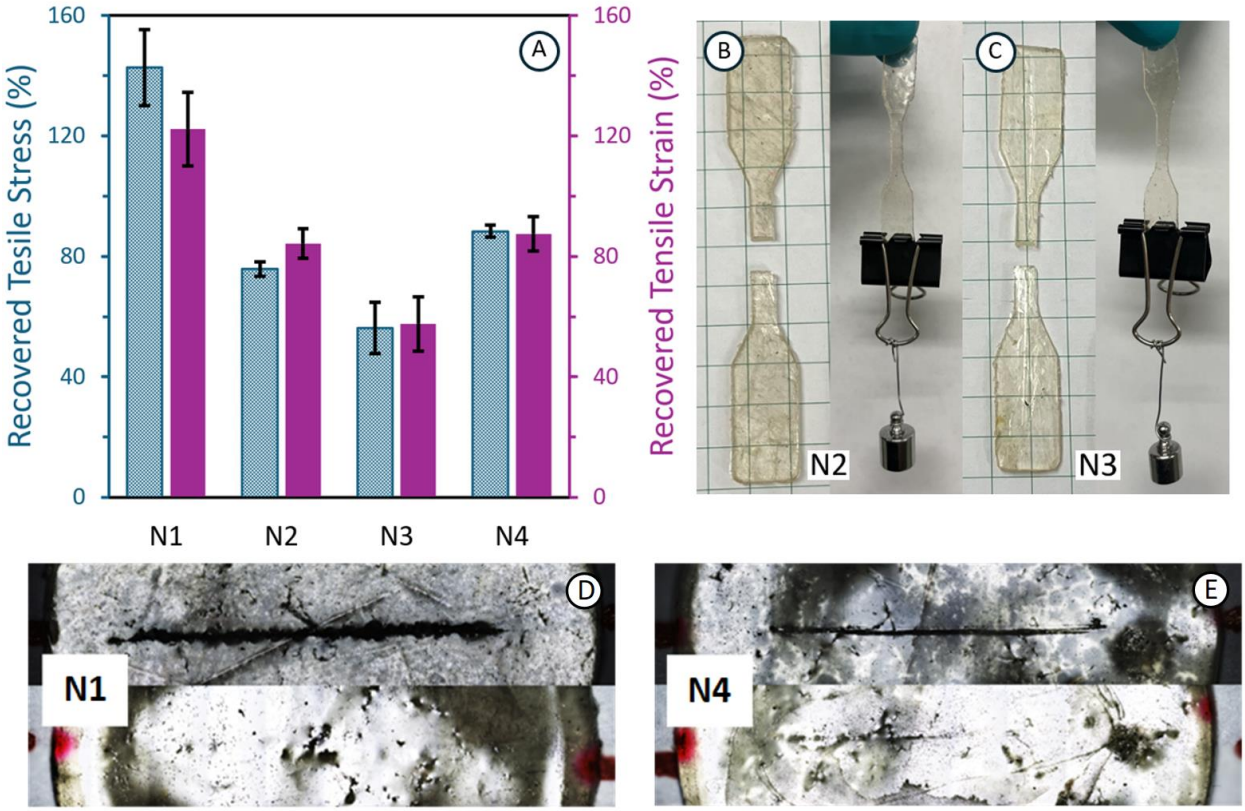

Figure 4.7. Self-healing: (A) Recovered mechanical properties relative to R×0 values from uniaxial tensile testing of test bars that underwent bulk-healing at their middle; (B) Images before and after bulk-healing of N2; and (C) of N3; (D) Images before and after (24 hours) scratch repair of N1; (E) Images before and after (50 hours) scratch repair of N4.

Following bulk healing success, surface scratch healing was also examined. Samples were manually scratched with a sharp scalpel and monitored over 24 hours at 60°C. N1 completely closed its defect within this period (Figure 4.7), while other networks displayed slower healing. Adding a drop of water to the scratched areas—thereby promoting the breakage of moisture-sensitive boronic acid bonds—and extending the time by 25 hours enabled N4 to nearly eliminate its scratch. The high cross-link density and rigidity of N4 initially inhibited healing, but added moisture permitted greater chain movement due to release of the boronic acid cross-links near the scratch, leading to defect closure. Importantly, block-copolymer networks N2 and N3 also showed partial healing. Although their improved creep resistance and phase-separated microstructure limited complete scratch removal, some regions visibly closed. All the scratch healing images can

be seen in Figure B28. The hard PMMA microphase-separated domains in N2 and N3 limited the bulk chain motion, yet areas where the scratch contacted itself were repaired.

4.5 Conclusion

We investigated the influence of hard-soft AB block copolymers on the rheo-mechanical and self-healing properties of dynamic networks. Nitroxide mediated polymerization was employed to synthesize 3 prepolymers of (1) diol-functional statistical, (2) boronic acid-functional statistical, and (3) boronic acid-functional AB diblock copolymers. Diblock polymer (3) used PMMA as the first block, giving p(MMA)-*block*-p(C13MA-*co*-VPBA).

Four different networks were then synthesized. Homogenous network N1 was formed from blending statistical polymer (1) with statistical polymer (2). Similarly, network N4 was formed by blending statistical polymer (1) with a difunctional small molecule cross-linker (BDB). In contrast, block copolymer-based networks (N2 and N3) were formed from cross-linking statistical polymer (1) with AB diblock polymer (3). SAXS confirmed the existence of spherical PMMA microphase separated domains within N2 and N3. Incorporating PMMA hard blocks proved effective in improving the tensile strength and hardness of the networks, when compared to homogenous blends of equal cross-linking. While N4 (BDB cross-linked) had the highest toughness of the networks, N3 had the greatest hardness due to its PMMA content. Through three rounds of recycling, all the networks exhibited a retention of their mechanical properties.

Rheological studies confirmed a rubbery plateau in all the networks. Next, frequency sweep tests revealed the elastic modulus of block containing networks N2 and N3 were less temperature dependent compared to homogeneous counterparts. In addition, stress relaxation tests showed slower relaxation times in blocky networks which was attributed to microphase separation. Regardless, full and relatively rapid stress relaxation was observed in all the networks ($\tau^* < 33$ s). Creep resistance and recovery were found to be greatly improved in the N2 and N3 blocky networks. The PMMA micro domains anchored the network both below and above the T_g of the PMMA. In addition, all networks displayed bulk-healing under ambient conditions after being cut.

These findings highlight the potential to tailor mechanical properties, such as creep resistance and self-healing, by leveraging polymer-polymer cross-linking within vitrimer networks of AB copolymers. Our strategy, which combines polymer-polymer cross-linking with the addition of as

little as 10 wt% PMMA microphase-separated domains, could significantly improve rheo-mechanical properties while preserving self-healing capabilities.

4.6 References

(1) Mavroeidi, E.; Dubois, M.; Dellink, R.; Bibas, R.; Lanzi, E., Plastic waste projections to 2060. In *Global Plastics Outlook*, OECD Publishing: Paris, 2022.

(2) Lorero, I.; Rodríguez, A.; Campo, M.; Prolongo, S. G., Thermally remendable, weldable, and recyclable epoxy network crosslinked with reversible Diels-alder bonds. *Polymer* **2022,** *259*, 125334.

(3) Yang, S.; Park, S.; Kim, S.; Kim, S.-K., Vitrimer with dynamic imine bonds as a solid-state electrolyte for lithium metal batteries. *Materials Today Energy* **2024,** *45*, 101690.

(4) Van Zee, N. J.; Nicolaÿ, R., Vitrimers: Permanently crosslinked polymers with dynamic network topology. *Progress in Polymer Science* **2020,** *104*, 101233.

(5) Denissen, W.; Winne, J. M.; Du Prez, F. E., Vitrimers: Permanent organic networks with glass-like fluidity. *Chemical Science* **2016,** *7* (1), 30-38.

(6) Yue, L.; Bonab, V. S.; Yuan, D.; Patel, A.; Karimkhani, V.; Manas-Zloczower, I., Vitrimerization: A novel concept to reprocess and recycle thermoset waste via dynamic chemistry. *Global Challenges* **2019,** *3* (7), 1800076.

(7) Miravalle, E.; Bracco, P.; Brunella, V.; Barolo, C.; Zanetti, M., Improving sustainability through covalent adaptable networks in the recycling of polyurethane plastics. *Polymers* **2023,** *15* (18).

(8) Kumar, A.; Connal, L. A., Biobased transesterification vitrimers. *Macromolecular Rapid Communications* **2023,** *44* (7), 2200892.

(9) Lucherelli, M. A.; Duval, A.; Avérous, L., Biobased vitrimers: Towards sustainable and adaptable performing polymer materials. *Progress in Polymer Science* **2022,** *127*, 101515.

(10) Wu, J.; Yu, X.; Zhang, H.; Guo, J.; Hu, J.; Li, M.-H., Fully biobased vitrimers from glycyrrhizic acid and soybean oil for self-healing, shape memory, weldable, and recyclable materials. *ACS Sustainable Chemistry & Engineering* **2020,** *8* (16), 6479-6487.

(11) Dhers, S.; Vantomme, G.; Avérous, L., A fully bio-based polyimine vitrimer derived from fructose. *Green Chemistry* **2019,** *21* (7), 1596-1601.

(12) Asempour, F.; Marić, M., Vitrification: Versatile method to modulate properties of myrcene-based rubbers. *ACS Applied Polymer Materials* **2023,** *5* (8), 6364-6376.

(13) Li, L.; Chen, X.; Jin, K.; Torkelson, J. M., Vitrimers designed both to strongly suppress creep and to recover original cross-link density after reprocessing: Quantitative theory and experiments. *Macromolecules* **2018,** *51* (15), 5537-5546.

(14) Asempour, F.; Laurent, E.; Ecochard, Y.; Maric, M., Reprocessable biobased statistical and block copolymer methacrylic-based vitrimers with a shape memory effect. *ACS Applied Polymer Materials* **2024,** *6* (1), 956-966.

(15) Lessard, J. J.; Scheutz, G. M.; Sung, S. H.; Lantz, K. A.; Epps, T. H., III; Sumerlin, B. S., Block copolymer vitrimers. *Journal of the American Chemical Society* **2020,** *142* (1), 283-289.

(16) Ishibashi, J. S. A.; Pierce, I. C.; Chang, A. B.; Zografos, A.; El-Zaatari, B. M.; Fang, Y.; Weigand, S. J.; Bates, F. S.; Kalow, J. A., Mechanical and structural consequences of associative dynamic cross-linking in acrylic diblock copolymers. *Macromolecules* **2021,** *54* (9), 3972-3986.

(17) Weerathaworn, S.; Meyer, A.; Abetz, V., Vitrimers based on block copolymers with diverse block sequences. *Polymer* **2024,** *308*, 127311.
(18) Wang, J.; Zhang, X.; Jiang, L.; Qiao, J., Advances in toughened polymer materials by structured rubber particles. *Progress in Polymer Science* **2019,** *98*, 101160.
(19) Krishnakumar, B.; Pucci, A.; Wadgaonkar, P. P.; Kumar, I.; Binder, W. H.; Rana, S., Vitrimers based on bio-derived chemicals: Overview and future prospects. *Chemical Engineering Journal* **2022,** *433*, 133261.
(20) Terriac, L.; Helesbeux, J.-J.; Maugars, Y.; Guicheux, J.; Tibbitt, M. W.; Delplace, V., Boronate ester hydrogels for biomedical applications: Challenges and opportunities. *Chemistry of Materials* **2024,** *36* (14), 6674-6695.
(21) Aung, Y.-Y.; Kristanti, A. N.; Lee, H. V.; Fahmi, M. Z., Boronic-acid-modified nanomaterials for biomedical applications. *ACS Omega* **2021,** *6* (28), 17750-17765.
(22) Gosecki, M.; Gosecka, M., Boronic acid esters and anhydrates as dynamic cross-links in vitrimers. *Polymers* **2022,** *14* (4).
(23) Tajbakhsh, S.; Hajiali, F.; Guinan, K.; Marić, M., Highly reprocessable, room temperature self-healable bio-based materials with boronic-ester dynamic cross-linking. *Reactive and Functional Polymers* **2021,** *158*, 104794.
(24) Röttger, M.; Domenech, T.; van der Weegen, R.; Breuillac, A.; Nicolaÿ, R.; Leibler, L., High-performance vitrimers from commodity thermoplastics through dioxaborolane metathesis. *Science* **2017,** *356* (6333), 62-65.
(25) Jiang, C.; Wang, C.; Zhang, S.; Bi, H.; Wu, Y.; Wang, J.; Zhu, Y.; Qin, J.; Zhao, Y.; Shi, X.; Zhang, G., Reprocessable and self-healable boronic-ester based poly(styrene-b-isoprene-b-styrene) vitrimeric elastomer with improved thermo-mechanical property and adhesive performance. *Reactive and Functional Polymers* **2024,** *198*, 105893.
(26) Lamontagne, H. R.; Lessard, B. H., Nitroxide-mediated polymerization: A versatile tool for the engineering of next generation materials. *ACS Applied Polymer Materials* **2020,** *2* (12), 5327-5344.
(27) Nicolas, J.; Dire, C.; Mueller, L.; Belleney, J.; Charleux, B.; Marque, S. R. A.; Bertin, D.; Magnet, S.; Couvreur, L., Living character of polymer chains prepared via nitroxide-mediated controlled free-radical polymerization of methyl methacrylate in the presence of a small amount of styrene at low temperature. *Macromolecules* **2006,** *39* (24), 8274-8282.
(28) Savelyeva, X.; Chondon, D.; Marić, M., Vinyl phenylboronic acid controlling co-monomer for nitroxide mediated synthesis of thermoresponsive poly(2- morpholinoethyl methacrylate). *Journal of Polymer Science Part A: Polymer Chemistry* **2016,** *54* (11), 1560-1572.
(29) Brutman, J. P.; Delgado, P. A.; Hillmyer, M. A., Polylactide vitrimers. *ACS Macro Letters* **2014,** *3* (7), 607-610.
(30) Denissen, W.; Rivero, G.; Nicolaÿ, R.; Leibler, L.; Winne, J. M.; Du Prez, F. E., Vinylogous urethane vitrimers. *Advanced Functional Materials* **2015,** *25* (16), 2451-2457.
(31) Mo, R.; Yu, D.; Li, W.; Sheng, X.; Zhang, X., Storage-stable and self-crosslinkable combinations of boronic acid containing polymers and diol containing polymers enabled by the latex system. *Polymer* **2024,** *299*, 126977.
(32) Man, Y.; Peng, G.; Lv, X.; Liang, Y.; Wang, Y.; Chen, Y.; Deng, Y., Microchip-grafted p(nipaam-co-vpba) with thermoresponsive boronate affinity for capture–release of cis-diol biomolecules. *Chromatographia* **2015,** *78* (3), 157-162.

(33) McKenzie, A.; Hoskins, R.; Swift, T.; Grant, C.; Rimmer, S., Core (polystyrene)–shell [poly(glycerol monomethacrylate)] particles. *ACS Applied Materials & Interfaces* **2017,** *9* (8), 7577-7590.
(34) Watanabe, K.; Katsuhara, S.; Mamiya, H.; Yamamoto, T.; Tajima, K.; Isono, T.; Satoh, T., Downsizing feature of microphase-separated structures via intramolecular crosslinking of block copolymers. *Chemical Science* **2019,** *10* (11), 3330-3339.
(35) Formon, G. J. M.; Storch, S.; Delplanque, A. Y. G.; Bresson, B.; Van Zee, N. J.; Nicolaÿ, R., Overcoming the tradeoff between processability and mechanical performance of elastomeric vitrimers. *Advanced Functional Materials* **2023,** *33* (52), 2306065.
(36) Bates, F. S.; Fredrickson, G. H., Block copolymer thermodynamics: Theory and experiment. *Annual Review of Physical Chemistry* **1990,** *41* (Volume 41), 525-557.
(37) Hamley, I. W.; Castelletto, V., Small-angle scattering of block copolymers: In the melt, solution and crystal states. *Progress in Polymer Science* **2004,** *29* (9), 909-948.
(38) Kim, G.; Libera, M., Morphological development in solvent-cast polystyrene−polybutadiene−polystyrene (sbs) triblock copolymer thin films. *Macromolecules* **1998,** *31* (8), 2569-2577.
(39) Wang, Z.; Gu, Y.; Ma, M.; Chen, M., Strong, reconfigurable, and recyclable thermosets cross-linked by polymer–polymer dynamic interaction based on commodity thermoplastics. *Macromolecules* **2020,** *53* (3), 956-964.
(40) Montarnal, D.; Capelot, M.; Tournilhac, F.; Leibler, L., Silica-like malleable materials from permanent organic networks. *Science* **2011,** *334* (6058), 965-968.
(41) Fang, H.; Gao, X.; Zhang, F.; Zhou, W.; Qi, G.; Song, K.; Cheng, S.; Ding, Y.; Winter, H. H., Triblock elastomeric vitrimers: Preparation, morphology, rheology, and applications. *Macromolecules* **2022,** *55* (24), 10900-10911.
(42) Schrickx, H. M.; Sen, P.; Balar, N.; O'Connor, B. T., Strain alignment of conjugated polymers: Method, microstructure, and applications. *Cell Reports Physical Science* **2024,** *5* (7), 102076.
(43) Beiermann, B. A.; Kramer, S. L. B.; May, P. A.; Moore, J. S.; White, S. R.; Sottos, N. R., The effect of polymer chain alignment and relaxation on force-induced chemical reactions in an elastomer. *Advanced Functional Materials* **2014,** *24* (11), 1529-1537.

Chapter 5: General Discussion and Future Work

The development of eco-friendly polymers is a complex and multifaceted challenge requiring the consideration of many factors. Opinions vary on which challenge should take priority, from utilizing renewable sourcing, designing for recyclability, and biodegradability to lifecycle energy requirements, carbon footprint, mechanical performance, durability, and economic viability.[79] Determining the best balance of these considerations is, in most cases, subjective, and highly application dependent. Reaching a consensus on the definition of a "green" material and establishing standardized methods to quantify its impact are needed to streamline research and accelerate development. Additionally, regulatory frameworks and public awareness will be crucial in achieving meaningful progress in sustainable polymer adoption.

In this thesis, we considered methods of incorporating renewable feedstocks into polymeric materials and focused on how to improve upon their mechanical properties to make them more competitive with commodity polymers. Specifically, itaconic acid was initially picked as a promising biomolecule to increase the renewable content of polymers. Due to its poor behaviour in polymerization reactions,[36] it was hypothesized that functionalizing it with a methacrylate group could allow for its easier polymerization into higher molecular weight products and more complex and useful architectures. Through a four-step synthesis procedure, an itaconic-acid based methacrylate was obtained, and it was shown to readily polymerize using standard methods of reversible deactivation radical polymerization. While it is interesting to demonstrate an alternative way to obtain polymers of itaconic acid with predictable polymerization results due to its methacrylate functionality, the four-step synthesis procedure to obtain the monomer undoubtedly impedes this method from being "green". The demanding synthetic route used in this work caused challenges in trying to scale up the monomer production. To conduct experiments on mechanical properties, or bulk material properties, the material and labour investments for the monomer production using the synthetic route in this work would be very great. However, that is not to say this method of functionalizing biomolecules for polymer applications is impractical, but rather that the synthetic route used in this work to functionalize itaconic acid would require modification.

This study demonstrated a pathway for obtaining polymers with enhanced bio-content due to the functionalization of itaconic acid, and future work in refining the synthetic pathway could improve its relevance. The current route, requiring organic solvents, metal catalysts, and two

rounds of purification undoubtedly counteracts any environmental benefit of using itaconic acid as opposed to a petroleum-based molecule. Determining the atom economy of the process would emphasize the negative aspects of this method, but as a preliminary study, it demonstrated how renewable molecules may be used to increase the renewable content of polymers. To increase the feasibility of these itaconic acid-based methacrylate's, developing a single step, or one-pot synthesis procedure for the monomer would be beneficial. Alternatively, efforts could be made to generate methacrylic families of other biomolecules that can be functionalized in an easier process.

If a low cost, renewable feedstock could be functionalized in fewer steps, then there could be high potential for this method. Lignin, chitosan, plant cellulose and vegetable oils, functionalized with methacrylates previously, may be viable options.[8, 53] To generate a fully renewable monomer, however, this would require an alternative production method be developed for methacryloyl chloride or methacrylic anhydride. This presents a roundabout dilemma, as efforts to improve the green production of these molecules could instead be put towards developing the green production of methyl methacrylate itself, to produce renewably sourced polymers of the same chemical identity as those already adopted by the market. To simplify the implementation of products on a larger scale, developing ways to obtain chemically identical species such as ethylene, styrene, or methyl methacrylate that use renewable feedstocks is likely the most promising route to move the polymer industry away from petroleum dependence.

Being able to directly polymerize renewable feedstocks is a second viable alternative. While this requires property modulation after polymerization, it offers the ability to obtain fully renewable materials. Polylactic acid (PLA) is the third most used renewable polymer, after bio-sourced derivatives of polyethylene terephthalate and polyethylene.[80] As PLA is the only one of the top three with a chemical structure distinct from petroleum alternatives, it exemplifies the potential for polymers of renewable sources to be polymerized, and implemented at a large scale, despite the fact it requires additives to achieve useful mechanical properties.[81] However, the broader acceptance of additives for performance tuning in the industry already suggests this should not be seen as a limitation, but rather as part of the design process in renewable polymer development. Innovation is required regardless of the method chosen to develop renewable polymers, whether creating renewable analogs of conventional polymers, polymerizing biomolecules and tuning the final properties, or functionalizing biomolecules and then tuning the

properties. However, the first two methods may require fewer innovations be made, making the prospect of their success more readily realized.

Advanced polymer networks, like vitrimer networks, offer promising prospects for recyclability and mechanical adaptability.[18] Vitrimers could revolutionize the market by replacing non-recyclable rubbers and providing a way to enhance the properties of biobased polymers.[82] Additionally, they could even serve to functionalize post-consumer waste, allowing existing polymers to be recycled or upcycled into new products.[83] With this approach, vast amounts of already-produced polymers could become resources for sustainable materials, creating a more circular economy. However, achieving strong creep resistance in vitrimer networks remains challenging. Using dynamic covalent chemistries with slower bond exchange rates, incorporating mixed static and dynamic networks, or inducing microphase separation could unlock greater mechanical stability for these materials, potentially seeing their greater breakthrough in transforming the polymer industry.

Building from the work reported in Chapter 4, incorporating diblock copolymers into vitrimers networks could offer an opportunity to control creep. Specifically, block copolymers with a high T_g component are not commonly reported, but as it was shown in this work, have the potential to improve and tune macroscopic material properties. Further studies on the amount of the hard block to include in the network, the influence of the diblock hard:soft ratio, and comparing diblock-diblock polymer cross-linked networks with diblock-small molecule cross-linked networks, would provide meaningful information on how to best utilize microphase separation to obtain desirable properties in vitrimer networks.

Developing the ability to use renewable sources for polymeric materials is, however, just one of many considerations to be made. The product's end of life is also a significant factor, which has great influence on the environmental impact of the material. Although about 80% of plastics produced are thermoplastics [84]—meaning they are technically recyclable—actual recycling rates are low, with less than 9% of plastics being recycled.[85] This underscores a breadth of problems. A lack of policies regulating or mandating recycling, lack of education on recycling, insufficient infrastructure, and added difficulties when using recycled materials as opposed to virgin materials all contribute to manufacturers continuing to use virgin materials. Thus, a reform is required for the end-of-life of polymer materials. Developing renewably sourced, and recyclable polymers is

not of great benefit if the recycling never occurs, and the renewably sourced material's end of life represents a source of waste in the environment.

Increasing recycling rates, while not impossible, requires the collaboration and agreement from a multitude of groups. The energy requirements of collecting, sorting, and recycling of materials can outweigh the energy requirements of using virgin material.[86] This is no different for vitrimeric materials. For their "recyclability" to be a benefit, they would need to be sorted with their own types and reprocessed before re-use. Essentially, the current recycling dilemma would need to be fixed, and recycling rate increased beyond their current 9% if the recyclability of vitrimers is to have a positive impact on the thermoset polymer industry.

As polymer scientists, we can contribute to improving the end-of-life of polymer materials by developing not only recycling strategies, but by designing biodegradable materials. Of potentially more significance than using renewable sources, developing materials that do not persist on the earth for centuries or millennia is an opportunity to minimize the industry's footprint. Some may argue this requires the development of composting facilities, infrastructure, and public awareness to ensure the biodegradation occurs, but this argument is no different than what already exists for improving recycling, and in this case, the degradation would see the removal of the material from the land.

Vitrimers could offer an interesting method of increasing the biodegradability of polymeric materials. Due to the reversible nature of covalent chemistries used in vitrimer networks, incorporating a high degree of the reversible cross-linking between small chain polymer oligomers could also allow for network degradation. If short-chain polymers could be small enough that biodegradation may be feasible, cross-linking them to a high degree could offer the opportunity to generate a material, that after a service life, could be un-cross-linked and degraded. Future research projects into what vitrimer chemistry would be best suited for this application, what polymer should be used for the short chain oligomers, and if this is a feasible method of breaking down materials would be highly exciting.

Developing eco-friendly polymers will require a balance of renewable sourcing, recyclability and biodegradability while maintaining current performance levels. In addition to these scientific developments, reducing the overall consumption of polymers has the potential to lessen the strain of the industry. Currently, projections predict the use of polymers to continue to increase,[87] but the

importance of encouraging the reduction of their use cannot be downplayed. In shifting the industry to more sustainable practices, collaboration across disciplines, industries, governments and citizens will be required. Defining how to rank an environmentally friendly material will help streamline innovations, while improving recycling and composting infrastructure, and promoting alternatives will see a considerable shift occur on a market level. Although incremental advances in policy and academia might appear small individually, cumulative efforts can drive the comprehensive change needed to transition the polymer industry towards sustainability. The combined development of renewable sources, engineering practices for material properties, and end-of-life solutions will be essential to meet the diverse demands polymers fulfill today.

Chapter 6: Conclusions

This thesis aimed to answer first if renewably source materials could be incorporated into polymeric materials with controlled polymerization kinetics, predictable molecular weights and narrow dispersities. Secondly, it sought to determine how the properties of renewable polymeric materials may be made more comparable to market standards

To address the first objective, itaconic acid was transformed in a four-step synthesis scheme to see the addition of a methacrylate group at its backbone. This allowed for a novel family of bio-soured itaconic acid-based methacrylates to be developed, demonstrating how bio-derived feedstocks can be functionalized to allow their incorporation into polymeric materials with enhanced renewable content. By the addition of a methacrylate group, the difficulties in polymerizing itaconic acid which had previously hindered its use in polymeric materials could be circumvented, allowing for the new monomers to display reliable polymerization kinetics typically expected of methacrylates. The resulting polymers were thermally stable, and adjusting the pendant arms of the itaconic acid allowed for the resulting polymers to give glass transition temperatures across a 60°C range. The predictable polymerization kinetics could be exploited to give designed molecular architectures, namely diblock copolymers.

Thermal and rheological testing of the polymers revealed the ability to tune these properties by means of adjusting the polymer's molecular weight. Copolymerizing into diblock copolymers also gave a greater ability to impart elastic behaviour to the polymers, thus leading the way into addressing the second objective of the thesis. This second objective was to explore methods of improving the macroscopic material properties of renewable polymers. Specifically, the influence of various molecular architectures in bio-based vitrimer networks on material properties was examined. Vitrimers, networks cross-linked by associative dynamic covalent chemistries, have the potential to replace thermosets with recyclable analogs, and serve as a mechanism of enhancing the material properties of renewable feedstocks which are not serviceable on their own. Their poor creep resistance, however, has prevented this from occurring so far. In the second project of this work, AB type diblock copolymers were cross-linked with statistical polymers, and compared to networks of just statistical, and statistical-small molecule kinds. Since the "A" in the diblock copolymers was a high T_g polymer, and was a minor phase in the networks, this cross-linking resulted in small and hard spherical microphase inclusions within a soft cross-linked matrix.

Rheological, mechanical, and thermal properties were reported, as was the ability of the networks to be reprocessed, and self-heal. Most notably, the small microphase separated inclusions were highly effective in reducing the susceptibility to creep, and recover from creep, when compared to the two homogenous networks both below and above the glass transition temperature of the A block. This did not however, impede their ability to relieve stress, be reprocessed, or self-heal.

By incorporating reversible cross-linking into the renewably sourced polymer matrix and inducing microphase separation from the inclusion of diblock copolymers in the blend, the second project of this work demonstrated methods to significantly improve the macroscopic properties of bio-sourced C13MA. Structure could be imparted to the material by the addition of the cross-linking, and creep could be better controlled by using diblock copolymers. Adjusting the ratio of cross-linking and diblock polymer within the blends can allow for a breadth of macroscopic properties to be designed, allowing for biobased materials to behave like their petroleum derived counterparts on the market.

In summary, this work demonstrated an approach for incorporating renewable feedstocks into polymeric materials and highlighted how molecular architecture in vitrimer networks significantly influences material properties, offering a promising method for property tuning in sustainable polymers. Future studies into functionalizing biomolecules in a simpler route, various vitrimer architectures, and degradation mechanisms could further enhance the capabilities of bio-based vitrimer networks, enabling the creation of more sustainable, high-performance materials capable of meeting market demands.

References

(1) Shanthi, G.; Beula Isabel, J.; Thankachan, R.; Premalatha, M., Sustainable strategies towards better utilization of synthetic polymers. *Biopolymers* **2024,** *115* (4), e23581.

(2) Beena Unni, A.; Muringayil Joseph, T., Enhancing polymer sustainability: Eco-conscious strategies. *Polymers* **2024,** *16*, 1769.

(3) Karali, N.; Khanna, N.; Shah, N. *Climate Impact of Primary Plastic Production*; LBNL-2001585; Lawrence Berkeley National Laboratory: 2024.

(4) Hamilton, L. A.; Feit, S. *Plastic & Climate: The Hidden Costs of a Plastic Planet*; Center for International Environmental Law: 2019.

(5) Iadrat, P.; Wattanakit, C., Bioethanol upgrading to renewable monomers using hierarchical zeolites: Catalyst preparation, characterization, and catalytic studies. *Catalysts* **2021,** *11* (10).

(6) Swetha, T. A.; Bora, A.; Mohanrasu, K.; Balaji, P.; Raja, R.; Ponnuchamy, K.; Muthusamy, G.; Arun, A., A comprehensive review on polylactic acid (PLA) – Synthesis, processing and application in food packaging. *International Journal of Biological Macromolecules* **2023,** *234*, 123715.

(7) Schneiderman, D. K.; Hillmyer, M. A., 50th anniversary perspective: There is a great future in sustainable polymers. *Macromolecules* **2017,** *50* (10), 3733-3749.

(8) Zhu, Y.; Romain, C.; Williams, C. K., Sustainable polymers from renewable resources. *Nature* **2016,** *540* (7633), 354-362.

(9) Palladino, F.; Marcelino, P. R.; Schlogl, A. E.; José, Á. H.; Rodrigues, R. D.; Fabrino, D. L.; Santos, I. J.; Rosa, C. A., Bioreactors: Applications and innovations for a sustainable and healthy future—A critical review. *Applied Sciences* **2024,** *14* (20).

(10) Werpy, T.; Peterson, G. *Top Value Added Chemicals from Biomass*; U.S. Department of Energy: 2004.

(11) De Carvalho, J.; Magalhaes, A.; Soccol, C., Biobased itaconic acid market and research trends - Is it really a promising chemical? *Chimica oggi* **2018,** *36*, 56.

(12) Lea Sollka, K. L., Progress in the free and controlled radical homo- and co-polymerization of itaconic acid derivatives: Toward functional polymers with controlled molar mass distribution and architecture. *Macromolecular Rapid Communications* **2021,** *42* (4).

(13) Farah, S.; Anderson, D. G.; Langer, R., Physical and mechanical properties of PLA, and their functions in widespread applications — A comprehensive review. *Advanced Drug Delivery Reviews* **2016,** *107*, 367-392.

(14) Quiles-Carrillo, L.; Montanes, N.; Lagaron, J. M.; Balart, R.; Torres-Giner, S., In situ compatibilization of biopolymer ternary blends by reactive extrusion with low-functionality epoxy-based styrene–acrylic oligomer. *Journal of Polymers and the Environment* **2019,** *27* (1), 84-96.

(15) Hahn, C.; Göttker-Schnetmann, I.; Tzourtzouklis, I.; Wagner, M.; Müller, A. H. E.; Floudas, G.; Mecking, S.; Frey, H., Nopadiene: A pinene-derived cyclic diene as a styrene substitute for fully biobased thermoplastic elastomers. *Journal of the American Chemical Society* **2023,** *145* (49), 26688-26698.

(16) Montarnal, D.; Capelot, M.; Tournilhac, F.; Leibler, L., Silica-like malleable materials from permanent organic networks. *Science* **2011,** *334* (6058), 965-968.

(17) Krishnakumar, B.; Sanka, R. V. S. P.; Binder, W. H.; Parthasarthy, V.; Rana, S.; Karak, N., Vitrimers: Associative dynamic covalent adaptive networks in thermoset polymers. *Chemical Engineering Journal* **2020,** *385*, 123820.
(18) Van Zee, N. J.; Nicolaÿ, R., Vitrimers: Permanently crosslinked polymers with dynamic network topology. *Progress in Polymer Science* **2020,** *104*, 101233.
(19) Feng, Y.; Qiu, H.; Deng, P.; Nie, Z.; Chen, J.; Gong, K.; Fan, X.; Qi, S., Tuning the static and dynamic properties of epoxy vitrimers through modulation of cross-link density. *European Polymer Journal* **2023,** *196*, 112308.
(20) *Plastics-the Facts 2022*; Plastics Europe: Berlin, 2022.
(21) Constable, D. J. C., What do patents tell us about the implementation of green and sustainable chemistry? *ACS Sustainable Chemistry & Engineering* **2020,** *8* (39), 14657-14667.
(22) Paul Anastas, N. E., Green chemistry: Principles and practice. *Royal Society of Chemistry* **2010,** *39*, 301-312.
(23) Moustafa, E.-S. I., Nonrenewable resources. In *Environmental Geology*, Springer Netherlands: Dordrecht, 1999; pp 436-438.
(24) Robert, T.; Friebel, S., Itaconic acid – A versatile building block for renewable polyesters with enhanced functionality. *Green Chemistry* **2016,** *18* (10), 2922-2934.
(25) Khunnonkwao, P.; Thitiprasert, S.; Jaiaue, P.; Khumrangsee, K.; Cheirsilp, B.; Thongchul, N., The outlooks and key challenges in renewable biomass feedstock utilization for value-added platform chemical via bioprocesses. *Heliyon* **2024,** *10* (10), e30830.
(26) Willke, T.; Vorlop, K. D., Biotechnological production of itaconic acid. *Applied microbiology and biotechnology* **2001,** *56* (3-4), 289-95.
(27) Arti Mahto, S. M., Guar gum grafted itaconic acid: A solution for different waste water treatment. *Journal of Polymers and the Environment* **2021,** *29*.
(28) Kirimura, K.; Honda, Y.; Hattori, T., Gluconic and Itaconic Acids. In *Comprehensive Biotechnology (Second Edition)*, Moo-Young, M., Ed. Academic Press: Burlington, 2011; pp 143-147.
(29) Yang, J.; Xu, H.; Jiang, J.; Zhang, N.; Xie, J.; Wei, M.; Zhao, J., Production of itaconic acid through microbiological fermentation of inexpensive materials. *Journal of Bioresources and Bioproducts* **2019,** *4* (3), 135-142.
(30) Lies Dwiarti, M. O., Shigenobu Miura, Masaaki Yaguchi, Mitsuyasu Okabe, Itaconic acid production using sago starch hydrolysate by Aspergillus terreus TN484-M1. *Bioresource Technology* **2007,** *98* (17), 3329-3337.
(31) Ahmed El-Imam, A. M.; Kazeem, M. O.; Odebisi, M. B.; Oke, M. A.; Abidoye, A. O., Production of itaconic acid from jatropha curcas seed cake by Aspergillus terreus. *Notulae Scientia Biologicae* **2013,** *5* (1), 57-61.
(32) *Itaconic Acid Market - By Derivative (Styrene Butadiene, Methyl Methacrylate, Polyitaconic Acid), By Application (SBR Latex, Synthetic Latex, Chillant Dispersant Agent, Superabsorbent Polymer), & By Region - Global Industry Analysis, Size, Share, Growth, Trends & Forecast | 2022 to 2027*; Market Data Forecast: 2022.
(33) Jain, S.; Kumar, S., A comprehensive review of bioethanol production from diverse feedstocks: Current advancements and economic perspectives. *Energy* **2024,** *296*, 131130.
(34) IEA *Net Zero Roadmap: A Glabl Pathway to Keep the 1.5°C Goal in Reach*; International Energy Agency: Paris, 2023.

(35) Marvel, C. S.; Shepherd, T. H., Polymerization reactions of itaconic acid and some of its derivatives. *The Journal of Organic Chemistry* **1959,** *24* (5), 599-605.
(36) S. Nagai, T. U., K. Yoshida, Studies on polymerizations and polymers of itaconic acid derivatives. *Kobunshi Kagaku* **1958,** *15*, 550--554.
(37) Hidemasa Azuma, Y. K., Shinichi Yamabe, Steric effects upon transition states of radical addition polymerizations. *Polymer Chemistry* **1996,** *34* (8), 1407-1414.
(38) Nagai Susumu, Y. K., The polymerization and polymers of itaconic acid derivatives. Viii. A cation exchange resin from itaconic anhydride. *Bulletin of the Chemical Society of Japan* **1965,** *38* (8), 1402-1403.
(39) Ogo, Y., Polymerizations at high pressures. *Journal of Macromolecular Science, Part C* **1984,** *24* (1), 1-48.
(40) Corrigan, N.; Jung, K.; Moad, G.; Hawker, C. J.; Matyjaszewski, K.; Boyer, C., Reversible-deactivation radical polymerization (Controlled/living radical polymerization): From discovery to materials design and applications. *Progress in Polymer Science* **2020,** *111*, 101311.
(41) Hirano, T.; Takeyoshi, R.; Seno, M.; Sato, T., Chain-transfer reaction in the radical polymerization of Di-n-butyl itaconate at high temperatures. *Journal of Polymer Science Part A: Polymer Chemistry* **2002,** *40*, 2415-2426.
(42) Satoh, K.; Lee, D.-H.; Nagai, K.; Kamigaito, M., Precision synthesis of bio-based acrylic thermoplastic elastomer by raft polymerization of itaconic acid derivatives. *Macromolecular Rapid Communications* **2014,** *35* (2), 161-167.
(43) Singh, M.; Rathi, R.; Singh, A.; Heller, J.; Talwar, G. P.; Kopecek, J., Controlled release of LHRH-DT from bioerodible hydrogel microspheres. *International Journal of Pharmaceutics* **1991,** *76* (3), R5-R8.
(44) Guo, B.; Chen, Y.; Lei, Y.; Zhang, L.; Zhou, W. Y.; Rabie, A. B. M.; Zhao, J., Biobased poly(propylene sebacate) as shape memory polymer with tunable switching temperature for potential biomedical applications. *Biomacromolecules* **2011,** *12* (4), 1312-1321.
(45) Dai, J.; Ma, S.; Liu, X.; Han, L.; Wu, Y.; Dai, X.; Zhu, J., Synthesis of bio-based unsaturated polyester resins and their application in waterborne UV-curable coatings. *Progress in Organic Coatings* **2015,** *78*, 49-54.
(46) J. Retuert, M. Y.-P., F. Martínez, M. Jeria Soluble itaconic acid–ethylene glycol polyesters. *Bulletin of the Chemical Society of Japan* **1993,** *66* (6), 1707-1708.
(47) Barrett, D. G.; Merkel, T. J.; Luft, J. C.; Yousaf, M. N., One-step syntheses of photocurable polyesters based on a renewable resource. *Macromolecules* **2010,** *43* (23), 9660-9667.
(48) Tang, T.; Takasu, A., Facile synthesis of unsaturated polyester-based double-network gels via chemoselective cross-linking using Michael addition and subsequent UV-initiated radical polymerization. *RSC Advances* **2015,** *5* (2), 819-829.
(49) Tzoumani, I.; Soto Beobide, A.; Iatridi, Z.; Voyiatzis, G. A.; Bokias, G.; Kallitsis, J. K., Glycidyl methacrylate-based copolymers as healing agents of waterborne polyurethanes. *International Journal of Molecular Sciences* **2022,** *23* (15).
(50) Cañamero, P.; Fernández-García, M.; de la Fuente, J. L., Adhesives based on poly(glycidyl methacrylate-co-butyl acrylate) with controlled structure: curing behavior and adhesion properties on metal substrates. *Macromolecular Materials and Engineering* **2024,** *309* (2), 2300267.

(51) Fan, Y.; Yin, A.; Li, Y.; Gu, Q.; Zhou, Y.; Zhou, J.; Zhao, R.; Zhang, K., Fabrication of glycidyl methacrylate-modified silk fibroin/poly(L-lactic acid-co-ε-caprolactone)–polyethylene glycol diacrylate hybrid 3D nanofibrous scaffolds for tissue engineering. *Frontiers of Materials Science* **2023,** *17* (2), 230647.
(52) Tran, N.-P.-D.; Yang, M.-C.; Hasanah, N.; Tran-Nguyen, P. L., Effect of poly(ethylene glycol) methacrylate on the ophthalmic properties of silicone hydrogel contact lenses. *Colloids and Surfaces B: Biointerfaces* **2022,** *217*, 112713.
(53) Holmberg, A. L.; Reno, K. H.; Nguyen, N. A.; Wool, R. P.; Epps, T. H., III, Syringyl methacrylate, a hardwood lignin-based monomer for high-Tg polymeric materials. *ACS Macro Letters* **2016,** *5* (5), 574-578.
(54) Kolawole, O. M.; Lau, W. M.; Khutoryanskiy, V. V., Methacrylated chitosan as a polymer with enhanced mucoadhesive properties for transmucosal drug delivery. *International Journal of Pharmaceutics* **2018,** *550* (1), 123-129.
(55) Kong, D.-C.; Yang, M.-H.; Zhang, X.-S.; Du, Z.-C.; Fu, Q.; Gao, X.-Q.; Gong, J.-W., Control of polymer properties by entanglement: A review. *Macromolecular Materials and Engineering* **2021,** *306* (12), 2100536.
(56) Wool, R. P., Polymer entanglements. *Macromolecules* **1993,** *26* (7), 1564-1569.
(57) Everaers, R.; Sukumaran, S. K.; Grest, G. S.; Svaneborg, C.; Sivasubramanian, A.; Kremer, K., Rheology and microscopic topology of entangled polymeric liquids. *Science* **2004,** *303* (5659), 823-826.
(58) Hiss, R.; Hobeika, S.; Lynn, C.; Strobl, G., Network stretching, slip processes, and fragmentation of crystallites during uniaxial drawing of polyethylene and related copolymers. A comparative study. *Macromolecules* **1999,** *32* (13), 4390-4403.
(59) van Melick, H. G. H.; Govaert, L. E.; Meijer, H. E. H., On the origin of strain hardening in glassy polymers. *Polymer* **2003,** *44* (8), 2493-2502.
(60) Pawlak, A.; Krajenta, J., Entanglements of macromolecules and their influence on rheological and mechanical properties of polymers. *Molecules* **2024,** *29* (14).
(61) Fetters, L. J.; Lohse, D. J.; Milner, S. T.; Graessley, W. W., Packing length influence in linear polymer melts on the entanglement, critical, and reptation molecular weights. *Macromolecules* **1999,** *32* (20), 6847-6851.
(62) Spyriouni, T.; Tzoumanekas, C.; Theodorou, D.; Müller-Plathe, F.; Milano, G., Coarse-grained and reverse-mapped united-atom simulations of long-chain atactic polystyrene melts: Structure, thermodynamic properties, chain conformation, and entanglements. *Macromolecules* **2007,** *40* (10), 3876-3885.
(63) Chatterjee, D. P.; Mandal, B. M., Triblock thermoplastic elastomers with poly(lauryl methacrylate) as the center block and poly(methyl methacrylate) or poly(tert-butyl methacrylate) as end nlocks. Morphology and thermomechanical properties. *Macromolecules* **2006,** *39* (26), 9192-9200.
(64) Gilbert, M., Relation of Structure to Thermal and Mechanical Properties. In *Brydson's Plastics Materials (Eighth Edition)*, Gilbert, M., Ed. Butterworth-Heinemann: 2017; pp 59-73.
(65) Alarifi, I. M., Synthetic polymers. In *Synthetic Engineering Materials and Nanotechnology*, Alarifi, I. M., Ed. Elsevier: 2022; pp 33-58.
(66) Yang, X.; Guo, L.; Xu, X.; Shang, S.; Liu, H., A fully bio-based epoxy vitrimer: Self-healing, triple-shape memory and reprocessing triggered by dynamic covalent bond exchange. *Materials & Design* **2020,** *186*, 108248.

(67) Moreno, A.; Morsali, M.; Sipponen, M. H., Catalyst-free synthesis of lignin vitrimers with tunable mechanical properties: Circular polymers and recoverable adhesives. *ACS Applied Materials & Interfaces* **2021,** *13* (48), 57952-57961.
(68) Zhao, S.; Abu-Omar, M. M., Catechol-mediated glycidylation toward epoxy vitrimers/polymers with tunable properties. *Macromolecules* **2019,** *52* (10), 3646-3654.
(69) Singh, G.; Varshney, V.; Sundararaghavan, V., Understanding creep in vitrimers: Insights from molecular dynamics simulations. *Polymer* **2024,** *313*, 127667.
(70) Meng, F.; Saed, M. O.; Terentjev, E. M., Rheology of vitrimers. *Nature Communications* **2022,** *13* (1), 5753.
(71) Montoya-Ospina, M. C.; Verhoogt, H.; Ordner, M.; Tan, X.; Osswald, T. A., Effect of cross-linking on the mechanical properties, degree of crystallinity and thermal stability of polyethylene vitrimers. *Polymer Engineering & Science* **2022,** *62* (12), 4203-4213.
(72) Zhu, L.; Xu, L.; Jie, S.; Li, B., Polybutadiene vitrimers with tunable epoxy ratios: Preparation and properties. *Polymers* **2021,** *13* (23).
(73) Li, L.; Chen, X.; Jin, K.; Torkelson, J. M., Vitrimers designed both to strongly suppress creep and to recover original cross-link density after reprocessing: Quantitative theory and experiments. *Macromolecules* **2018,** *51* (15), 5537-5546.
(74) Wang, S.; Ma, S.; Li, Q.; Xu, X.; Wang, B.; Huang, K.; liu, Y.; Zhu, J., Facile preparation of polyimine vitrimers with enhanced creep resistance and thermal and mechanical properties via metal coordination. *Macromolecules* **2020,** *53* (8), 2919-2931.
(75) Formon, G. J. M.; Storch, S.; Delplanque, A. Y. G.; Bresson, B.; Van Zee, N. J.; Nicolaÿ, R., Overcoming the tradeoff between processability and mechanical performance of elastomeric vitrimers. *Advanced Functional Materials* **2023,** *33* (52), 2306065.
(76) Lessard, J. J.; Scheutz, G. M.; Sung, S. H.; Lantz, K. A.; Epps, T. H., III; Sumerlin, B. S., Block copolymer vitrimers. *Journal of the American Chemical Society* **2020,** *142* (1), 283-289.
(77) Ishibashi, J. S. A.; Pierce, I. C.; Chang, A. B.; Zografos, A.; El-Zaatari, B. M.; Fang, Y.; Weigand, S. J.; Bates, F. S.; Kalow, J. A., Mechanical and structural consequences of associative dynamic cross-linking in acrylic diblock copolymers. *Macromolecules* **2021,** *54* (9), 3972-3986.
(78) Fang, H.; Gao, X.; Zhang, F.; Zhou, W.; Qi, G.; Song, K.; Cheng, S.; Ding, Y.; Winter, H. H., Triblock elastomeric vitrimers: Preparation, morphology, rheology, and applications. *Macromolecules* **2022,** *55* (24), 10900-10911.
(79) Hanifah, A.; Arfiathi; Mahardika, M.; Sumirat, R.; Nissa, R. C.; Nurhamiyah, Y., Recent Updates on Biopolymers: Precursors, Process, Properties, Challenge, and Future Perspectives. In *Biomass Conversion and Sustainable Biorefinery: Towards Circular Bioeconomy*, Springer Nature Singapore: Singapore, 2024; pp 19-42.
(80) Shen, L.; Worrell, E.; Patel, M., Present and future development in plastics from biomass. *Biofuels, Bioproducts and Biorefining* **2010,** *4* (1), 25-40.
(81) da Silva Pens, C. J.; Klug, T. V.; Stoll, L.; Izidoro, F.; Flores, S. H.; de Oliveira Rios, A., Poly (lactic acid) and its improved properties by some modifications for food packaging applications: A review. *Food Packaging and Shelf Life* **2024,** *41*, 101230.
(82) Asempour, F.; Marić, M., Vitrification: Versatile method to modulate properties of myrcene-based rubbers. *ACS Applied Polymer Materials* **2023,** *5* (8), 6364-6376.

(83) Yue, L.; Bonab, V. S.; Yuan, D.; Patel, A.; Karimkhani, V.; Manas-Zloczower, I., Vitrimerization: A novel concept to reprocess and recycle thermoset waste via dynamic chemistry. *Global Challenges* **2019,** *3* (7), 1800076.
(84) Al-Salem, S. M.; Lettieri, P.; Baeyens, J., Recycling and recovery routes of plastic solid waste (PSW): A review. *Waste Management* **2009,** *29* (10), 2625-2643.
(85) Dubois, M.; Bibas, R.; Fouré, J., Plastics flows and their impacts on the environment. In *Global Plastics Outlook*, OECD Publishing: Paris, 2022.
(86) Tsuchimoto, I.; Kajikawa, Y., Recycling of plastic waste: A systematic review using bibliometric analysis. *Sustainability* **2022,** *14* (24).
(87) Mavroeidi, E.; Dubois, M.; Dellink, R.; Bibas, R.; Lanzi, E., Plastic waste projections to 2060. In *Global Plastics Outlook*, OECD Publishing: Paris, 2022.

Appendix A: Supporting Information to Chapter 3

A1 Experimental Methods

A1.1 Materials and Reagents

All materials purchased were reagent grade. Azobisisobutyronitrile (AIBN, Millipore Sima, ≥98.0%) was recrystallized from methanol and dried in vacuum before being used. Methyl methacrylate (MMA, ≥99.0%, Millipore Sigma) and styrene (≥99.0%, Millipore Sigma) were passed through a column of basic alumina mixed with 5 wt% calcium hydride to remove inhibitors before being used. 2-cyano-2-propyl benzodithioate (RAFT agent) was purchased from Sigma Aldrich. BlocBuilder™ (alkoxyamine for NMP) was obtained from Arkema. 1-heptanol (≥99.9%, Oleris) was purchased from Arkema. Bis(pinacolato)diboron (B_2Pin_2, ≥99.0%) was purchased from Chem Impex. Itaconic acid (IA, ≥99.0%), benzyl alcohol (≥99.0%), butylated hydroxytoluene (BHT, ≥99.0%), *para*-toluene sulfonic acid monohydrate (pTSOH·H_2O, ≥99.0%), benzyl alcohol (≥99.0%), anhydrous magnesium sulfate ($MgSO_4$, ≥97.0%), copper (I) chloride (CuCl, ≥99.0%), sodium tert-butoxide (NaOtBu, ≥97.0%), sodium perborate tetrahydrate ($NaBO_3 \cdot 4H_2O$, ≥96.0%), methacryloyl chloride (≥97.0%), triethylamine (≥99.5%), ethyl α-bromoisobutyrate (EbiB, ≥98%), copper (I) bromide (CuBr, ≥99%), N,N,N′,N″,N″-pentamethyldiethylenetriamine (PMDETA, ≥99%), anhydrous tetrahydrofuran (THF, ≥99.9%), deuterated chloroform ($CDCl_3$, ≥99.0%), silica gel 60 (230-400 Mesh ASTM) and celite were all purchased from Millipore Sigma. Bis[(2-diphenylphosphino)phenyl] ether (DPEPhos, ≥98.0%), tetrahydrofuran (THF, HPLC grade), methanol (≥99.8%), ethyl acetate (≥99.0%), hexanes (≥99.0%), dichloromethane (≥99.8%), toluene (≥99.0%), and 1,4-dioxane (≥99.0%) were all purchased from Fisher Scientific.

A1.2 ^{1}H NMR Spectroscopy

^{1}H NMR spectra were obtained using a Bruker AVIIIHD 500 MHz Spectrometer using an average of 16 scans in deuterated chloroform ($CDCl_3$) at room temperature.

A1.3 Gel Permeation Chromatography

Samples for gel permeation chromatography were run on two independent instruments.

For samples collected during the polymerizations for kinetic analysis, the molecular weight and dispersity was collected using gel permeation chromatography (Waters Breeze) calibrated with

narrow molecular weight distribution MMA) standards. HPLC grade THF at a flowrate of 0.3mL/min was used as the mobile phase for detection by a differential refractive index detector (RI 2414). The instrument was equipped with three Waters Styragel HR columns which were heated to 40°C during the analysis. The Mark-Houwink-Sakurada equation was not applied for the analysis of these samples, and the resulting molecular weight and dispersity data is therefore relative to the calibration from the p(MMA) standards. The p(MMA) standards obtained from Varian ranged from 2 710 g/mol to 1 677 000 g/mol.

For final polymers the samples were first dried under reduced pressure at 70°C overnight to remove any moisture. The following day, solutions of the samples were prepared in HPLC grade THF in concentrations of approximately 2 mg/mL, and these solutions were then allowed to fully dissolve overnight in the fridge. The samples were then filtered through 2 μm filters and added to an Agilent 1260 Infinity II multidetector suite system equipped with refractive index and multi-angle light scattering detector. Calibration of the system was completed using Varian narrow p(MMA) standards (2 710 g/mol to 1 677 000 g/mol). This system had two Polypore separation columns, set at 40°C and a flowrate of 0.3 mL/min with HPLC grade THF as the eluent. Determination of absolute molecular weight and *dn/dc* by light scattering using the Agilent software assumed all the injected sample mass eluted from the column and was contained within the integration peak of the sample.

A1.4 Differential Scanning Calorimetry

The glass transition temperatures for the sets of polymers were determined by differential scanning calorimetry using a TA Instruments Discovery 2500 under a nitrogen atmosphere, following a heat/cool/heat cycle. The samples were equilibrated at -90°C for 5 minutes before being heated to 20°C at a rate of 2°C/min, held at 20°C for 5 minutes, and cooled back to -90°C at a rate of 2°C/min. They were then once again held at -90°C for 5 minutes and then heated a final time to 20°C at 2°C/min. The glass transition temperature was taken from the second heating cycle using the glass/step transition analysis tool in the TA Instruments Universal Analysis 2000 software where the inflection point is reported as the glass transition temperature.

A1.5 Thermal Gravimetric Analysis

The thermal stability of the synthesized polymers was evaluated using a TA Instruments Discovery 5500 instrument under a nitrogen flowrate of 25 mL/min. Samples were loaded onto

platinum sample pans, and heated from 25 to 700°C at a rate of 10°C/min. The onset temperature at a weight loss of 10% is reported, obtained from using the weight loss at temperature tool in the TA Instruments TRIOS software.

A1.6 Rheology

Prior to rheological assessment, the samples were dried under vacuum for 48 hours at 40°C. An Anton Paar MCR 302 instrument was used for rheology and viscosity tests, equipped with a 25 mm parallel plate sample mount. Samples were added to the parallel plate apparatus using a spatula, except for MbH1 which was first hot-pressed into a disk shape due to being more rigid. Frequency sweep tests were performed at a strain of 0.1%, and the samples were allowed to equilibrate at the testing temperature for 10 minutes before being run.

A1.7 Thin Film Preparation

Approximately 0.2 g of diblock polymer samples were dissolved in minimal amounts of THF, and then applied using a glass pipette onto a glass microscope plate. The samples were then added to an oven at 120°C and ambient pressure for 3 hours, after which reduced pressure was applied. The oven was then turned off and allowed to cool to room temperature overnight.

A1.8 Small Angle X-RAY Scattering

SAXS patterns were obtained on a SAXSpoint 2.0 (Anton Paar) instrument using a Cu Ka radiation source with an Eiger R 1M horizontal detector. The detector was set at 557 mm, with the radiation source giving a wavelength of 1.54 Å. The thin film samples were laid onto 10 mm x10 mm sample holders obtained from Anton Paar. The samples were exposed to X-Rays for 20 minutes per frame, for a total of three frames per sample; The SAXS patterns were corrected and given as a function of the scattering vector ($q=(4\pi/\lambda)sin\theta$, with 2θ being the scattering angle in degrees (°) and q in nm^{-1}).

A1.9 Synthesis of Monomer

An overview of the first synthesis step is shown in Schematic A1.

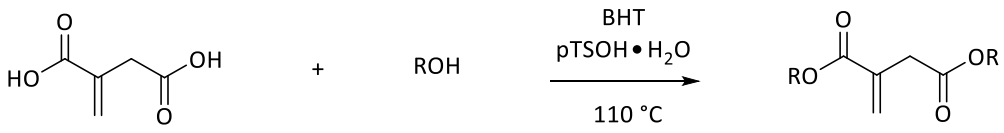

Schematic A1. Functionalization of itaconic acid via dehydration.

Step 1. Itaconic acid (23.74 g, 182.5 mmol, 1 eq.) was added to a 250 mL three-necked round bottom flask containing a magnetic Teflon stir bar along with *para*-toluene sulfonic acid monohydrate (pTSOH·H_2O) (2.37g, 10 wt% of itaconic acid) and butylated hydroxytoluene (BHT) (237 mg, 1wt% of itaconic acid). 1-heptanol (52.85 mL, 374.1 mmol, 2.05 eq.) was subsequently added and the flask was heated at 110°C under strong nitrogen bubbling for 2.5 hours via an oil bath, while connected to a Dean-Stark apparatus. The mixture was then cooled to room temperature and diluted with 400 mL of ethyl acetate in a separatory funnel. This organic fraction was first washed with 400 mL of saturated $NaHCO_3$ solution then 400 mL of brine, before being dried with $MgSO_4$, and filtered. Excess solvent was removed by rotary evaporation to obtain diheptyl itaconate (55.49 g, 170.0 mmol) as a colourless oil with 93% yield.

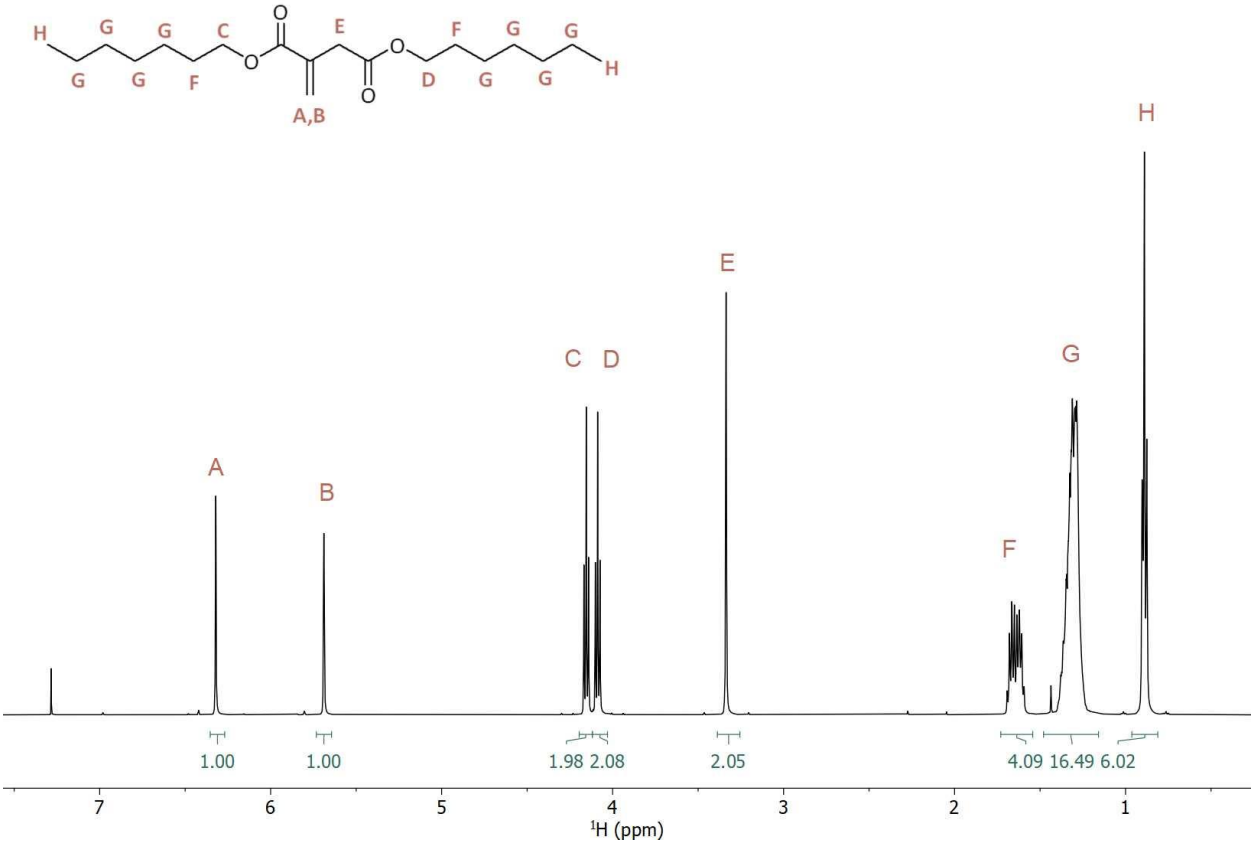

Figure A1. ^{1}H NMR of diheptyl itaconate: δ 6.32 (A) (s, 1H), 5.69 (B) (s, 1H), 4.15 (C) (t, 2H), 4.09 (D) (t, 2H), 3.34 (E) (s, 2H), 1.65 (F) (m, 4H), 1.31 (G) (m, 16H), 0.89 (H) (t, 6H).

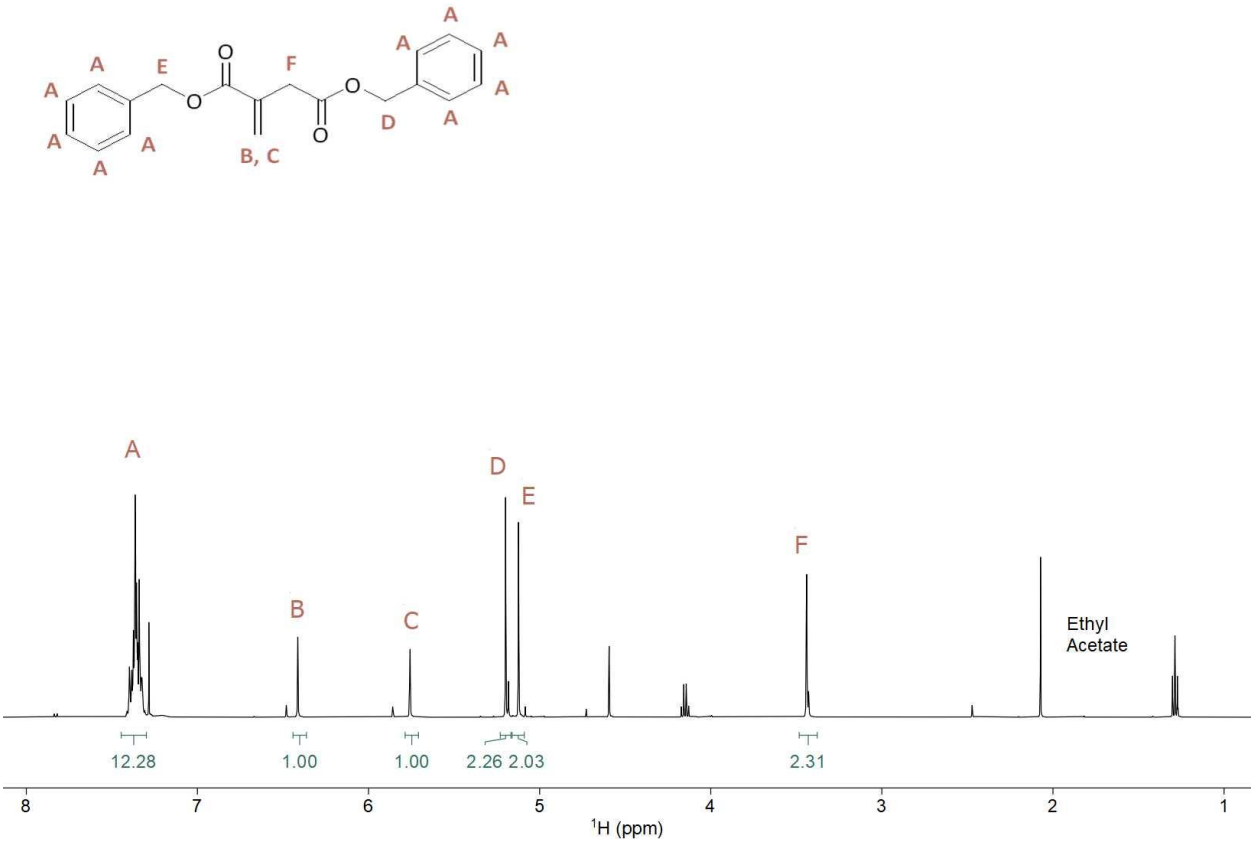

Figure A2. ^{1}H NMR of dibenzyl itaconate: δ 7.36 (A) (m, 10H), 6.41 (B) (s, 1H), 5.76 (C) (s, 1H), 3.43 (F) (d, 2H).

An overview of the second synthesis step is shown in Schematic A2.

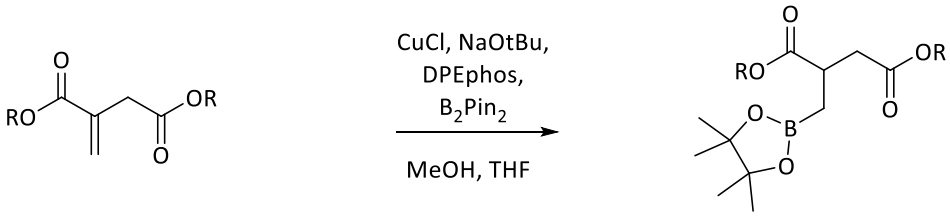

Schematic A2. Boration of the itaconic acid derivative.

Step 2. To a flame-dried and nitrogen-purged 250 mL round bottom flask containing a magnetic Teflon stir bar was added copper chloride (178.2 mg, 1.8 mmol, 0.06 eq.), sodium tert-butoxide (518.9 mg, 5.4 mmol, 0.18 eq.), bis[(2-diphenylphosphino)phenyl] ether (1.050 g, 1.8 mmol, 0.06 eq.) and lastly anhydrous tetrahydrofuran (60mL) before being stirred for 30 minutes under a

nitrogen atmosphere. Bis(pinacolato)diboron (8.380 g, 33 mmol, 1.1 eq.) was added with the remaining anhydrous tetrahydrofuran (30 mL) and stirred for 10 minutes. Previously synthesized diheptyl itaconate (9.794 g, 30 mmol, 1 eq.) was added with methanol[1] (4.87 mL, 120 mmol, 4 eq.) and left under nitrogen to stir overnight. The mixture was passed through a bed of celite the following day, and the solvent removed by rotary evaporation to yield a pale blue oil containing the excess bis(pinacolato)diboron. The product was used without further purification.

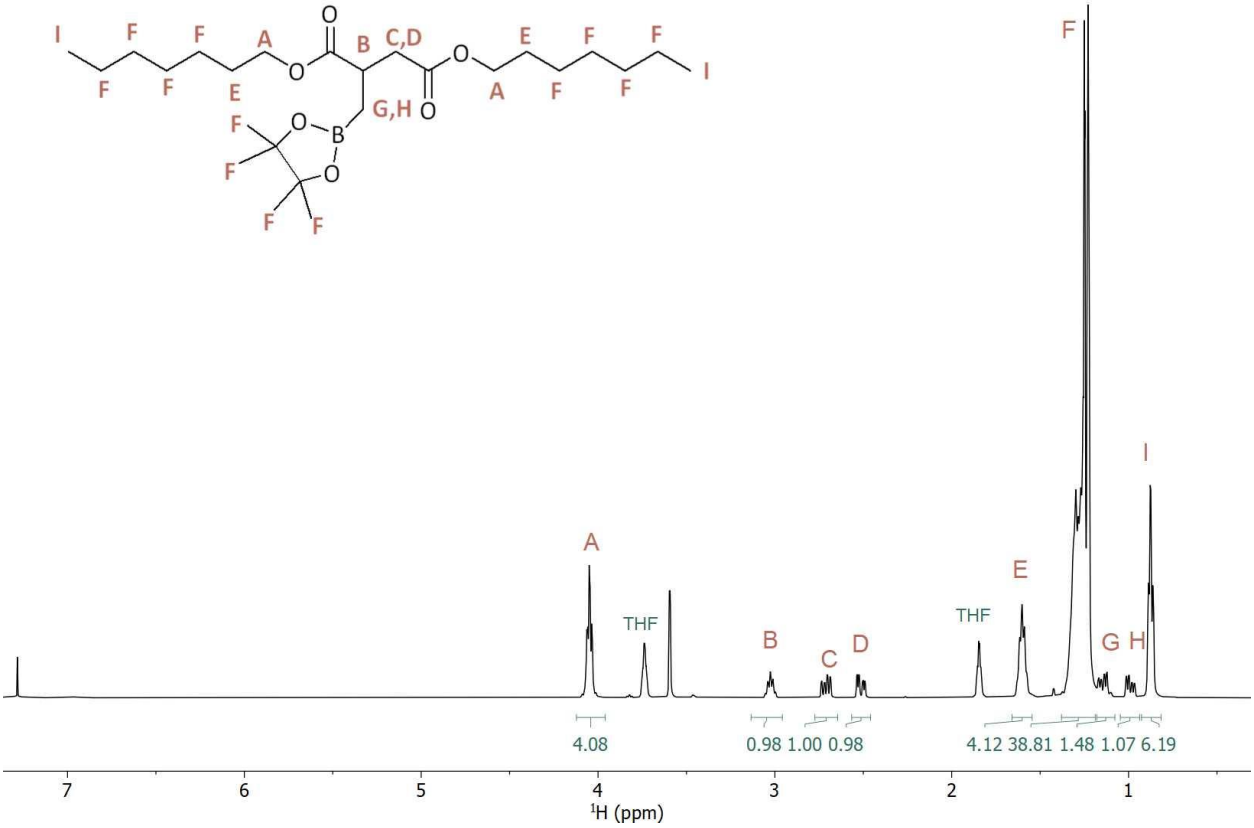

Figure A3. [1]H NMR of borated diheptyl itaconate: δ 4.05 (A) (td, 4H), 3.02 (B) (m, 1H), 2.71 (C) (dd, 1H), 2.51 (D) (dd, 1H), 1.61 (E) (q, 4H), 1.24 (F) (m, 16H), 1.15 (G) (dd, 1H), 0.99 (H) (dd, 1H), 0.88 (I) (td, 6H).

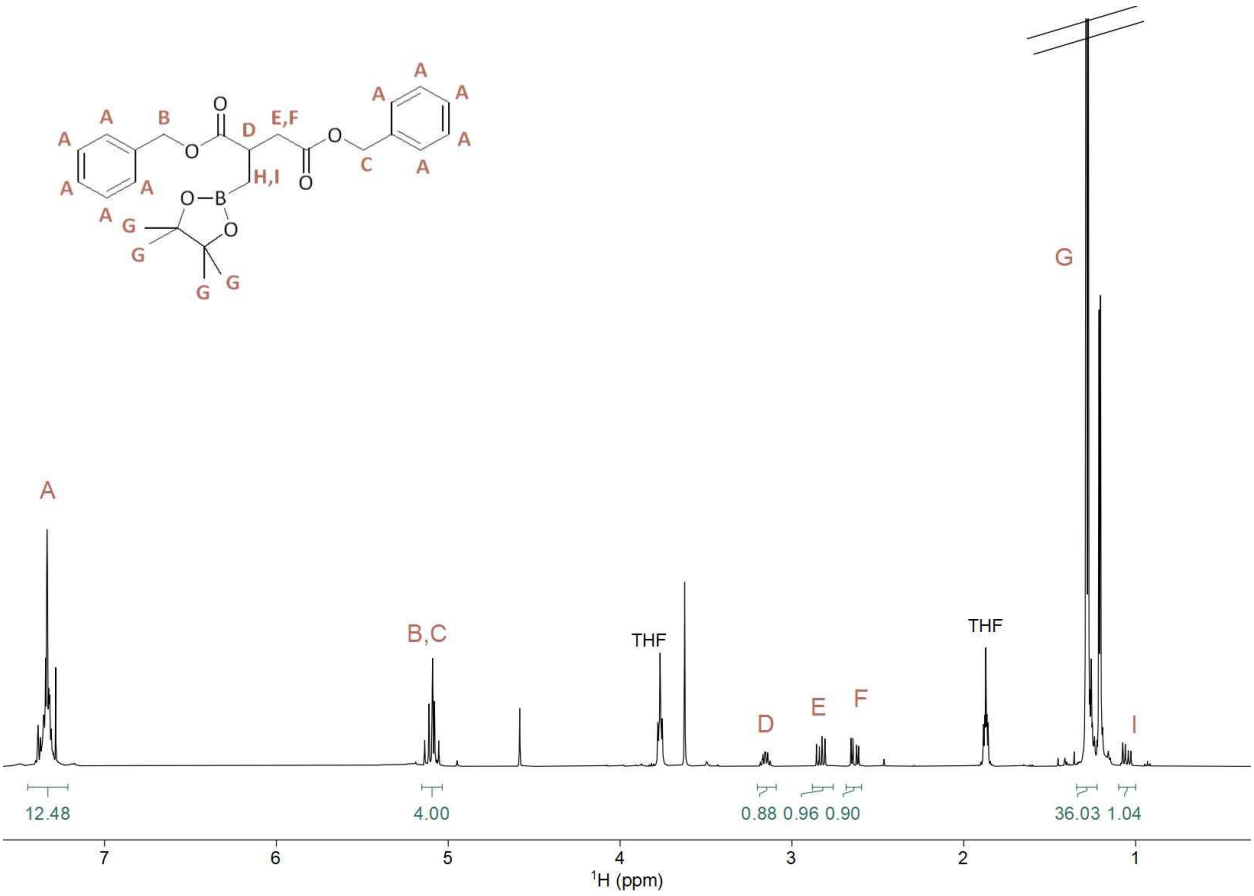

Figure A4. ^{1}H NMR of borated dibenzyl itaconate: δ 7.34 (A) (m, 10H), 5.09 (B, C) (m, 4H), 3.16 (D) (m, 1H), 2.83 (E) (dd, 1H), 2.63 (F) (dd 1H), 1.28 (G) (m, 12H), 1.05 (I) (dd, 1H).

An overview of the third synthesis step is shown in Schematic A3.

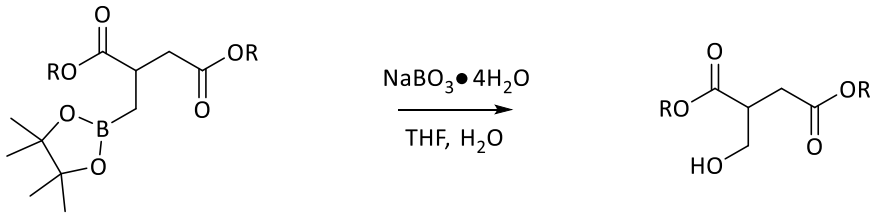

Schematic A3. Oxidation of borated adduct.

Step 3. The adduct from S2 (15 mmol, 1 eq.) was dissolved in tetrahydrofuran (60 mL) and reverse osmosis water (60 mL) in a 250 mL round bottom flask, to which was added sodium perborate tetrahydrate (6.924 g, 45 mmol, 3 eq.) and then stirred for 1.5 hours. The reaction was quenched by the addition of 90 mL reverse osmosis water and washed with 120 mL of brine, then extracted with 180 mL of ethyl acetate. Two more extractions of the aqueous phase were completed

using 120 mL of ethyl acetate. The combined organic fractions were washed with 150 mL of brine, before being dried with $MgSO_4$, filtered, and the excess solvent removed by rotary evaporation to obtain a yellow-green oil. Purification by column chromatography at 70:30 hexanes:ethyl acetate was monitored by thin line chromatography to isolate a colourless oil as the product (3.3 g, 9.58 mmol) in a 63.9 % yield across both Step 2 and Step 3.

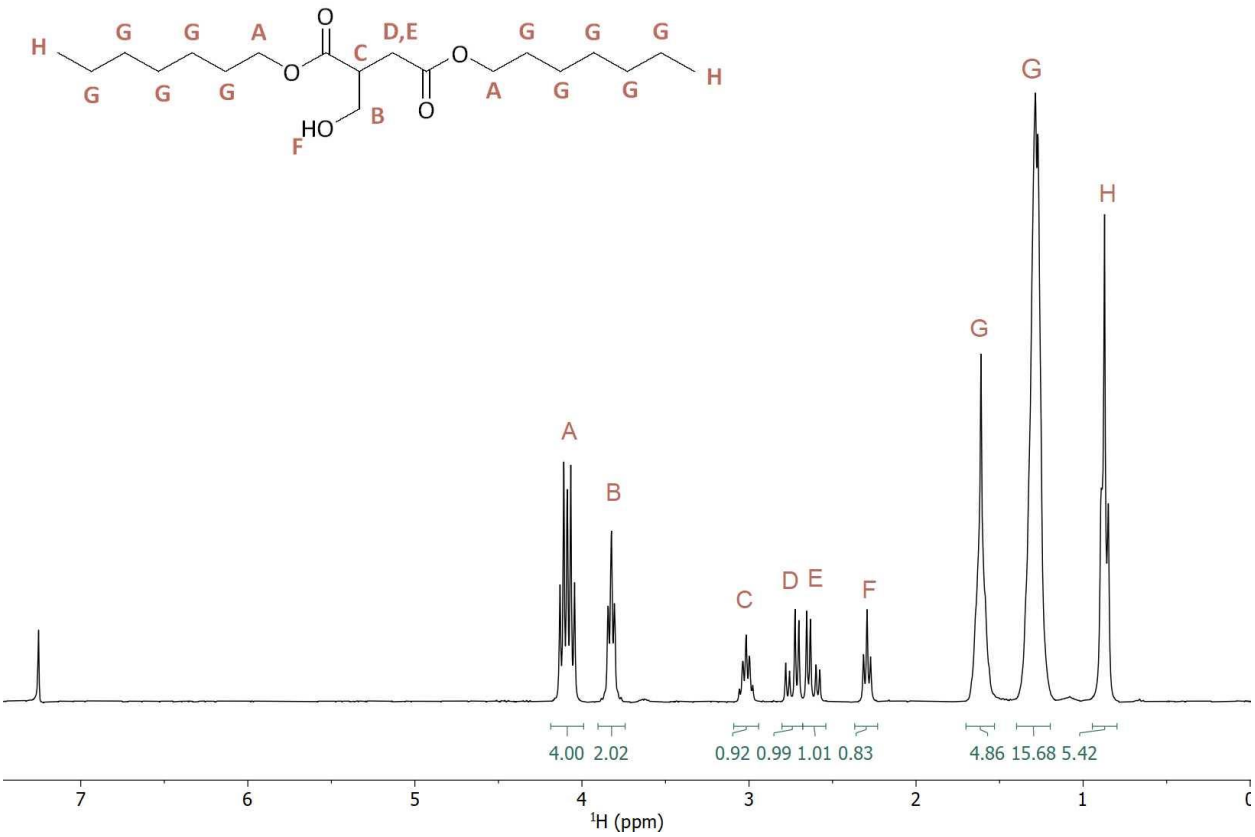

Figure A5. ^{1}H NMR of oxidized diheptyl itaconate: δ 4.09 (A) (dt, 4H), 3.82 (B) (t, 2H), 3.02 (C) (p, 1H), 2.72 (D) (dd, 1H), 2.62 (E) (dd, 1H), 2.29 (F) (t, 1H), 1.20-1.72 (G) (m, 20H), 0.88 (H) (m, 6H).

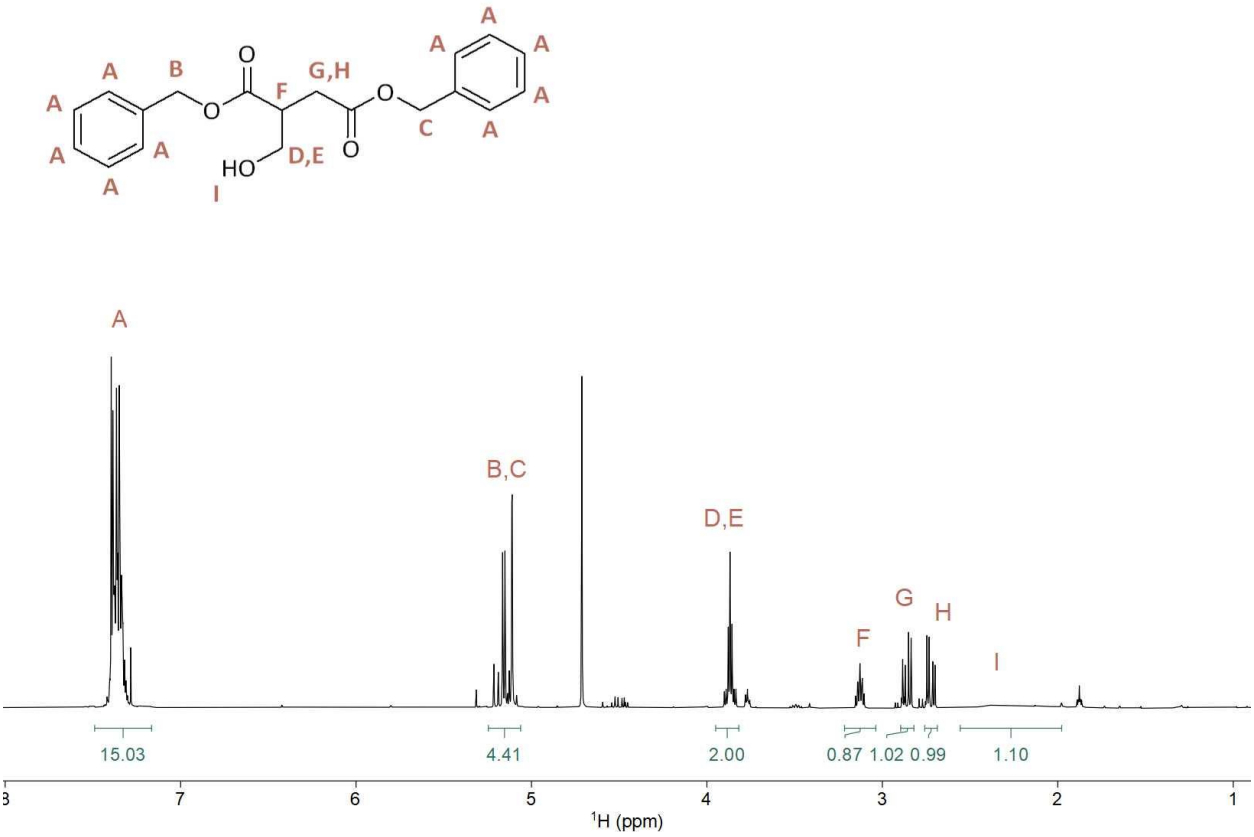

Figure A6. ^{1}H NMR of oxidized dibenzyl itaconate: δ 7.36 (A) (m 10H), 5.15 (B, C) (m 4H), 3.86 (D, E) (h, 2H), 3.13 (F) (tt, 1H), 2.86 (G) (dd, 1H), 2.72 (H) (dd, 1H), 1.98-2.58 (I) (br, 1H).

An overview of the fourth synthesis step is shown in Schematic A4.

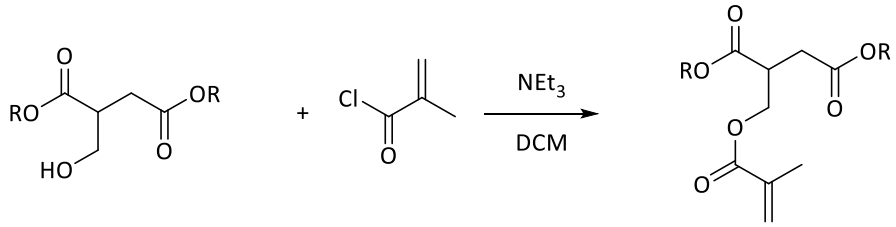

Schematic A4. Methacyrylation of oxidized itaconate.

Step 4. To a flame dried 1000 mL reactor containing a magnetic stir bar, 370 mL of dichloromethane was added, and subsequently cooled in an ice bath. The educt from S3 (17.47 g, 50.7 mmol, 1 eq.) was then dissolved into the solvent, and triethylamine was added (13.5 mL, 96.3 mmol, 1.9 eq.). Methacryloyl chloride (5.95 mL, 60.8 mmol, 1.2 eq.) was then added dropwise, and the mixture was allowed to warm to room temperature while being stirred overnight. The

reaction was quenched the following day by the addition of 150 mL of saturated $NaHCO_3$ solution. The resulting aqueous phase was extracted twice more with 150 mL of dichloromethane each time, and the combined organic phases washed with 150 mL of brine before being dried with anhydrous $MgSO_4$ and filtered. Evaporation of excess solvent by rotary evaporation produced a peach hued oil that was purified by column chromatography using hexanes: ethyl acetate at 70:30, in which the product was the first to elute from the column as a colourless oil yielding 76.2% (15.94 g, 38.6 mmol).

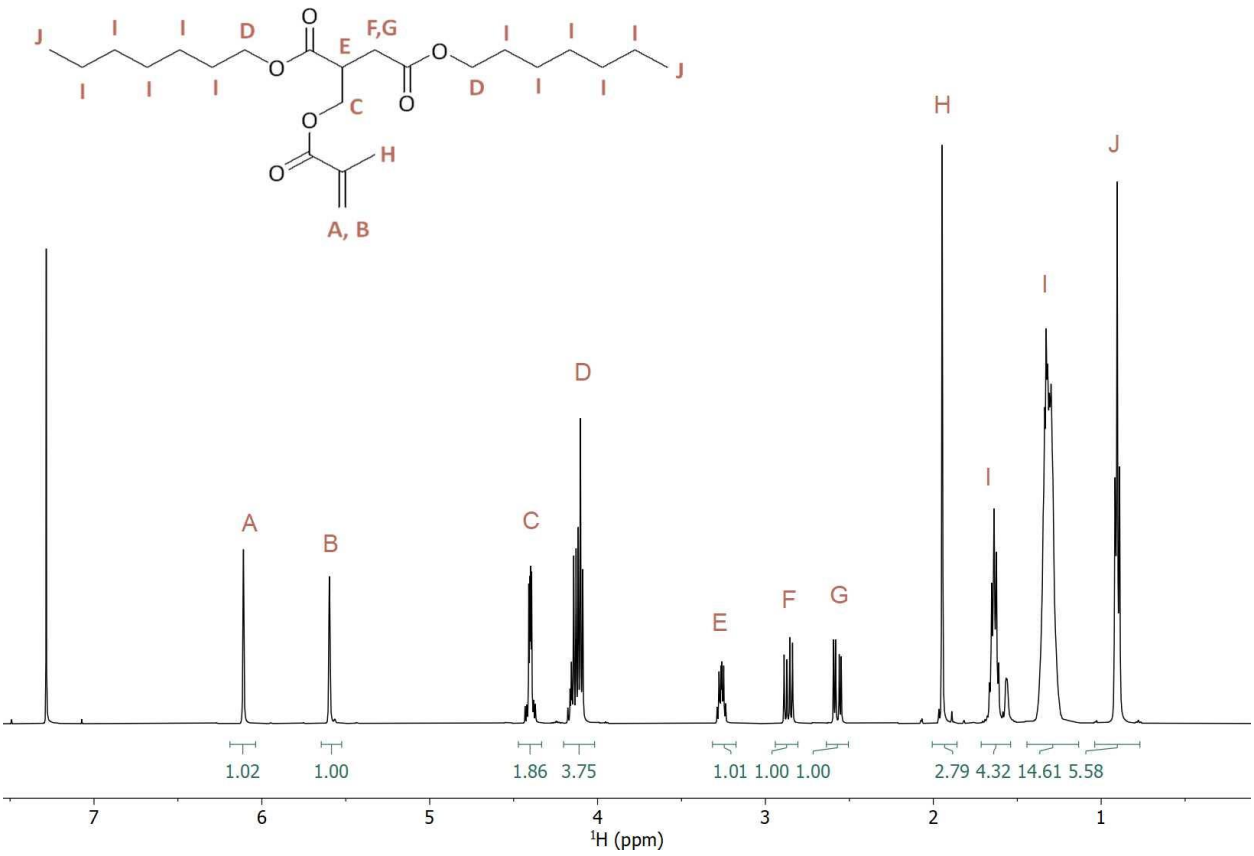

Figure A7. ^{1}H NMR of diheptyl itaconyl methacrylate: δ 6.11(A) (s, 1H), 5.6 (B) (s, 1H), 4.40 (C) (m, 2H), 4.12 (D) (dt, 4H), 3.26 (E) (dq, 1H), 2.86 (F) (dd, 1H), 2.57 (G) (dd, 1H), 1.95 (H) (s, 3H), 1.20-1.72 (I) (m, 20H), 0.91 (J) (td, 6H).

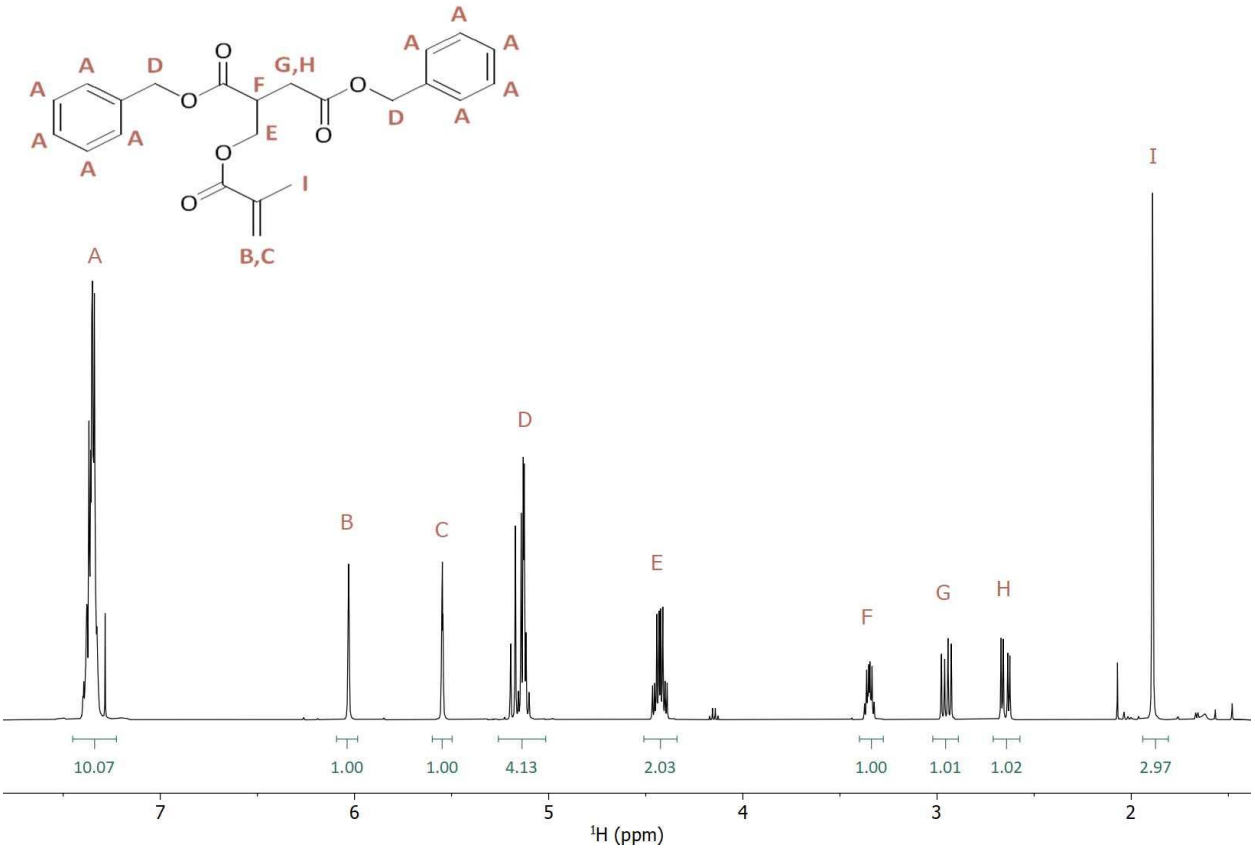

Figure A8. ^{1}H NMR of dibenzyl itaconyl methacrylate: δ 7.36 (A) (m, 10H), 6.03 (B) (s, 1H), 5.55 (C) (s, 1H), 5.15 (D) (m, 4H), 4.43 (E) (qd, 2H), 3.35 (F) (m, 1H), 2.95 (G) (dd, 1H), 2.65 (H) (dd, 1H), 1.89 (I) (s, 3H).

A1.10 Nitroxide Mediated Polymerization of DHIAMA

An overview of the polymerization is given in Schematic A5.

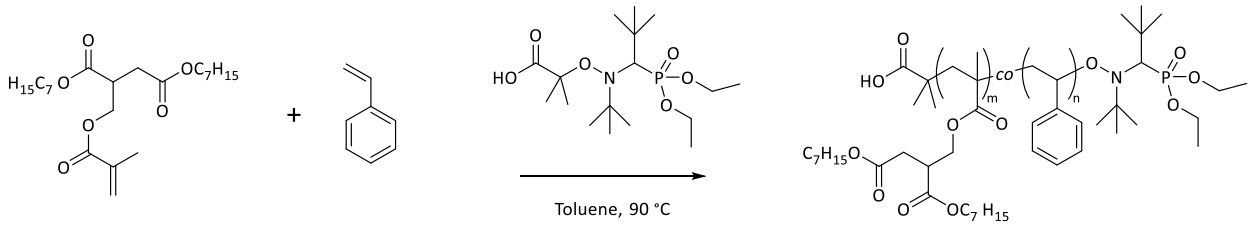

Schematic A5. Polymerization conditions via nitroxide mediated polymerization.

BlocBuilder was used as the nitroxide initiator and radical source during the nitroxide mediated polymerization of DHIAMA. Due to its methacrylic structure, styrene was used as a comonomer

in small amounts ~ 10 mol% with DHIAMA to impart control over the nitroxide mediated polymerization[2]. For the synthesis of the polymer, DHIAMA (1.466 g, 3.55 mmol), styrene (41 mg, 0.39 mmol), and BlocBuilder (23 mg, 0.06 mmol) were dissolved in an equivalent mass of toluene (1.76 mL) in a 10 mL three-neck round-bottom flask containing a magnetic stir bar, and fitted to a reflux condenser. Nitrogen gas was purged through the solution for 30 minutes before the flask was placed in an oil bath preheated to 90°C for 6 hours. Samples for ^{1}H NMR and GPC were taken periodically for kinetic analysis. The reaction was stopped by removing the flask from the oil bath and allowing the solution to cool to room temperature before being precipitated three times with methanol from THF. The resulting viscous liquid was dried overnight under reduced pressure at 40°C.

A1.11 Atom Transfer Radical Polymerization of DHIAMA

An overview of the polymerization is given in Schematic A6.

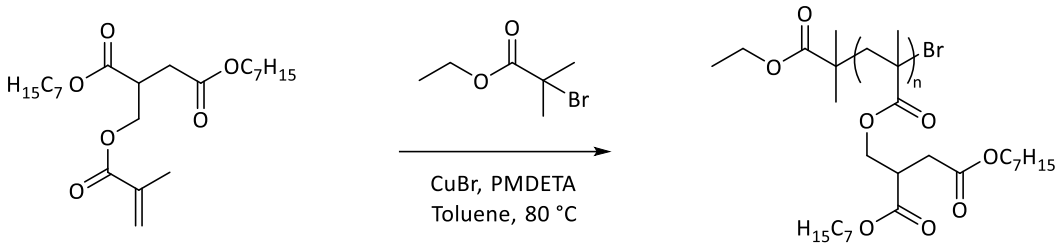

Schematic A6. Polymerization conditions via atom transfer radical polymerization.

A standard method of ATRP was employed to synthesize a homopolymer of DHIAMA. The target degree of polymerization, representing the number of repeat monomer units, was set to 50, with the degree of polymerization: ligand: catalyst: initiator ratio set to 1:1:0.5:1. For the synthesis, half the total volume of solvent dioxane (1.15 mL) was added into a 10mL three-necked-flask, to which the catalyst copper I bromide (4 mg, 0.027 mmol) and ligand PMDETA (9.6 mg, 0.055 mmol) were weighed in, and stirred by a magnetic stir bar under nitrogen purge for 15 minutes. Atop this setup was a reflux condenser. The DHIAMA (1.15 g, 2.78 mmol), remaining solvent (final solution 50wt% monomer and solvent) and initiator EBiB (10.8 mg, 0.055 mmol) were then introduced to the reactor, and the mixture was left to purge for an additional 15 minutes. To start the reaction, the three-necked-flask was submerged halfway into an oil bath preheated to 80°C. Samples for GPC and NMR were taken throughout the reaction to permit kinetic analysis. The

reaction was stopped by removing the reactor from the oil bath, with the polymer then being precipitated 3 times by methanol and THF.

A1.12 Reversible Addition Fragmentation Chain Transfer Polymerization of DHIAMA

An overview of the polymerization is given in Schematic A7.

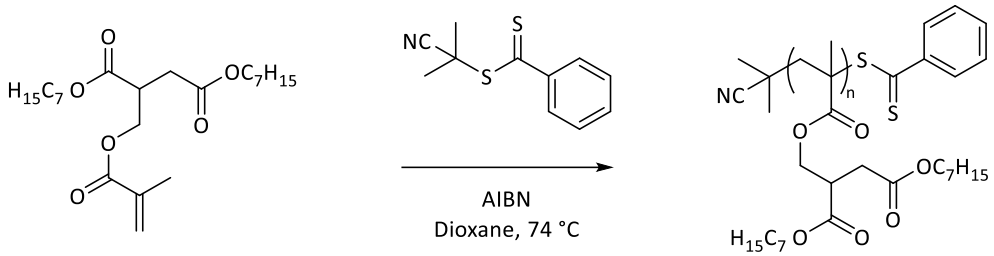

Schematic A7. Polymerization conditions via reversible addition-fragmentation chain transfer.

Reversible addition-fragmentation chain transfer polymerization was selected for the synthesis of the homopolymer series, for its ability to produce nearly monodisperse polymers with active chain ends. Having high control over the degree of polymerization and maintaining a low dispersity renders it favourable for producing samples where the molecular weight dependance of properties can be studied.

Aside from the runtime, reaction conditions were maintained constant for the homopolymer series. As an example for DH-20k, the reaction setup began with the addition of DHIAMA (1 g, 2.42 mmol), the chain transfer agent 2-cyano-2-propyl benzodithioate (11.19 mg, 0.051 mmol), the initiator AIBN (1.66 mg, 0.010 mmol) and the solvent, dioxane (2 mL, to reach a volumetric solution ratio of 1:2 for monomer: solvent), to a 10 mL three-necked-flask. A magnetic stir bar was added to the flask, and the mixture was stirred under nitrogen purge for 30 minutes before being added to a preheated oil bath at 72°C to begin the reaction. Samples for GPC and NMR were taken throughout to allow for kinetic analysis, and the reaction was terminated by removing the flask from the oil bath and cooling the mixture. Polymers were obtained by being precipitated three times using methanol and THF.

A1.13 Block Copolymer Synthesis

An overview of the two-step polymerization is given in Schematic A8.

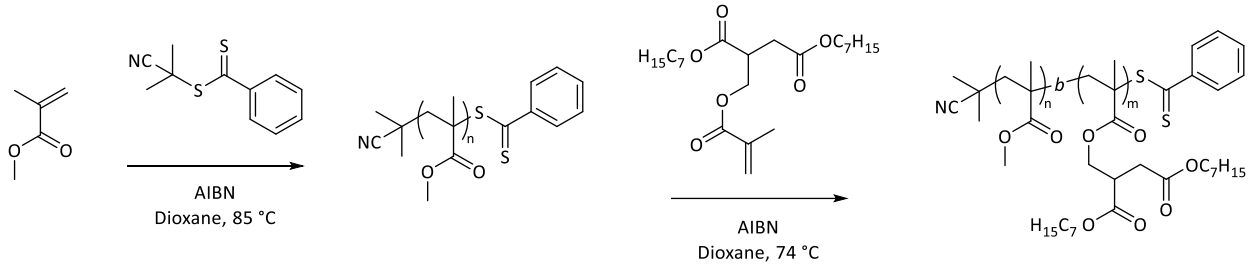

Schematic A8. Two-step polymerization conditions of diblock copolymers via reversible addition-fragmentation chain transfer.

Preparation of the macro-RAFT CTA agent was completed following the method outlined in Section A1.12 above, using methyl methacrylate (MMA) as the monomer, a volumetric solution volume of 1:1 (monomer:dioxane) and a temperature of 85°C. Following three precipitation cycles, the macro-RAFT agent was then dried in a fume hood for 24 hours and then under reduced pressure at 40°C for 24 hours to remove any remaining solvent. Chain extensions of the macro-RAFT agent again followed the procedure outlined above. As an example for MbH1: p(MMA) macro-RAFT agent (800 mg, 0.080 mmol), AIBN (3.94 mg, 0.024 mmol), DHIAMA (840 mg, 2.04 mmol) and dioxane (3 mL, to reach an approximate polymer/monomer: solvent ratio of 2:1) were added to a 10mL three-necked-flask. The mixture was stirred under nitrogen purge for 30 minutes before being added to a preheated oil bath at 74°C to initiate polymerization. The reaction was stopped by cooling the mixture, and the polymer precipitated three times from THF using methanol.

A2 Homopolymers

A2.1 Nuclear Magnetic Resonance

An example NMR spectra of p(DHIAMA) is given in Figure A9 and for p(DBIAMA) in Figure A10.

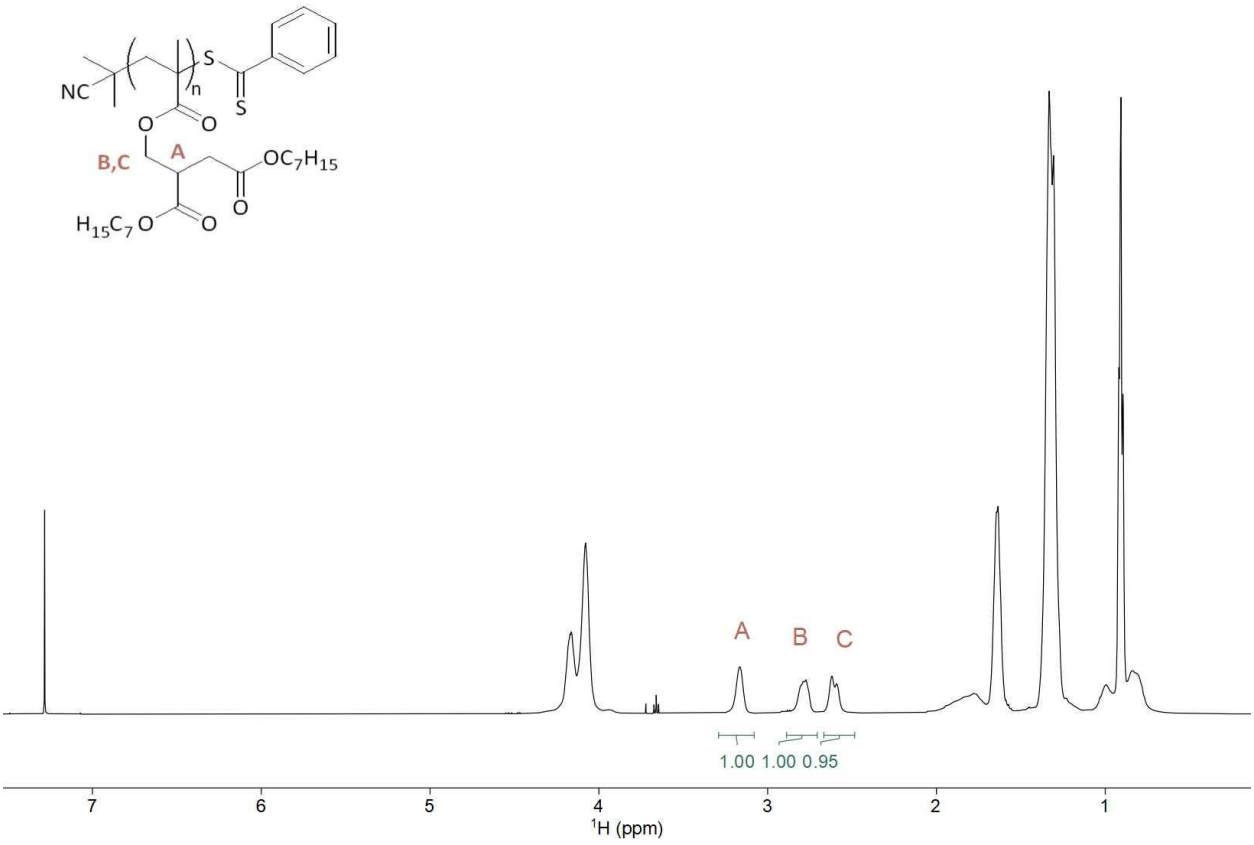

Figure A9. ^{1}H NMR of p(DHIAMA): δ 3.07-3.25 (A) (br, 1H), 2.71-2.89 (B) (br, 1H), 2.48-2.67 (C) (br, 1H).

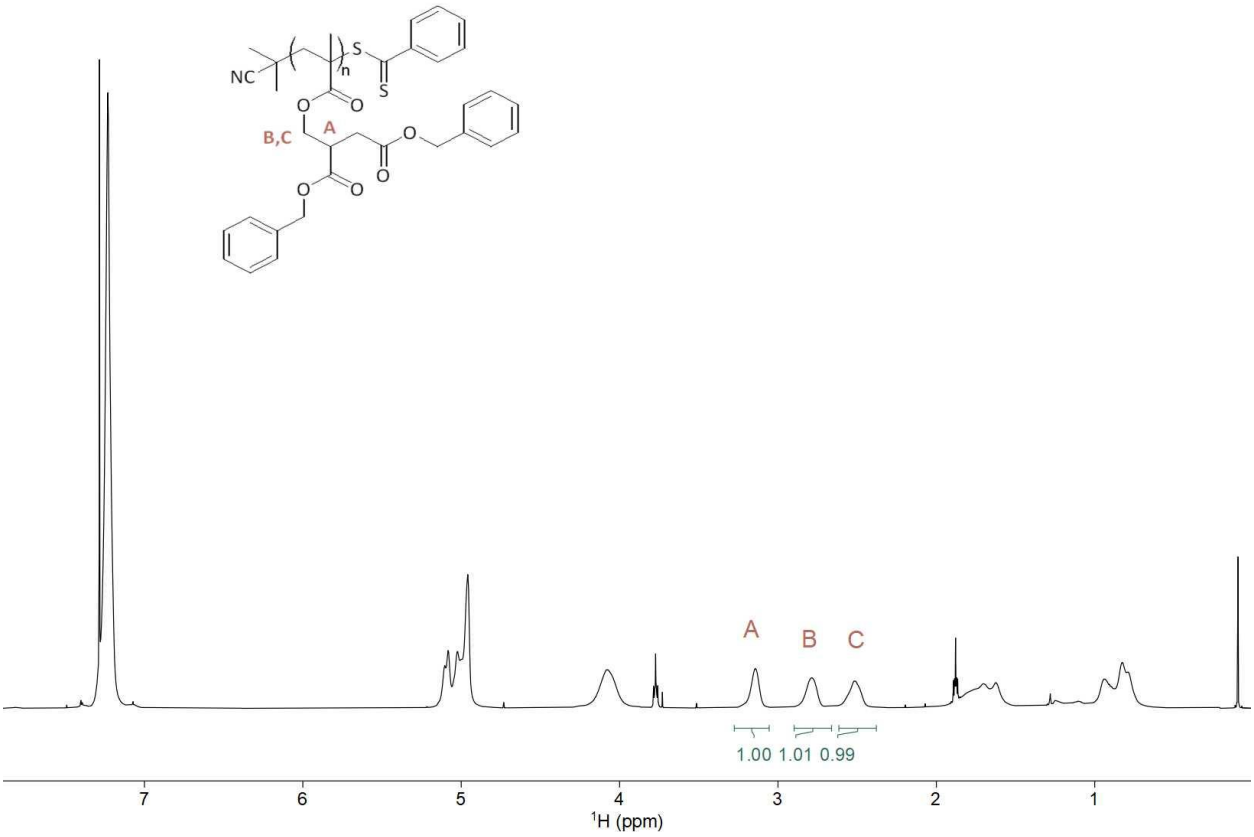

Figure A10. ^{1}H NMR of p(DBIAMA): δ 3.07-3.25 (A) (br, 1H), 2.71-2.89 (B) (br, 1H), 2.48-2.67 (C) (br, 1H), (trace impurities at 1.85 and 3.76 from THF).

A2.2 p(DBIAMA) Reaction Kinetics

Polymerization kinetics of p(DBIAMA) following the procedure outlined in Section A1.12 are shown in Figure A11 and A12.

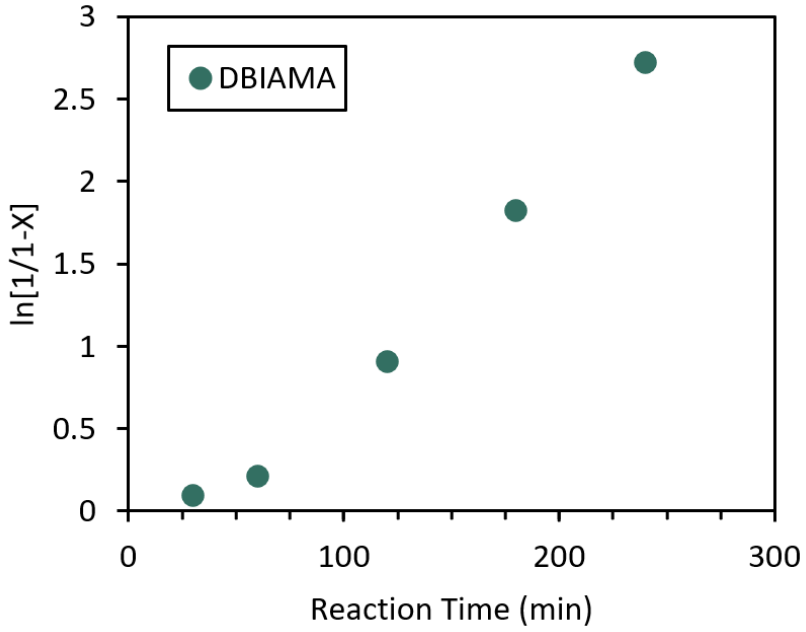

Figure A11. Pseudo-first order monomer conversion with time for a standard polymerization of dibenzyl itaconyl methacrylate using RAFT at 74°C. Monomer conversion was determined from the integration of monomer peaks in NMR samples.

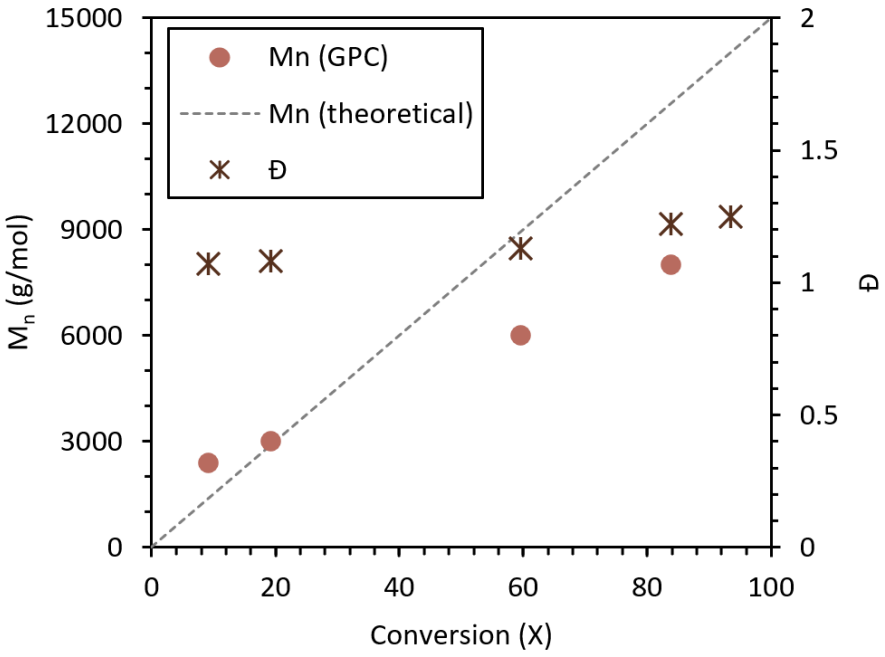

Figure A12. Molecular weight and dispersity of the growing polymer chains during the polymerization of DBIAMA by RAFT. Molecular weight and dispersity values were determined from GPC samples analyzed by an RI detector.

A2.3 Thermal Gravimetric Analysis

Results from TGA following the methods outlined in Section A1.5 are shown in Figure A13 and A14.

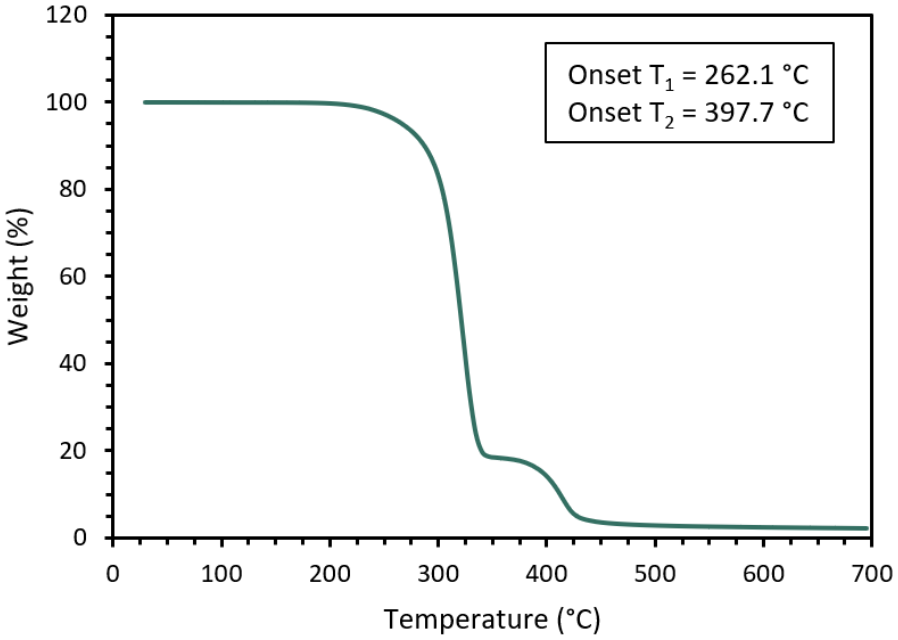

Figure A13. Thermal gravimetric results of p(DHIAMA) (H7), indicating a two-step decomposition process.

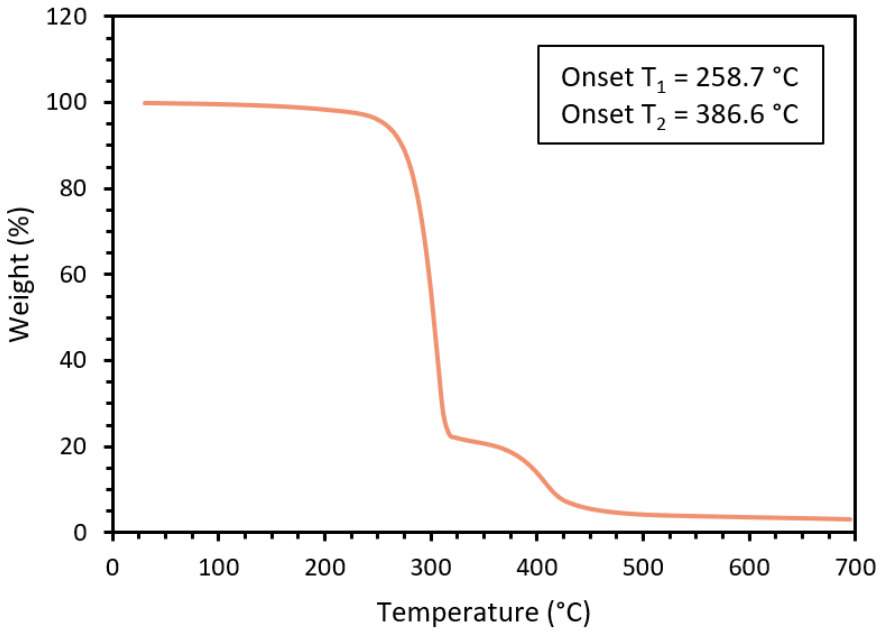

Figure A14. Thermal gravimetric analysis results of p(DBIAMA) (B4), indicating a two-step decomposition process.

A2.4 p(DHIAMA) Viscosity Sweep

Viscosity sweeps conducted on the p(DHIAMA) series are shown in Figure A15.

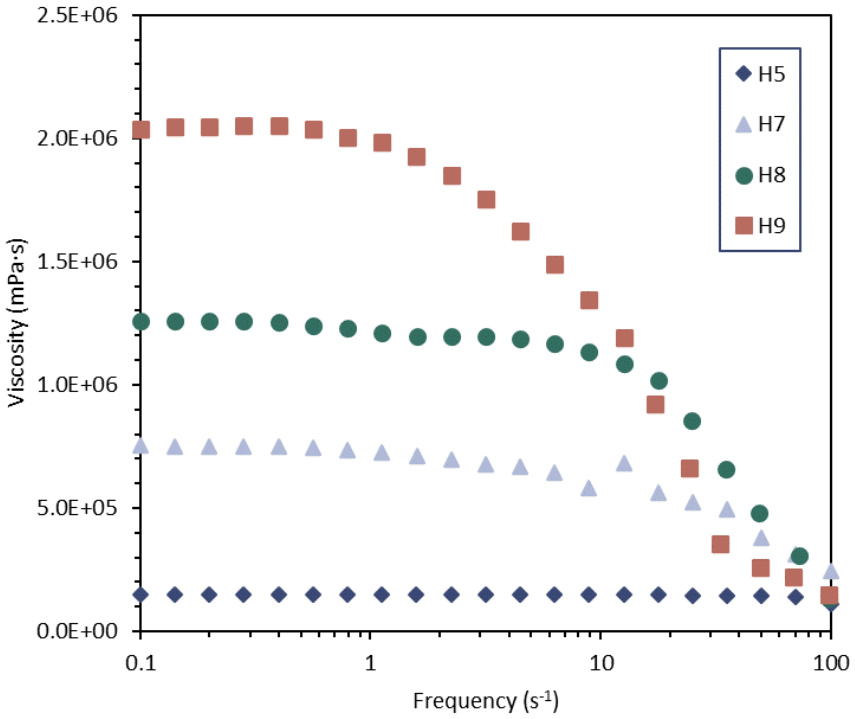

Figure A15. Example viscosity curves of p(DHIAMA) homopolymers from which zero-shear viscosity values were obtained from the plateau at low frequencies.

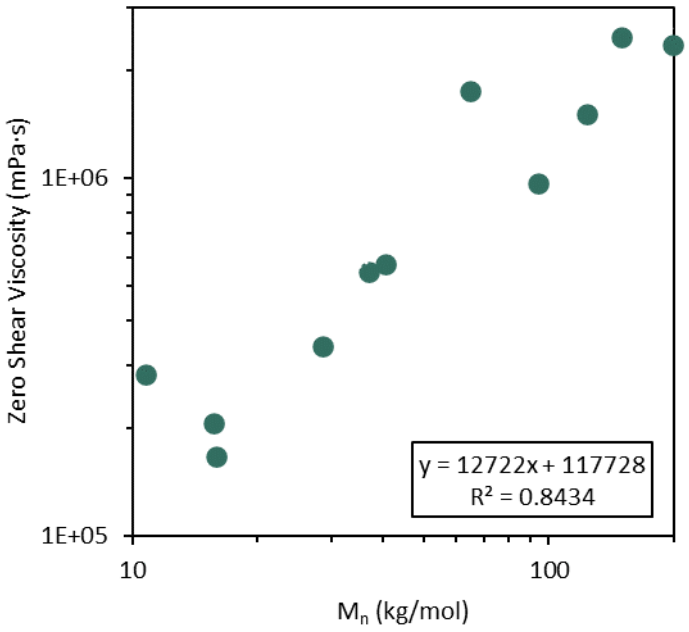

Figure A16. Zero-shear viscosities gave a good linear fit (R^2=0.8434) with molecular weight under the tested homopolymers. The molecular weight of entanglement was not in the synthesized range.

A3 Block Copolymers

A3.1 Solubility Parameter Calculation p(DHIAMA)

The Hoftyzer-Van Krevelen method was used to estimate the solubility parameter of DHIAMA (δ_{DHIAMA}) using group contribution[3]. In this approach, the solubility parameter is given by Equation A1:

$$\delta^2 = \delta_d^2 + \delta_p^2 + \delta_h^2 \tag{A1}$$

where:

$$\delta_d = \frac{\sum F_{di}}{V};\ \delta_p = \frac{\sqrt{\sum F_{pi}^2}}{V};\ \delta_h = \sqrt{\frac{\sum E_{hi}}{V}} \tag{A2}$$

The parameters of the relevant functional groups in DHIAMA can be found in literature.

Table A1. Structural group solubility parameter contributions[3]

Structural Group	F_d ($J^{0.5}cm^{1.5}mol^{-1}$)	F_p ($J^{0.5}cm^{1.5}mol^{-1}$)	E_h ($J\ mol^{-1}$)
-CH3	420	0	0
-CH2-	270	0	0
>CH-	80	0	0
=CH2	400	0	0
=C<	70	0	0
-COO-	390	490	7000

A pycnometer was used to find the density of p(DHIAMA) as $\rho = 1.05\ g/cm^3$, leading to a molar volume of $V_{p(DHIAMA)}$ being 392.8 cm^3/mol. Thus, the solubility parameter was estimated as $\delta_{DHIAMA} = 18.8\ (J/cm^3)^{0.5}$.

A3.2 Flory-Huggins Interaction Parameter Calculation

The interaction parameter of p(DHIAMA) and p(MMA) systems can be calculated using the Flory-Huggins method by:

$$\chi = \frac{\bar{V}}{RT}(\delta_{DHIAMA} - \delta_{MMA})^2 \quad \text{(A3)}$$

with the average volume given by Equation A4.

$$\bar{V} = \sqrt{V_{DHIAMA} V_{MMA}} \quad \text{(A4)}$$

where R is the universal gas constant and T is the absolute temperature.

From literature, the molar volume of p(MMA) is 86.5 cm^3/mol and $\delta_{MMA} = 23.5\ (J/cm^3)^{0.5}$ [4].

Their interaction parameter can then be estimated as $\chi = 1.627$ at 25°C. To expect phase separation in the polymer, the (χN) value must exceed 10.5, where N is the total degree of polymerization. Using this, the block copolymers were designed such that the degree of polymerization for the target composition would be expected to result in microphase separation, as shown in the table.

Table A2. χN values of the targeted p(MMA-*b*-DHIAMA) block copolymers.

Copolymer	M_n p(MMA), GPC	M_n p(DHIAMA), target	N_{total}, expected	(χN)
MbH1	10 000	10 500	125	203.4
MbH2	10 000	24 000	158	257.1
MbH3	10 000	85 000	306	497.9
MbH4	10 000	118 000	386	628.0
MbH5	32 300	137 000	655	1 065.7

With the χN values falling over an order of magnitude above 10.5, it is estimated the diblock polymers will likely exhibit phase separation if synthesized as designed.

A3.3 Block Copolymer Reaction Kinetics

Example reaction kinetics using the methods outlined in Section A1.13 for the synthesis of a diblock copolymer are given in Figure A17 through A20.

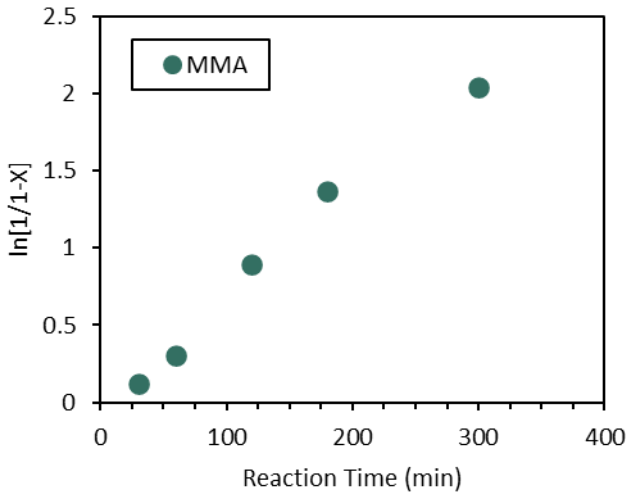

Figure A17. Pseudo first-order conversion of MMA during polymerization by RAFT.

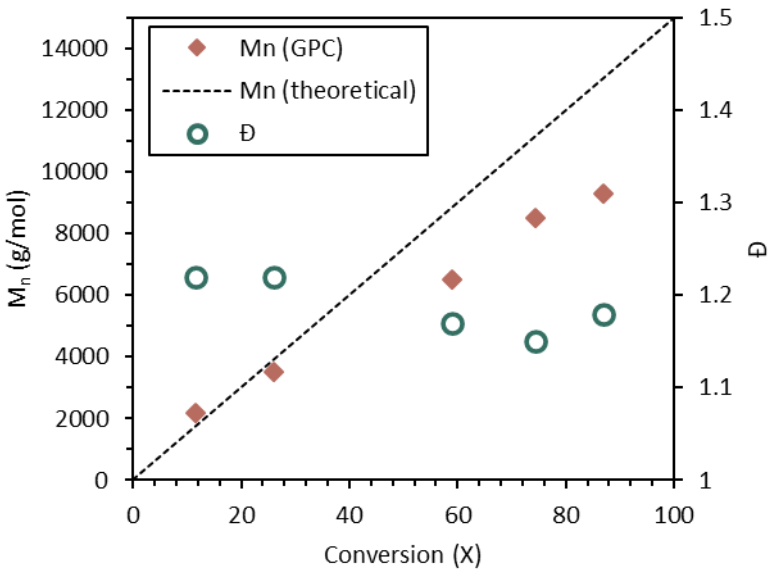

Figure A18. Molecular weight and dispersity values during the polymerization of MMA to generate the macro-RAFT agent.

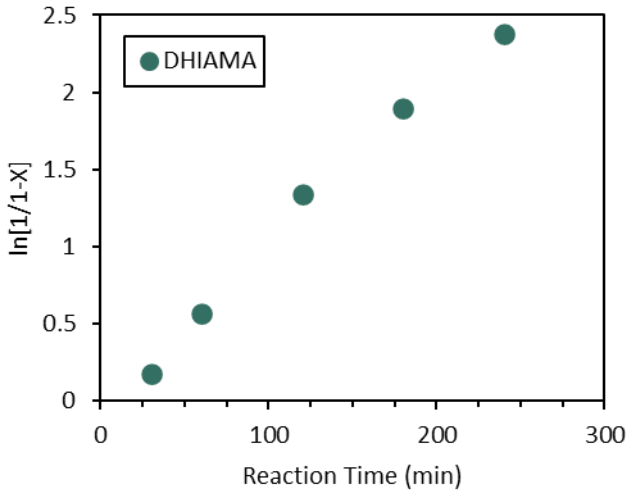

Figure A19. Pseudo first-order conversion of DHIAMA during the chain extension of the p(MMA) macro-RAFT agent to give a diblock copolymer.

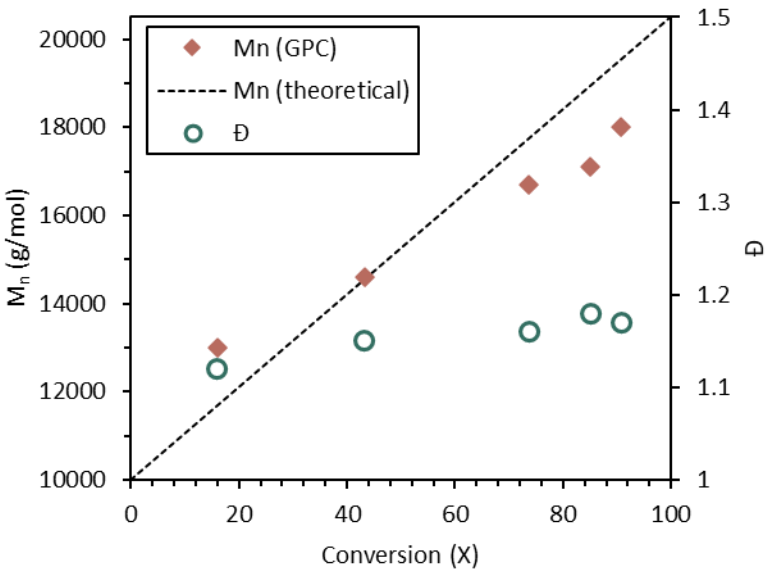

Figure A20. Molecular weight and dispersity of the growing polymer during the chain extension reaction to produce p(MMA-*b*-DHIAMA).

A3.4 Nuclear Magnetic Resonance

An example of a NMR spectra of a diblock copolymer is given in Figure A21.

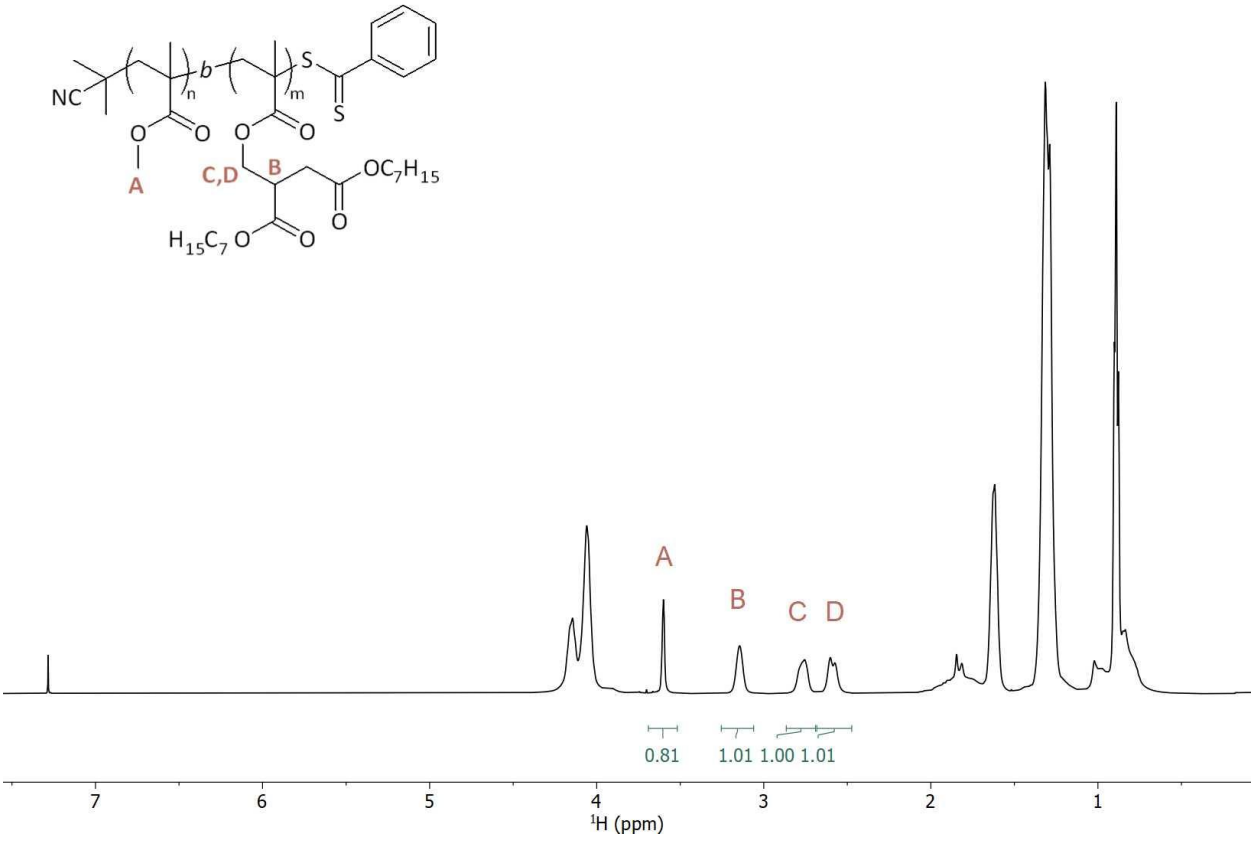

Figure A21. ^{1}H NMR of p(MMA-*b*-DHIAMA): δ 3.50-3.65 (A) (3H, p(MMA)), 3.07-3.25 (B) (1H, p(DHIAMA)), 2.71-2.89 (C) (1H, p(DHIAMA)), 2.48-2.67 (D) (1H, p(DHIAMA)).

A3.5 Copolymer Composition Calculation

The composition of the diblock copolymers was determined using the ^{1}H NMR spectrum of the dried samples. The integration values found from the chemical shifts were used in Equation A5 to determine the composition:

$$F_i = \frac{\left(\int_{\text{range start}}^{\text{range end}} \left(\frac{1}{\text{Number of Hydrogens}}\right)\right)_i}{\sum_1^{N\ components} \int_{\text{range start}}^{\text{range end}} \left(\frac{1}{\text{Number of Hydrogens}}\right)} \quad \text{(A5)}$$

A3.6 Differential Scanning Calorimetry

The results of DSC on the diblock copolymers, following the method outlined in Section A1.4, are given in Figure A22.

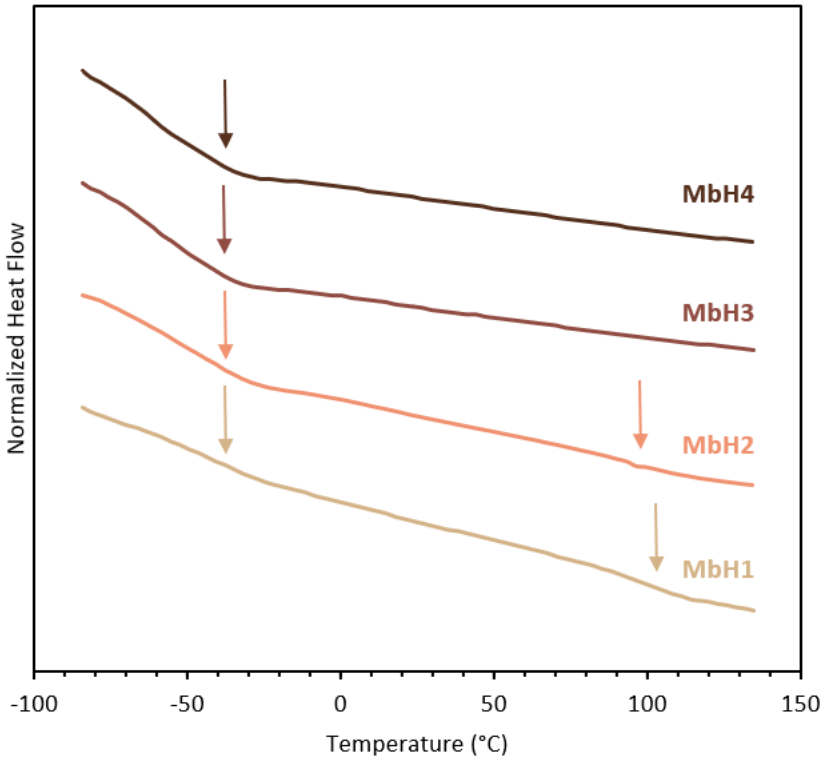

Figure A22. Differential scanning calorimetry results of the p(MMA-*b*-DHIAMA) series with discernable glass transition temperatures indicated by arrows.

A4 References

(1) Mun, S.; Lee, J.-E.; Yun, J., Copper-catalyzed β-boration of α,β-unsaturated carbonyl compounds: Rate acceleration by alcohol additives. *Organic Letters* **2006,** *8* (21), 4887-4889.

(2) Zaremski, M. Y.; Plutalova, A. V.; Lachinov, M. B.; Golubev, V. B., A concept for quasiliving nitroxide-mediated radical copolymerization. *Macromolecules* **2000,** *33* (12), 4365-4372.

(3) Krevelen, D. W.; Te, K., Cohesive Properties and Solubility. 2009; pp 189-227.

(4) Arnold, J. C., 6.06 - Environmental Effects on Crack Growth in Polymers. In *Comprehensive Structural Integrity*, Milne, I.; Ritchie, R. O.; Karihaloo, B., Eds. Pergamon: Oxford, 2003; pp 281-319.

Appendix B: Supporting Information to Chapter 4

B1 Experimental Methods

B1.1 Materials and Reagents

All chemicals were used as received, unless otherwise stated here. VISIOMER® Terra C13-methacrylate (C13MA, Evonik), styrene (MilliporeSigma), methyl methacrylate (MMA, MilliporeSigma), and acrylonitrile (AN, MilliporeSigma) were purified in a column of basic alumina and 5 wt% calcium hydride to remove inhibitors before use. Glycerol monomemthacrylate (GMMA) was purchased from Polysciences. 4-Vinylphenylboronic acid (VPBA, ≥95%) and 1,4-Benzenediboronic acid (98%) were purchased from AK Scientific. BlocBuilder™ (BB, alkoxyamine for NMP) was obtained from Arkema. 1,2-Propanediol (≥99.5%), pinacol (98%), deuterated chloroform (99.8%), dioxane (≥99.0%), dimethylformamide (DMF, ≥99.9%), toluene (≥99.5%) and molecular sieves were purchased from Millipore Sigma. Methanol, (MeOH, ≥99.8%), tetrahydrofuran (THF, HPLC grade, ≥99.9%), chloroform (≥99.8%), and anhydrous magnesium sulfate ($MgSO_4$) were purchased from Fisher.

B1.2 Instrumentation and Methods

B1.2.1 Proton Nuclear Magnetic Resonance (1H NMR)

^1H NMR spectra were collected using a Bruker AVIIHD 500 MHz spectrometer with an average of 32 scans using deuterated chloroform ($CDCl_3$) as the diluent. To dissolve the VPBA based copolymers in $CDCl_3$ for NMR analyses, excess amount of pinacol was added to the samples to cap the boronic acids.

B1.2.2 Fourier Transform Infrared (FTIR) Spectroscopy

FTIR spectra were collected using a Thermo Scientific Nicolet iS50 FTIR Spectrometer. The instrument was equipped with a single bounce diamond attenuated transmission reflectance (ATR) for solids. Samples were subjected to 32 scans in the range of 4000 - 400 cm^{-1}.

B1.2.3 Atomic Force Microscopy (AFM)

A Cypher VRS SPM (Asylum-Research-Oxford Instruments) machine was used in tapping mode for the atomic force microscopy phase imaging. The prepolymer was dissolved in THF and

transferred onto a Teflon plate to dry out overnight at room temperature followed by vacuum drying in an oven at 50°C. The dried polymer film was then transferred onto an AFM sample holder for analyses in air.

B1.2.4 Small Angle X-Ray Scattering (SAXS)

Measurements were taken of bulk samples on a SAXS point 2.0 (Anton Paar) instrument. A Cu Ka radiation source with a wavelength of 1.54 Å was used with an Eiger R 1M horizontal detector set at 557 mm. The samples of the bulk material were placed on a sample holder provided by Anton Paar, and exposed to X-ray for 20 minutes per frame, for three frames per sample. The SAXS patterns were corrected and given as a function of the scattering vector $q = (4\pi/\lambda)\sin\theta$, where 2θ is the scattering angle in degrees (°) and q is in nm^{-1}. The domain spacing was then determined by the following equation:

$$d = \frac{2\pi}{q*}$$

where q* is the principal peak, being the first major peak in the SAXS patterns.

B1.2.5 Gel Permeation Chromatography (GPC)

Samples taken during prepolymer synthesis and of final prepolymers were run on a Waters Breeze gel permeation chromatography instrument using HPLC-grade THF to determine the number average molecular weight (M_n), and the dispersity ($Đ = M_w/M_n$). A flowrate of 0.3mL/min was used to run the samples through the system operated at 40°C consisting of a guard column, 3 Styragel HR columns, and a refractive index (RI 2414) detector. The system calibration was completed with a series of poly(methyl methacrylate) (PMMA) standards from Varian (with a calibration range from 875 to 1 677 000 g/mol), and molecular weights reported are relative to those PMMA standards.

Polymer samples containing 4-vinylphenylboronic acid (VPBA) were capped using pinacol and molecular sieves prior to being analyzed by GPC.

B1.2.6 Thermogravimetric Analysis (TGA)

Thermal stability of prepolymers and networks was assessed by a TA Instrument Discovery 5500 under nitrogen, using platinum pans. For determining the temperature of decomposition, samples were heated at a rate of 10°C/min from 25°C to 600°C. In the TA Instruments TRIOS

software, the onset tool was used to determine the onset of 10 wt% degradation, with the corresponding temperature reported. For the isothermal test, the sample was first heated to 100°C and held for 30 min to remove any moisture, before being heated to 150°C and held isothermal for 180 min.

B1.2.7 Differential Scanning Calorimetry (DSC)

The glass transition temperature (T_g) of prepolymers and vitrimeric blends was evaluated using a TA Instruments Discover 2500 under a nitrogen atmosphere, in aluminum hermetic pin-hole pans. The samples were subjected to a heat/cool/heat cycle: first being held at -90°C for 3 min, then heated to 140°C at a heating rate of 10°C/min, held isothermal for 3 min, and cooled again at a rate of 10°C/min to -90°C, held isothermal for 3 min, and heated a final time to 140°C at 10°C/min. Using the second heating ramp, the T_g was determined using the as the curve inflection point and glass transition tool in the TA Instruments TRIOS software.

B1.2.8 Compression Molding of Test Bars and Disks

Dog-bone shaped test bars for tensile testing, as well as disks for rheological testing, were produced with a Carver manual hydraulic press with Watlow temperature controllers. Dried vitrimeric samples were cut into small fragments, and arranged in steel molds, sandwiched between Teflon plates before being transferred into the preheated press. The dimensions of each dog-bone were 3.2 mm wide × 1.5mm thick × 15.0 mm long while the disks were 25 mm in diameter and 1 mm in thickness. Bars and disks were pressed at 115°C and 6 metric tonnes (Mt) for 20 min, then 8 Mt for 20 min, and finally 12 Mt for 20 min, with 30 sec of degassing at 0 Mt between each pressure increase. The total press time was 60 ± 5 min. The hot press plates were cooled down to 30 ± 10°C using tap water, before releasing the pressure and removal of sample.

B1.2.9 Dynamic Mechanical Analysis (DMA) and Rheology

An Anton Paar MCR 302 was used for rheological and DMA testing. DMA tests were completed on 25 mm disks using a parallel plate geometry with a gap distance of 1 mm. The sample were heated from room temperature to 150°C at a rate of 5°C/min, and a frequency of 1 Hz. Rheological tests were also performed using the same parallel plate setup. Strain sweep tests were performed on the networks at 50 and 150°C to confirm the linear viscoelastic region (LVR) when subjected to a frequency of 1 Hz. Frequency sweep tests were performed at 0.1% strain and from

50 – 130°C. Stress relaxation tests were performed at 0.1% fixed strain from 90 to 130°C with 10°C increasing increments each for 1000 s with 1 N normal force. Creep-recovery tests were performed by applying 250 Pa for 300 s, followed by 0 Pa for 500 s, for a total test time of 800 s.

B1.2.10 Tensile Testing

Uniaxial tensile tests were conducted using a Shimadzu Easy Test instrument with a 500 N load cell as complying with ASTM standard D638-14. Test bars were clamped and tested at an overhead strain rate of 10 mm/min at room temperature. Stress-strain curves were used to determine the strain (% elongation) and stress at break.

B1.2.11 Indentation

A Nanovea M1 Hardness Tester Nano-indentator equipped with a Berkovich tip was used. A load of 20 mN with an approaching load rate and unloading rate of 40mN/min, and 20mN/min, respectively, were applied. An approach speed of 2.5 μm/min was selected, with a contact load of 0.3 mN that was held for 30 s between the loading and unloading phase. Nine tests were conducted on different locations of the network surface. The Nanovea software was used to calculate the hardness of the material.

B1.2.12 Swelling and Gel Fraction

The swelling ratio and gel fraction of the networks were assessed in toluene. The samples were added to a capped 20 mL vial and excess toluene at room temperature for 48 hours. Afterwards, the swollen samples were removed from the solvent, with excess solvent removed by gently dapping using a Kimwipes and weighed to determine the swelling ratio by Equation B1:

$$\text{Swelling Ratio} = \frac{m_s - m_0}{m_0} \times 100 \quad \text{(B1)}$$

where, m_s is the swollen sample mass and m_0 is the original sample mass before the swelling experiment.

The swollen samples were then dried under reduced pressure at 60°C for 24 hours, before weighing again. This dried sample mass (m_d) could then be used to determine the gel content of the networks by Equation B2:

$$\text{Gel Content (\%)} = \frac{m_d}{m_0} \times 100 \quad \text{(B2)}$$

B2 Synthesis and Characterization of Polymers and Crosslinker

B2.1 Statistical Copolymer: poly(GMMA-*co*-C13MA-*co*-Styrene): P1-S-GM

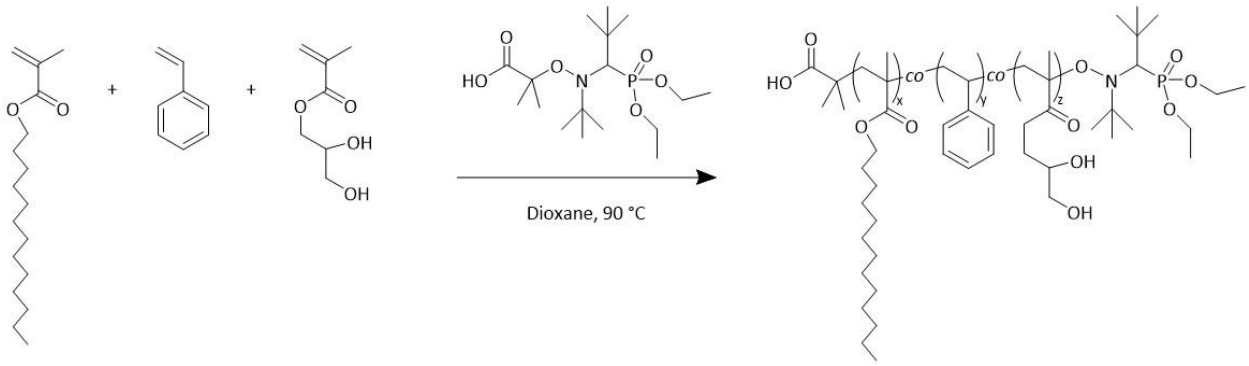

Figure B1. Synthesis of statistical P1-S-GM polymer via nitroxide mediated polymerization using BlocBuilder.

C13-methacrylate (25 g, f_{C13MA} = 0.8 mol %), GMMA (1.86 g , f_{GMMA} = 0.1 mol %), styrene (1.21 g, $f_{styrene}$ = 0.1 mol %), 0.4 g BlocBuilder (1.048 mmol, $M_{n,\ target}$ = 25 kg/mol at 100% conversion), dioxane (28.5 grams, 50 wt% of solution), and DMF (1 mL, as internal reference for NMR analyses) were added to a 250 mL three necked round bottom flask equipped with a Teflon stir bar and an overhead reflux condenser cooled to 5°C.

The solution was purged with ultrapure nitrogen gas for 45 min at room temperature prior to transferring the reactor to an oil bath preheated at 90°C, marking the start of the reaction. At this time zero, 0.2 mL of was drawn via syringe to be evenly split for GPC and NMR analysis. 0.2 mL aliquots were periodically taken throughout the reaction for GPC and NMR analysis to assess the polymerization kinetics. After 330 min, the reactor was removed from the oil bath to cool down to < 40°C. Subsequently, the reaction solution was transferred to a beaker and triply precipitated into excess MeOH, from THF , yielding a white polymer, which was then dried under reduced pressure.

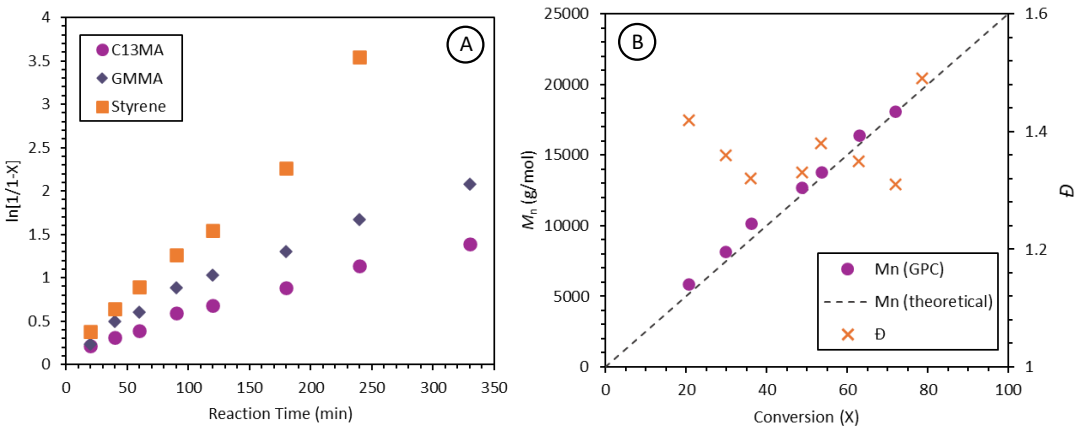

Figure B2. P1-S-GM synthesis reaction results: (A) Pseudo-first order kinetics of the statistical polymerization of poly(C13MA-*co*-Styrene-*co*-GMMA) (P1-S-GM) with C13MA (pink circles), GMMA (navy diamonds), and styrene (orange squares). Styrene appears to be preferentially polymerized and was fully incorporated by the final sample time of 330 minutes; (B) Number average molecular weight (M_n) (pink circles) as determined by GPC, theoretical molecular weight (dashed line) as determined by overall monomer conversion ($X_{overall} = \sum X_i f_{0,i}$ with $f_{0,i}$ initial mol% of the monomer i) from ^{1}H NMR, and dispersity ($Đ$) (orange crosses) determined by GPC.

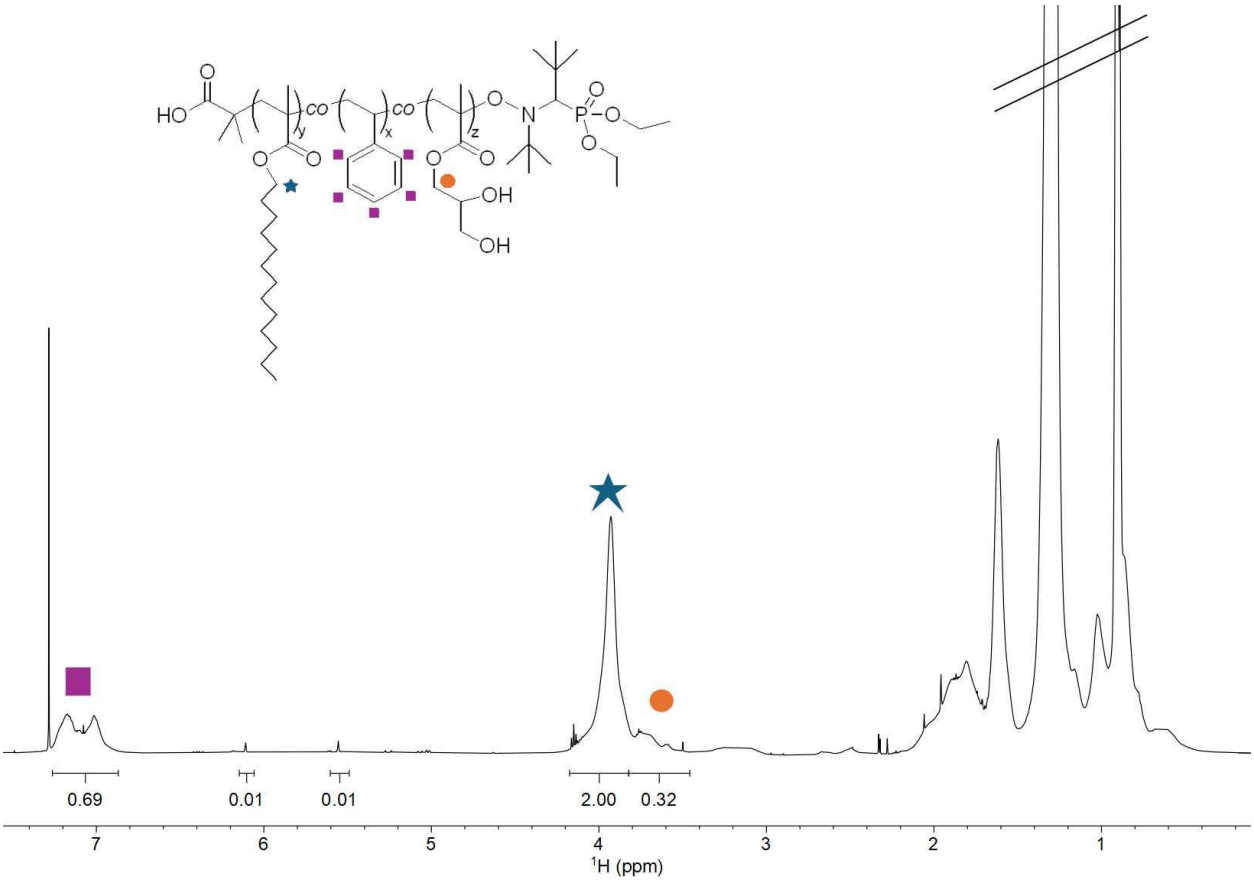

Figure B3. ^{1}H NMR of the final dried P1-S-GM polymer: δ 6.87 – 7.26 (purple square) (5H, Styrene), 3.82 – 4.17 (blue star) (2H, C13MA), 3.46 – 3.82 (orange circle) (2H, GMMA).

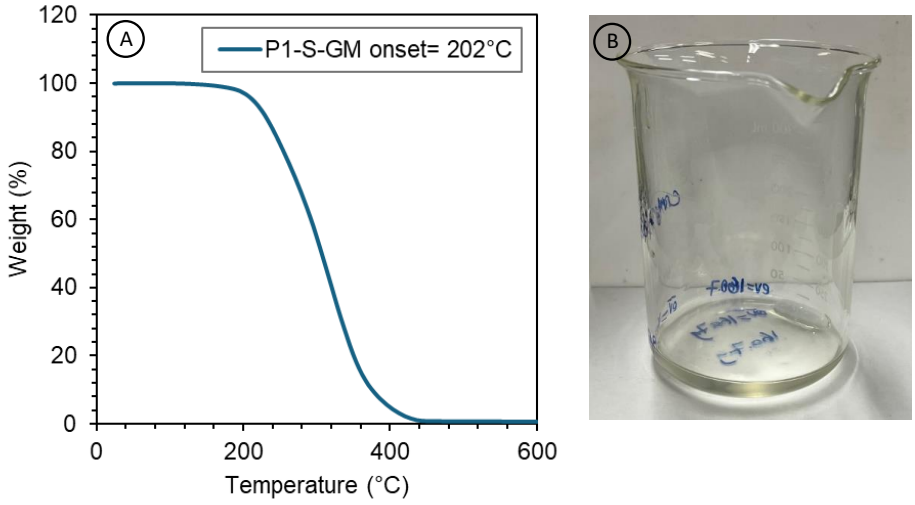

Figure B4. (A) TGA curve of P1-S-GM with the onset of 10 wt% degradation at 202°C; (B) image of P1-S-GM in a beaker.

B2.2 Statistical Copolymer: poly(VPBA-*co*-C13MA): P2-S-VP

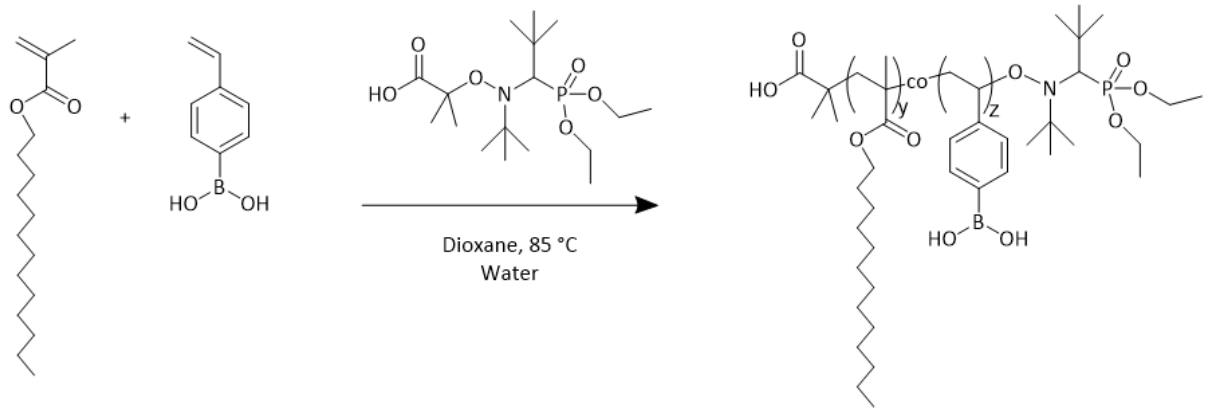

Figure B5. Synthesis of statistical poly(C13MA-*co*-VPBA) (P2-S-VP) copolymer via nitroxide mediated polymerization using BlocBuilder.

C13MA(C13MA18.52 g, f_{C13MA} = 0.9), VPBA (1.13 g , f_{VPBA} = 0.1), BlocBuilder (0.3 g, $M_{n,\,target}$ = 25 kg/mol at 100% conversion), dioxane (19.7 g, $\frac{m_{dioxane}}{\sum m_{monomers}} = 2$), water (1 mL) to open potential Broxines, and DMF (1 mL, for internal reference in NMR analysis) were added to a three necked flask with a Teflon stir bar, overhead reflux condenser, thermal coupleand the outlets capped with rubber septa. The solution was stirred to allow the BlocBuilder and VPBA to fully dissolve, before the reactor was attached to a reflux condenser chilled to 5°C. A nitrogen purge was then introduced to the solution and purged for 30 minutes, before the reactor was placed atop a heating mantle and heated to 85°C. Time zero was taken to be when the solution reached 70°C, and aliquots samples for GPC and NMR were taken periodically. After 340min, the solution was removed from the heating mantle and cooled before being transferred into a beaker and then precipitated in MeOH and reprecipitated from THF three times. The purified prepolymer, shown in Figure B8, was dried out at 40 ˚C under vacuum overnight.

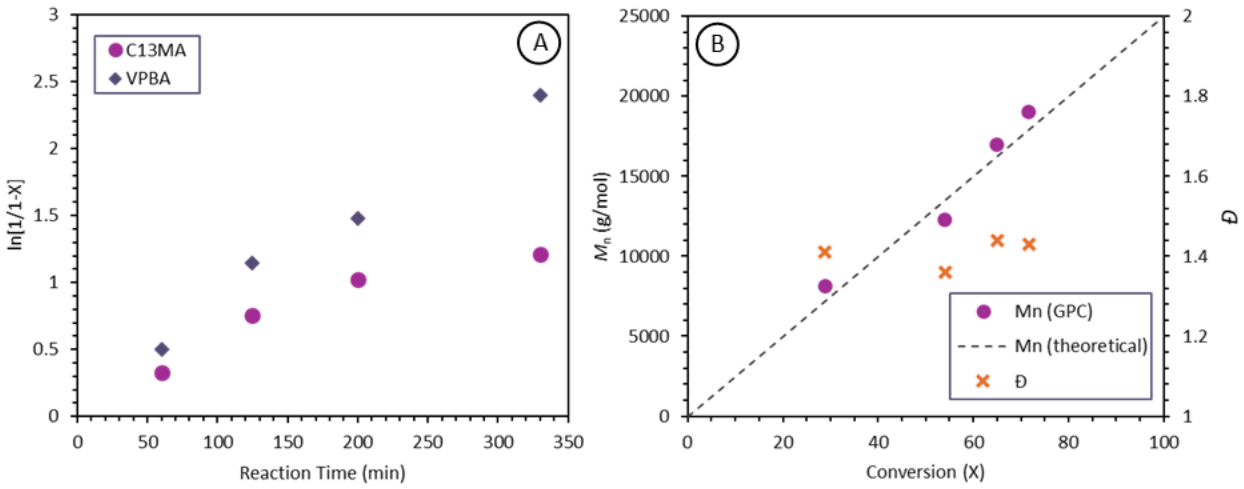

Figure B6. P2-S-VP synthesis reaction results: (A) Pseudo-first order kinetics of the statistical polymerization of P2-S-VP with C13MA (pink circles), and VPBA (navy diamonds) determined by ^{1}H NMR; (B) M_n (pink circles), dispersity (orange crosses) determined by GPC, and theoretical molecular weight (dashed line) versus overall monomer conversion throughout the polymerization.

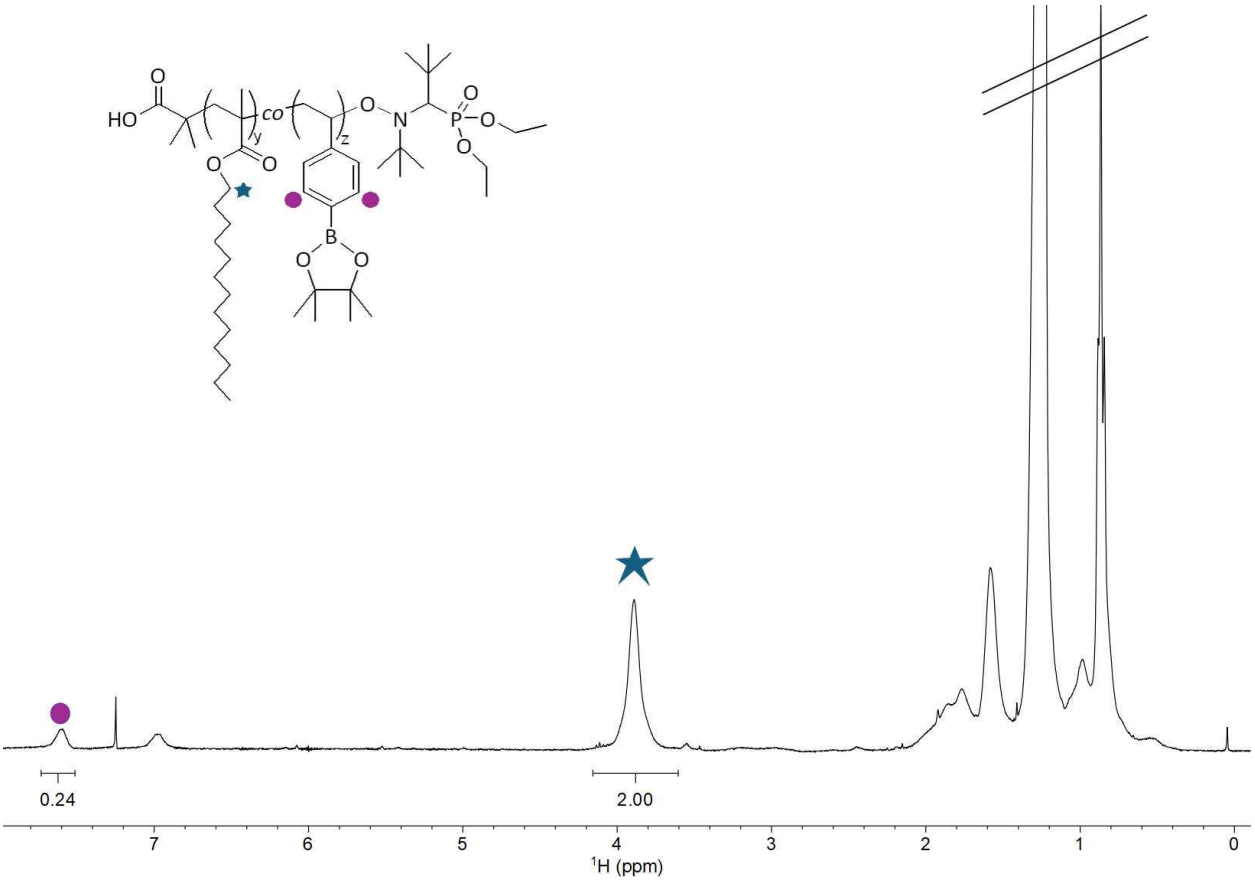

Figure B7. ^{1}H NMR of the final dried P2-S-VP polymer: δ 7.50 – 7.80 (purple circle) (2H, VPBA), 3.75 – 4.15 (blue star) (2H, C13MA).

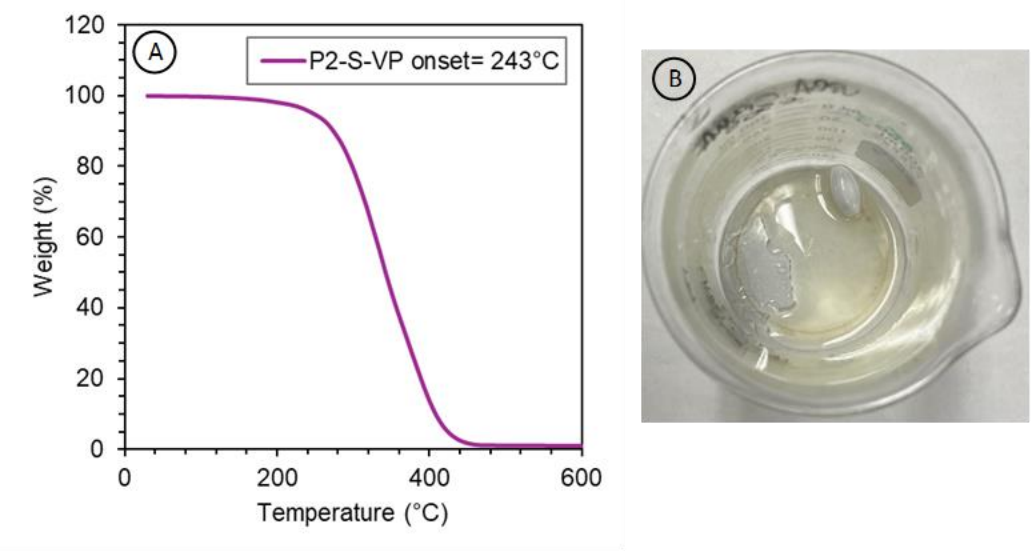

Figure B8. (A) TGA curve of P2-S-VP with the onset of 10 wt% degradation at 243°C; (B) Image of P2-S-VP.

B2.3 Block copolymer poly(MMA-*co*-AN)-*block*-poly(C13MA-*co*-VPBA): P3-B-VP

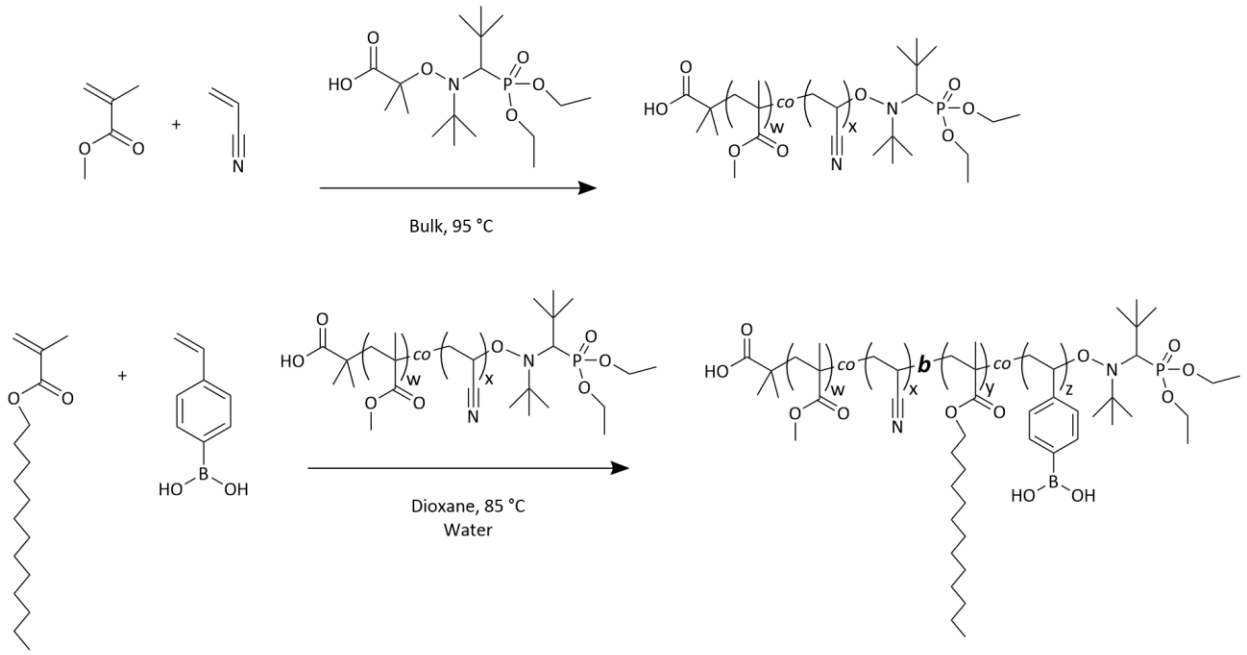

Figure B9. Sequential synthesis of block P3-B-VP copolymer via NMP using BlocBuilder. First, poly(MMA-*co*-AN) macroinitiator is synthesized in bulk and then the macroinitiator was dissolved in dioxane and chain extended with C13MA/VPBBA to form a diblock copolymer.

MMA (78.7 grams, f_{MMA} = 0.9), acrylonitrile (AN, 5.16 grams, f_{AN} =0.1) and BlocBuilder (0.80 gram) were added to a 250 mL 3-neck round bottom reactor with a Teflon stir bar and overhead reflux condenser chilled to 2°C. The solution was purged with ultrapure nitrogen for 45 minutes. The mixture was heated to 95°C using a heating mantel. Time zero was taken to be when the mixture reached 70°C, and aliquot samples were taken periodically for GPC and NMR analyses. After 65 minutes, the mixture was cooled (< 40 ˚C), and precipitated three times in cold MeOH from THF. The resulting white polymer (PMMA, M_n = 8100 g/mol, $Đ$ = 1.55) was dried under reduced vacuum at 40°C overnight.

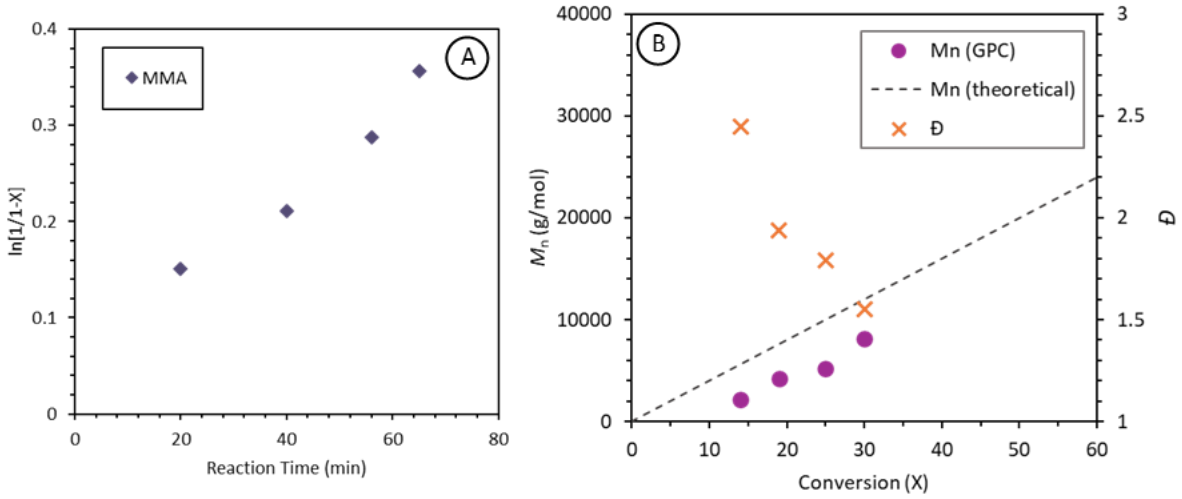

Figure B10. PMMA synthesis results: (A) Pseudo-first order kinetics of the PMMA macroinitiator synthesis in bulk at 95°C; (B) M_n (pink circles) and dispersity (orange crosses) determined by GPC, theoretical molecular weight (dashed line), versus overall monomer conversion throughout the polymerization.

For the chain extension polymerization, the PMMA macroinitiator (9.0 grams, ~ ca. 1.11 mmol) was first dissolved overnight in dioxane (51.6 g, ~60 wt% of polymerization solution) and along with C13MA (26.16 g, f_{C13MA} = 0.88) , VPBA (1.97 g, f_{VPBA}= 0.12), DMF (4 mL), and water (5 mL) were added into a 250 mL three-necked reactor with a thermal well, Teflon stir bar and overhead reflux condenser chilled to 3°C to prevent evaporation of solvent and monomer. The solution was purged with nitrogen for 45 minutes before being placed atop a heating mantle and heating at 85°C. The time zero was set to be when the solution reached 70°C. Aliquots samples were taken periodically for NMR and GPC analyses. After 180 min, the solution was transferred

to a beaker and precipitated in cold MeOH four times from THF. The resulting polymer was dried under vacuum at 40°C overnight.

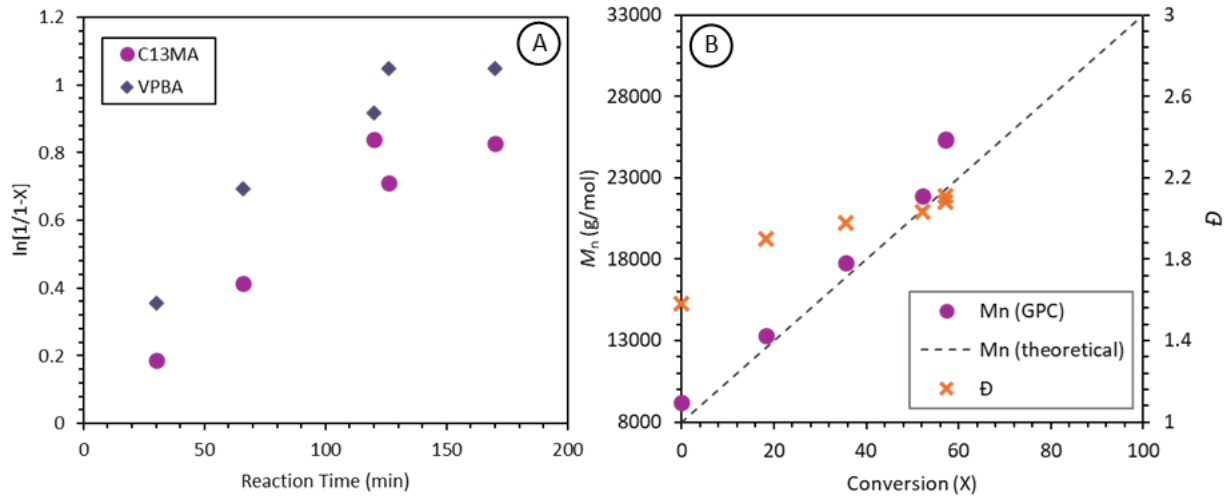

Figure B11. Block extension synthesis results: (A) Pseudo-first order kinetics of the PMMA-rich block extension polymerization of P3-B-VP with C13MA (pink circles), and VPBA (navy diamonds); (B) M_n (pink circles), dispersity (orange crosses) determined by GPC, and theoretical molecular weight (dashed line) versus overall monomer conversion throughout the polymerization.

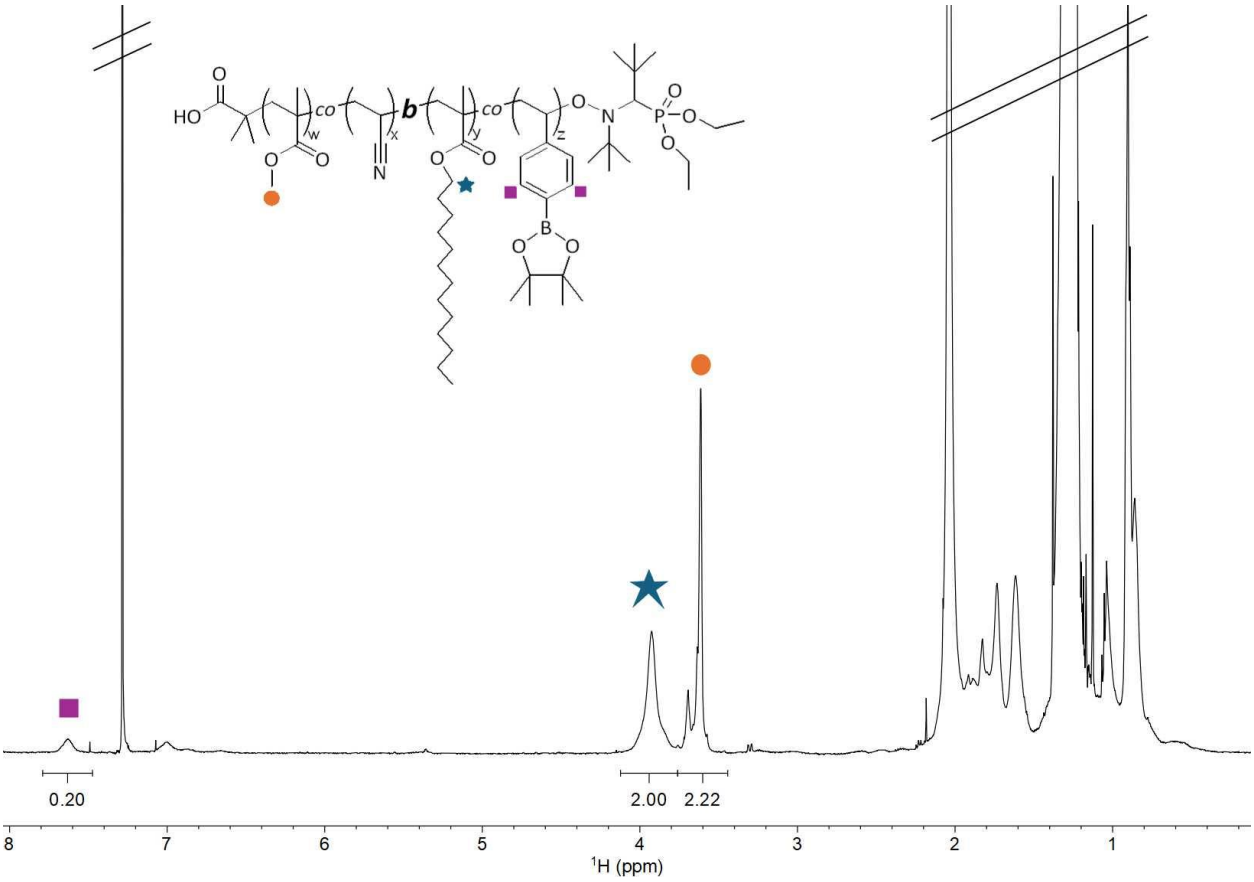

Figure B12. ^{1}H NMR of the final dried P3-B-VP polymer: δ 7.47 – 7.79 (purple square) (2H, VPBA), 3.76 – 4.12 (blue star) (2H, C13MA), 3.44 – 3.76 (orange circle) (3H, MMA). The VPBA was capped with pinacol for easier dissolution in $CDCl_3$.

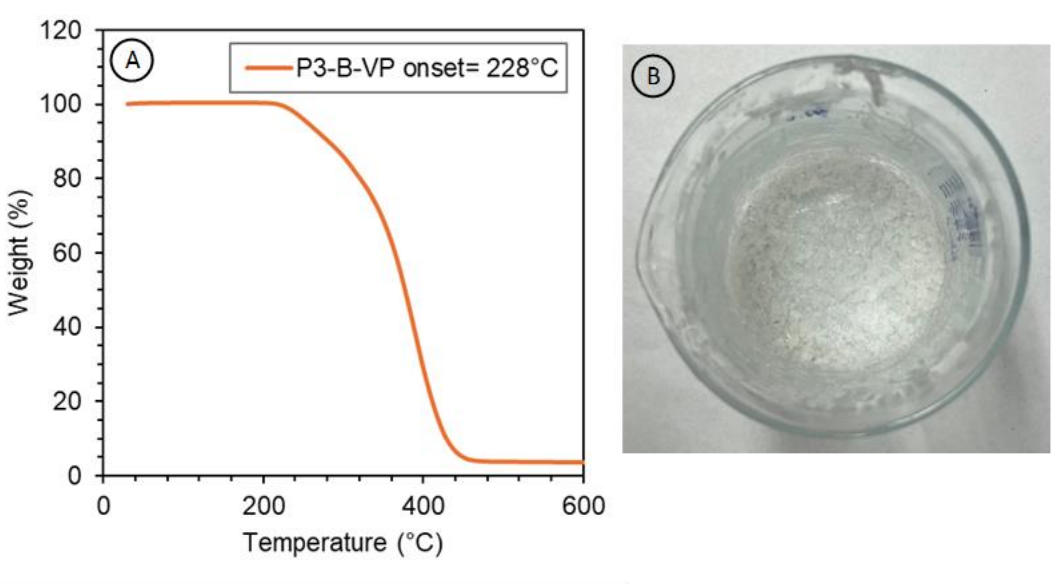

Figure B13. (A) TGA curve of P3-B-VP with the onset of 10 wt% degradation at 228°C; (B) Image of P3-B-VP.

B2.4 Gel Permeation Chromatography

The GPC results of the three prepolymers are given in Figure B14.

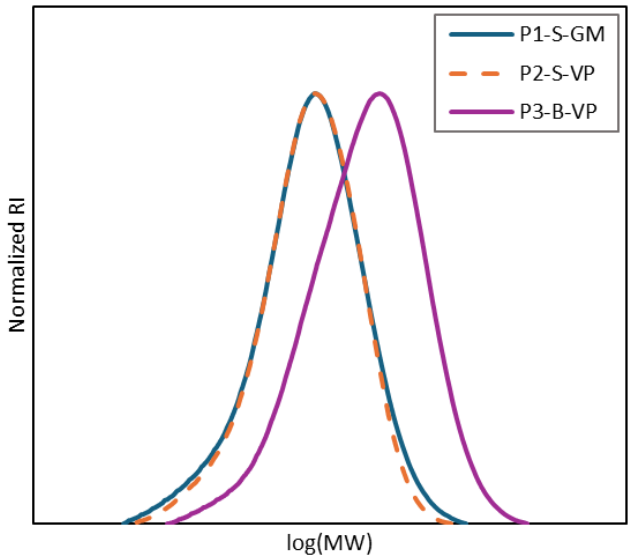

Figure B14. Gel permeation chromatography traces of the three prepolymers displaying monomodal distributions.

B2.5 Synthesis of Capped Benzene Diboronic (BDB) Acid Small Molecule Cross-linker

An overview of the BDB synthesis is given in Figure B15.

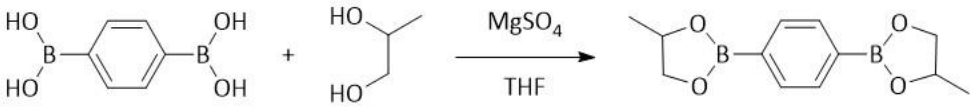

Figure B15. Synthesis of capped benzene diboronic acid.

A bifunctional small molecule cross-linker was synthesized based on previously published literature[1]. In brief, 1,4-phenylenediboronic acid (1.50 g, 9.0 mmol), 1,2-propanediol (1.38 g, 18.01 mmol), anhydrous THF (40 mL), and distilled water (0.2 mL) were combined in a round-bottom flask. The mixture was stirred at room temperature for 2 hours. Then, magnesium sulfate (3 g, 25 mmol) was added, and the reaction was allowed to proceed overnight at room temperature. The mixture was then filtered and concentrated under reduced pressure using a rotary evaporator. The resulting material was dissolved in hexanes, filtered, and concentrated to yield a white solid.

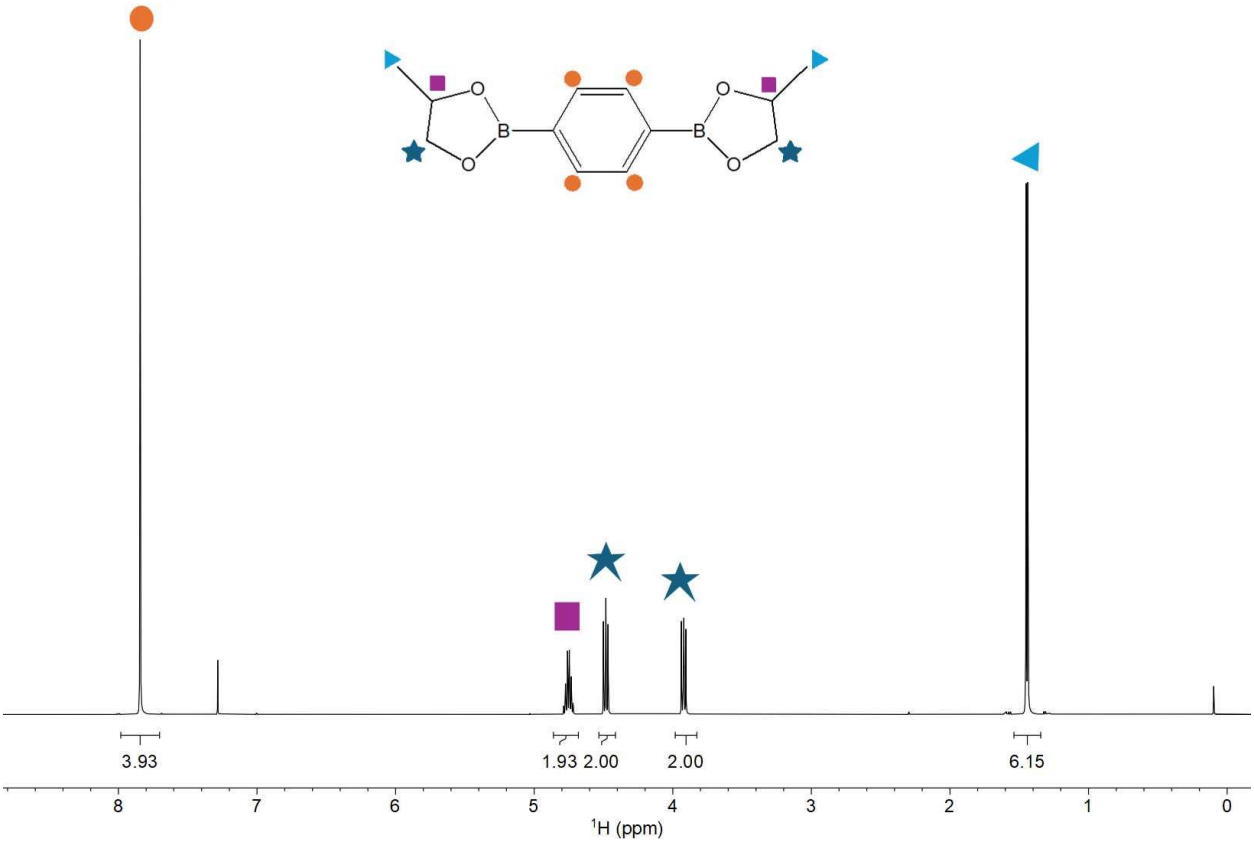

Figure B16. ^{1}H NMR of capped benzene diboronic acid: δ 7.84 (orange circle) (s, 4H), 4.76 (purple square) (m, 2H), 4.48 (blue star) (dd, 2H), 3.92 (blue star) (dd, 2H), 1.44 (blue triangle) (d, 6H).

B2.6 Calculating Polymer Composition

The composition of the prepolymers was determined from the ^{1}H NMR spectrum shown in the respective synthesis procedures. Table 1 summarizes the chemical shifts used to determine the incorporation of the various monomers into the final polymers.

Table B1. ^{1}H NMR shift ranges of polymer constituents

Component	Shift Range (ppm)	Number of Hydrogen Atoms
Poly(MMA)	3.50 – 3.70	3
Poly(C13MA)	3.75 - 4.15	2
Poly(VPBA)	7.50 - 7.80	2
Poly(GMMA)	3.00 – 3.50	2
Poly(styrene)	6.80 – 7.25	5

The values of these integrated regions were used in Equation B3 to determine the composition:

$$F_i = \frac{\left(\int_{\text{range start}}^{\text{range end}} \left(\frac{1}{\text{Number of Hydrogens}}\right)\right)_i}{\sum_1^{N\ components} \int_{\text{range start}}^{\text{range end}} \left(\frac{1}{\text{Number of Hydrogens}}\right)} \quad \text{(B3)}$$

For P3-B-VP, due to the overlapping NMR peaks, a stoichiometric incorporation of methyl methacrylate and acrylonitrile was assumed for the first block. Thus, the AN content of the polymer was taken to be 1:9 of the MMA content.

B3 Synthesis and Characterization of Networks

B3.1 Network Synthesis

Networks 1, 2, and 3 were prepared by the same method. Using network 1 as an example, P1-S-GM (8 grams, 4.58 mmol of GMMA) was dissolved in 8 grams of THF, and P2-S-VP (5 grams, 2.11 mmol of VPBA) was dissolved in 5 grams of THF. To the solutions of VPBA containing prepolymers, ~0.1 mL of methanol was added, to break boroxine crosslinking occurring between VPBA groups which caused the prepolymer to swell rather than dissolved in THF. The two prepolymer solutions were then combined and stirred, with gelling occurring rapidly after mixing.

Network 4 was prepared by dissolving P1-S-GM (4.5 grams, 2.45 mmol GMMA) in 3.5 mL of chloroform that had been dried for 48 hours over molecular sieves. BDB cross-linker (297.6 mg, 2.20 mmol boronic esters) was dissolved in 0.5 mL of the dried chloroform. The two solutions were then combined, and gelling was observed within five minutes of mixing. Following crosslinking, the networks were dried at 40°C and reduced pressure for at least 12 h to remove solvent and moisture.

B3.2 Differential Scanning Calorimetry

Following the method outlined in Section B1.2.7, DSC was conducted on the networks. Heat scans were completed on the material immediately following cross-linking and drying (R×0) as well as on two-times reprocessed (via hot-pressing) material (R×2). Minimal changes in the glass transition temperature indicate thermal properties were retained throughout processing. The results are shown in Figure B17, with the T_gs given in Table B2.

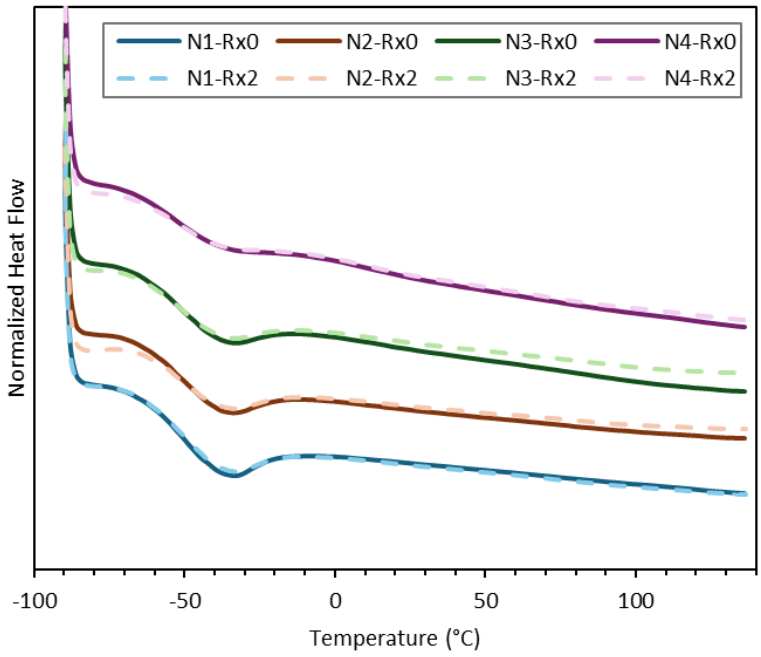

Figure B17. Differential scanning calorimetry (DSC) curves of the four networks.

Table B2. Glass transition temperatures of the unprocessed, and twice reprocessed networks.

	T_g (˚C) of networks			
Recycle	N1	N2	N3	N4
R×0	-50.5	-51.4	-50.1	-50.8
R×2	-50.8	-50.1	-50.1	-51.3

B3.3 Thermogravimetric Analysis

Following the method outlined in Section B1.2.6, TGA was conducted on the networks. Analysis was completed on the material following cross-linking and drying (R×0) as well as on the two-times reprocessed (via hot processing) material (R×2). An increase in the onset of degradation temperature was observed for the networks, indicating a fraction of the less thermally stable material was removed from the material during the reprocessing it had undergone. The results are shown in Figure B18, with the onset temperature of 10 wt% loss given in Table B3.

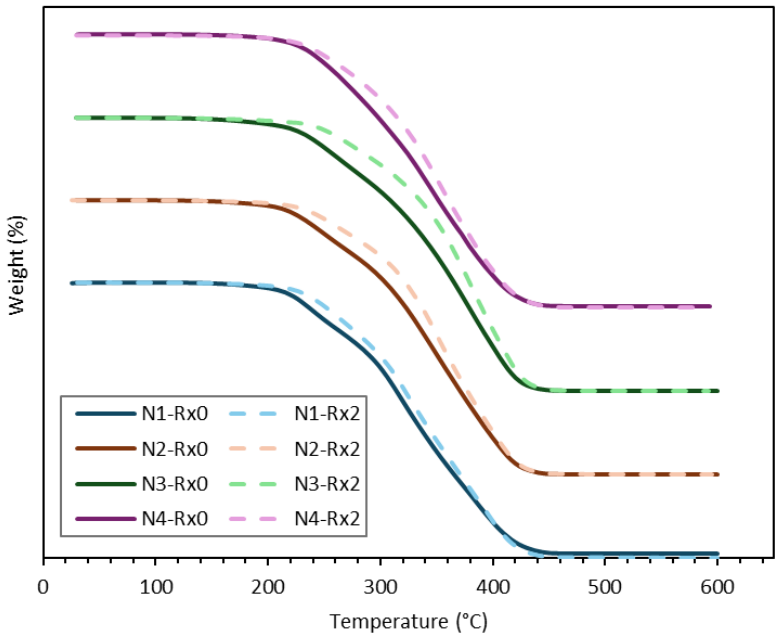

Figure B18. thermal gravimetric analysis (TGA) curves of the four networks.

Table B3. Onset temperature of 10 wt% decomposition of the unprocessed, and twice reprocessed networks.

	$T_{onset,\ 10\ wt\%}$ (˚C) of networks			
Recycle	N1	N2	N3	N4
R×0	209.53	209.36	214.96	219.75
R×2	224.01	225.66	241.20	225.09

An isothermal TGA experiment was also conducted on N2. This experiment showed marginal weight loss (< 3 wt%) when the sample was held at 150°C for 3 hours. The slight decrease in weight could be attributed to remaining moisture being driven off or probable degradation following the ramp in temperature. The resulting curve is given in Figure B19.

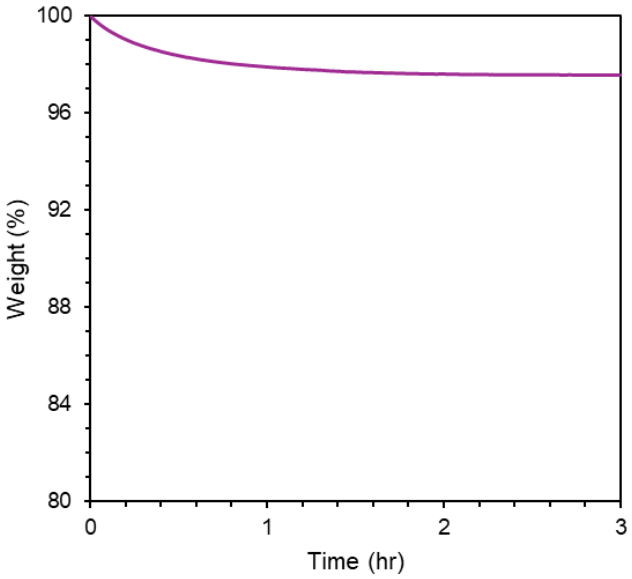

Figure B19. Isothermal TGA experiment on N2.

B3.4 Fourier Transform Infrared Spectroscopy

Following the method outlined in Section B1.2.2, ATR-FTIR was conducted on the prepolymers and their networks. An example spectra of N1 and its prepolymers (P1-S-GM and P2-S-VP) is shown in Figure B20. -OH stretching at 3200 cm^{-1} for P2-S-VP and 3450 cm^{-1} for P1-S-GM is reduced in the final network N1 due to the cross-linking between -BOH and -COH groups.

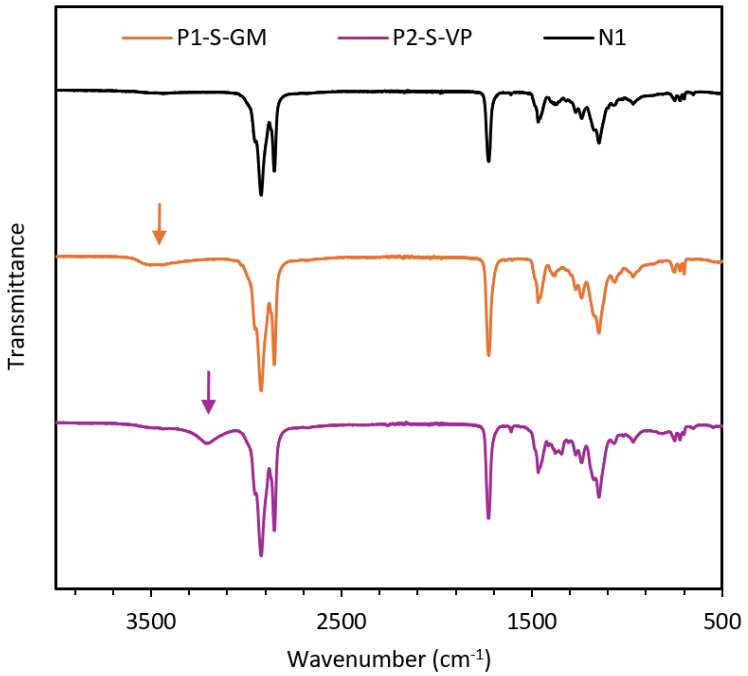

Figure B20. ATR-FTIR of prepolymers P1-S-GM and P2-S-VP and their respective network N1.

3.5 Swelling Ratio and Gel Content

Using the method outlined in Section B1.2.12, swelling and gel content tests were conducted on the networks. Equation B1 and B2 were used to determine the swelling ratio and gel content, and the results are given in Figure B21. Large swelling ratios are observed due to the relatively small amounts of crosslinking (~2 – 6 wt% of network). N4 dissolved in the swelling test: it is hypothesized the presence of moisture or the small capping molecules generated during its network formation could cleave the network bonds.

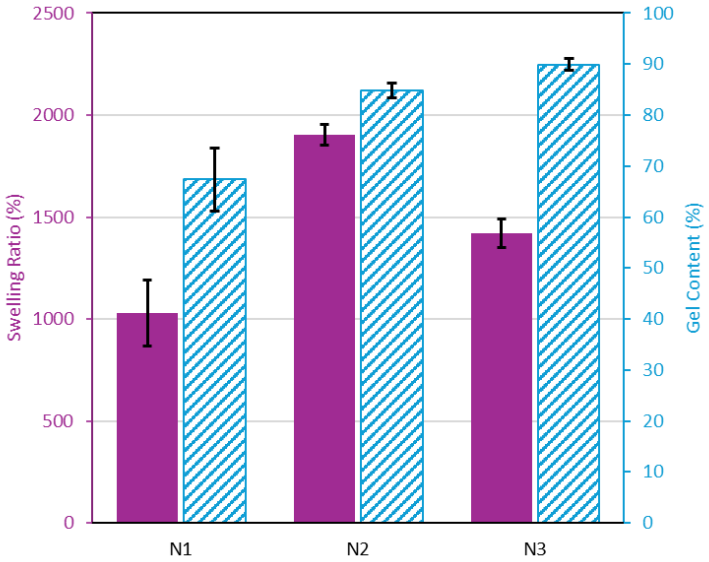

Figure B21. Swelling ratio and gel content of networks N1 through N3.

B3.6 Dynamic Mechanical Analysis and Rheology

B3.6.1 Strain Sweep Test and Linear Viscoelastic Region

The method detailed in Section B1.2.9 was used to determine the linear viscoelastic region of the networks under a constant frequency of 1 Hz prior to further rheological testing. The results are shown in Figure B22.

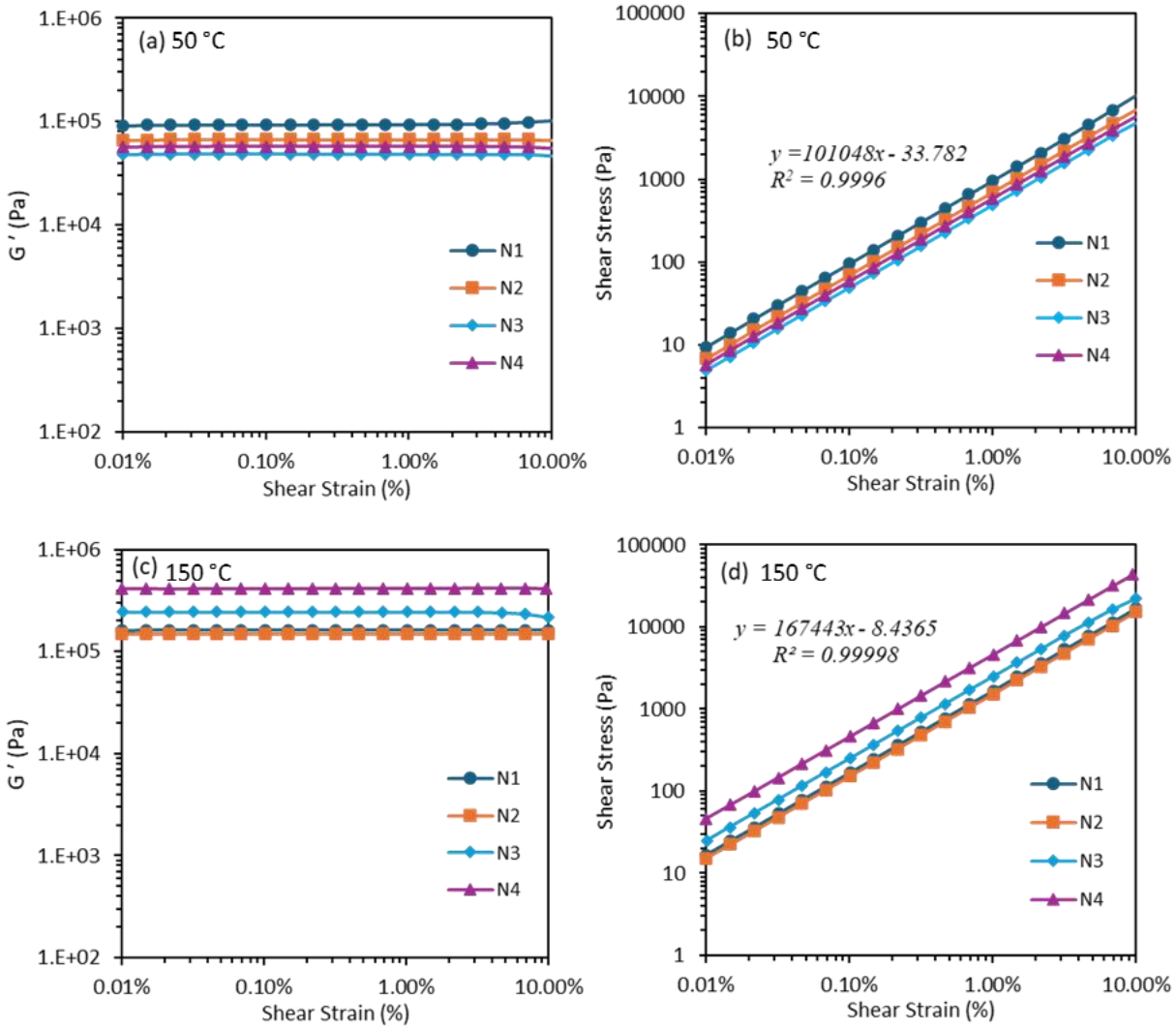

Figure B22. Evaluation of the linear viscoelastic region (LVR) of the vitrimers. Strain sweep tests (left) and stress-strain sweep tests (right) of the networks.

B3.6.2 Frequency Sweeps

Frequency sweeps under a constant strain of 0.1% were conducted on the networks as detailed in Section B1.2.9. The results are shown in Figure B23.

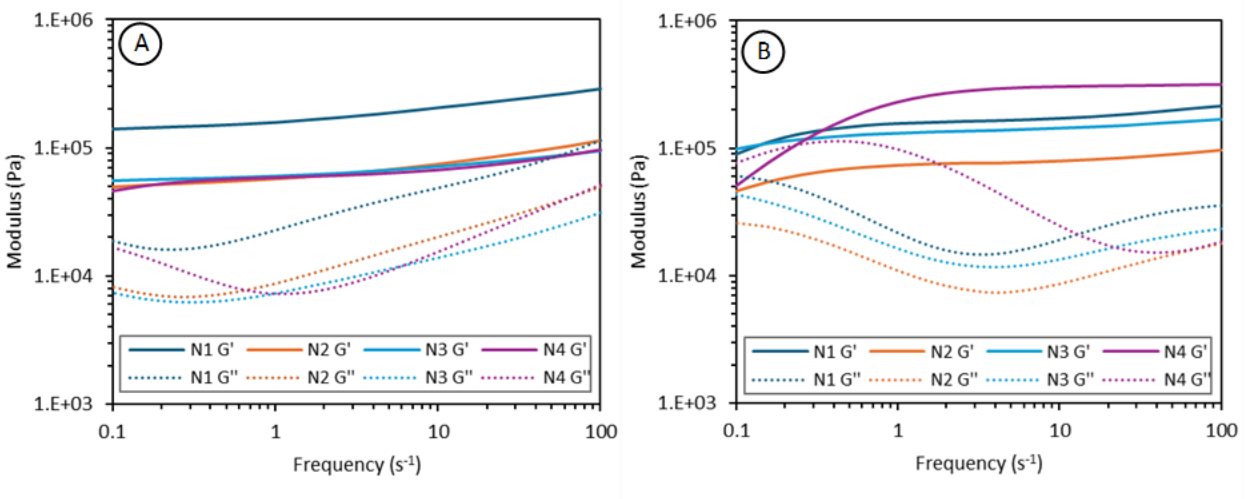

Figure B23. Frequency sweep tests: (A) at 50°C; and (B) at 90°C.

B3.6.3 Stress-Relaxation Tests

The networks were subjected to stress-relaxation tests between 90 and 130°C. The method of the test is detailed in Section B1.2.9.

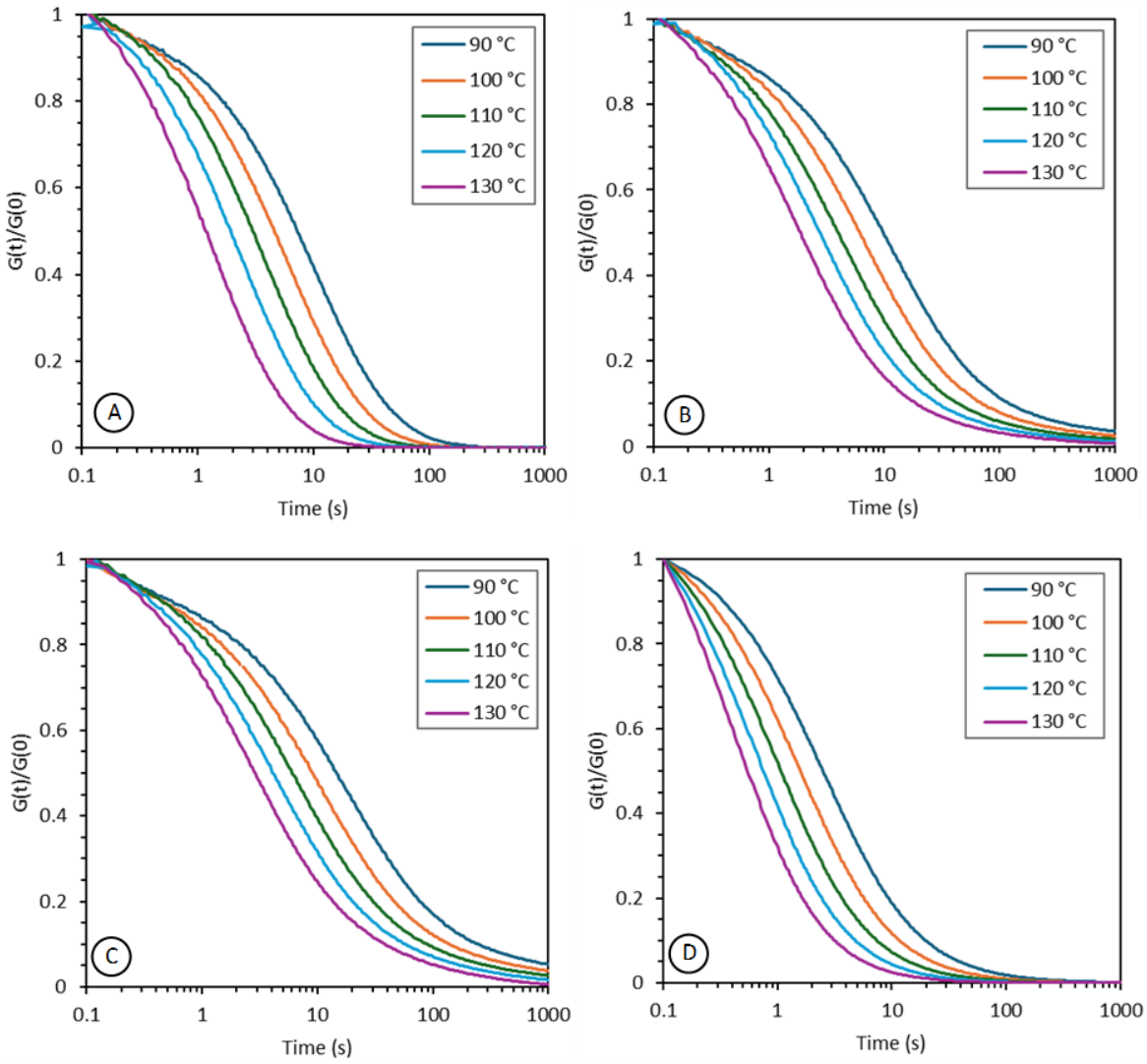

Figure B24. Stress-relaxation: (A) of N1; (B) of N2; (C) of N3; and (D) of N4.

The networks displayed Maxwellian stress-relaxation behaviour, undergoing full relaxation. The normalized stress-relaxation plots $G(t)/G_0$ were fit to a stretched exponential decay model to allow for the estimation of the characteristic relaxation time (τ^*) and β, where β relates to the breadth of the relaxation distribution. The decay model is shown by Equation B4, and the fitting parameters are summarized in Table B4.

$$\frac{G(t)}{G_0} = \exp\left(-\left(\frac{1}{\tau^*}\right)^{\beta}\right) \tag{B4}$$

Table B4. Characteristic relaxation times and β fitting parameters of the networks from 90 – 130°C

	T (°C)	τ^* (s)	β
N1	90	12.5	0.72
	100	7.8	0.76
	110	5.0	0.80
	120	3.2	0.81
	130	1.9	0.87
N2	90	20.6	0.57
	100	12.7	0.60
	110	8.2	0.62
	120	5.6	0.64
	130	3.8	0.65
N3	90	33.1	0.51
	100	20.1	0.53
	110	13.3	0.56
	120	9.0	0.57
	130	6.2	0.59
N4	90	4.7	0.70
	100	2.9	0.72
	110	2.0	0.75
	120	1.3	0.79
	130	1.0	0.84

The parameters were then fit to Equation B5 to determine the activation energy for viscous flow.

$$ln\tau^* = \frac{E_a}{RT} + ln\tau_0 \tag{B5}$$

where: E_a is the activation energy for viscous flow, R is the universal gas constant, T is the temperature, and τ_0 is the Arrhenius pre-factor. The goodness of fit of data to the equation are shown in Figure B25 and the activation energy for viscous flow is given in Table B5.

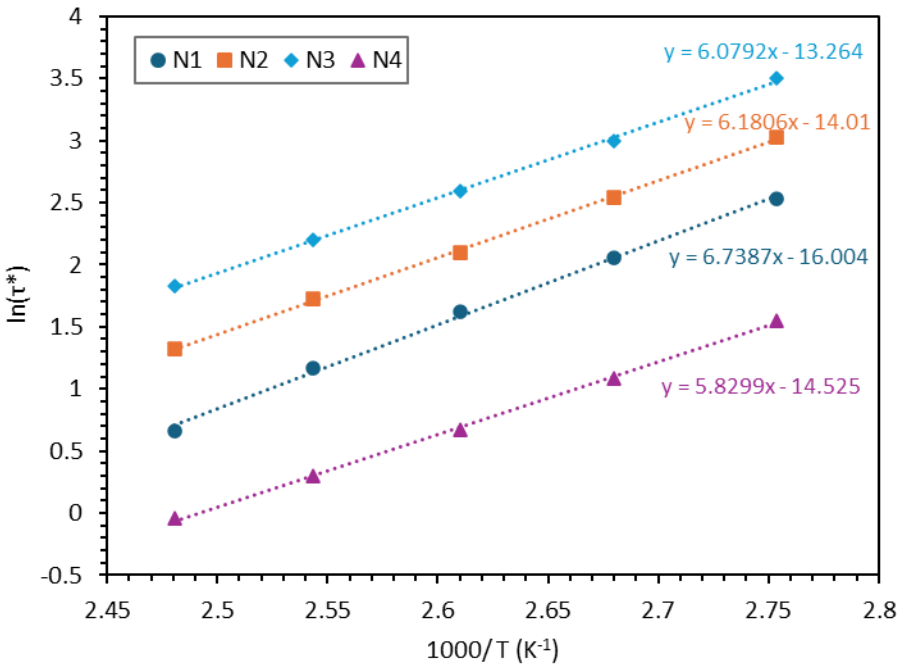

Figure B25. An Arrhenius relationship was observed between the relaxation time and temperature for the networks from stress-relaxation experiments.

Table B5. Activation energy for viscous flow for the networks.

Network	N1	N2	N3	N4
Activation energy (kJ/mol)	50.5	51.4	56.0	48.5

B3.6.4 Creep Tests

Creep tests using a pressure of 250 Pa for 300 seconds, followed by 0 Pa for 500 seconds were conducted on the networks. The results of the test at 130°C are given in Figure B26. The shear strain recovery of the networks from tests at 90°C and 130°C are given in Table B6.

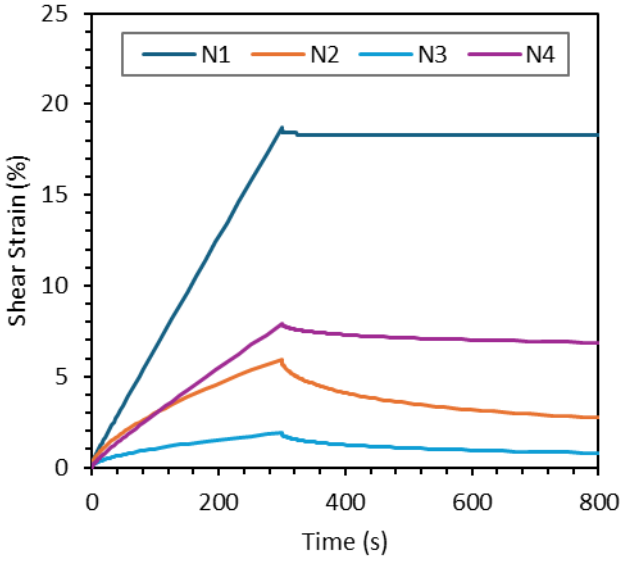

Figure B26. Creep recovery of the networks at 130°C.

Table B6. Creep recovery of the networks.

Test	N1	N2	N3	N4
Shear strain recovery at 90°C (%)	11.7	63.8	57.4	32.0
Shear strain recovery at 130°C (%)	2.1	54.2	58.3	13.1

B3.7 Self-Healing

B3.7.1 Bulk Healing

Bulk healing was completed by pressing tensile bars using the method in Section B1.2.8, and then cutting the bars at their center using a scalpel. The bars were manually placed together and held in place by the weight of an empty KimWipe box, under ambient conditions for 100 hours. The bars were then subjected to tensile testing using the method in Section B1.2.10. Photos of the process are given in Figure B27.

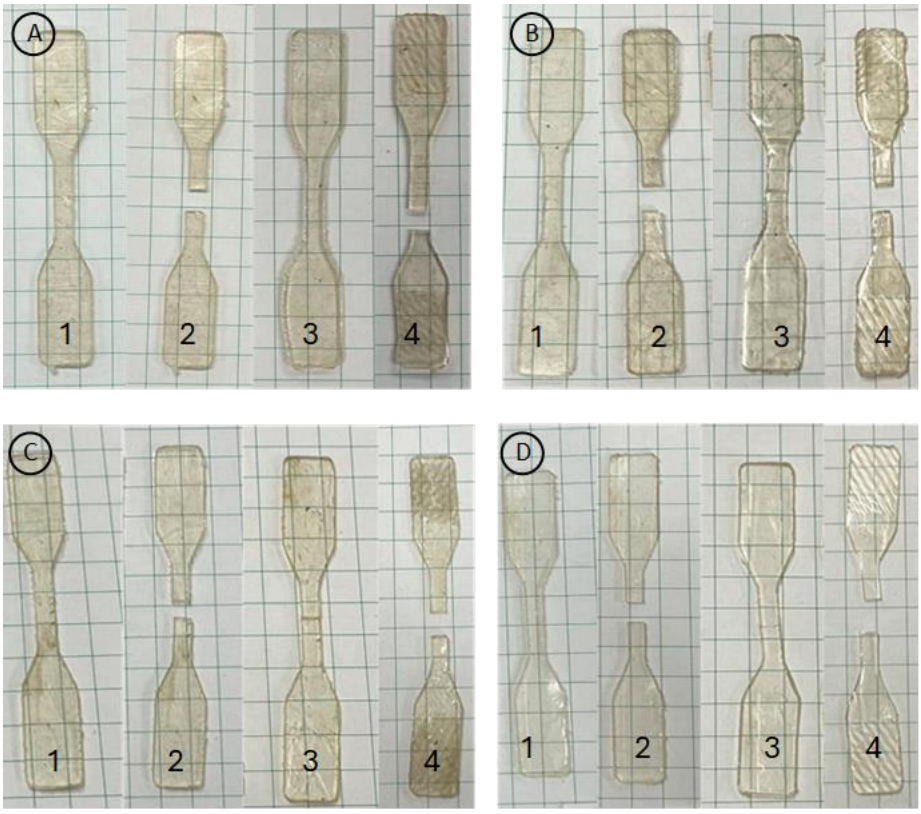

Figure B27. Bulk healing progression where 1 is precut, 2 is immediately post cut, 3 is post healing, and 4 is post tensile testing: (A) of N1; (B) of N2; (C) of N3; and (D) of N4.

B3.7.2 Scratch Healing

Scratch healing was conducted at 60°C for all networks. After 25 hours, scratches on N2 – N4 were exposed to a drop of water to encourage the reformation of boronic acid ester crosslinking. Figure B28 includes progression photos of scratch healing.

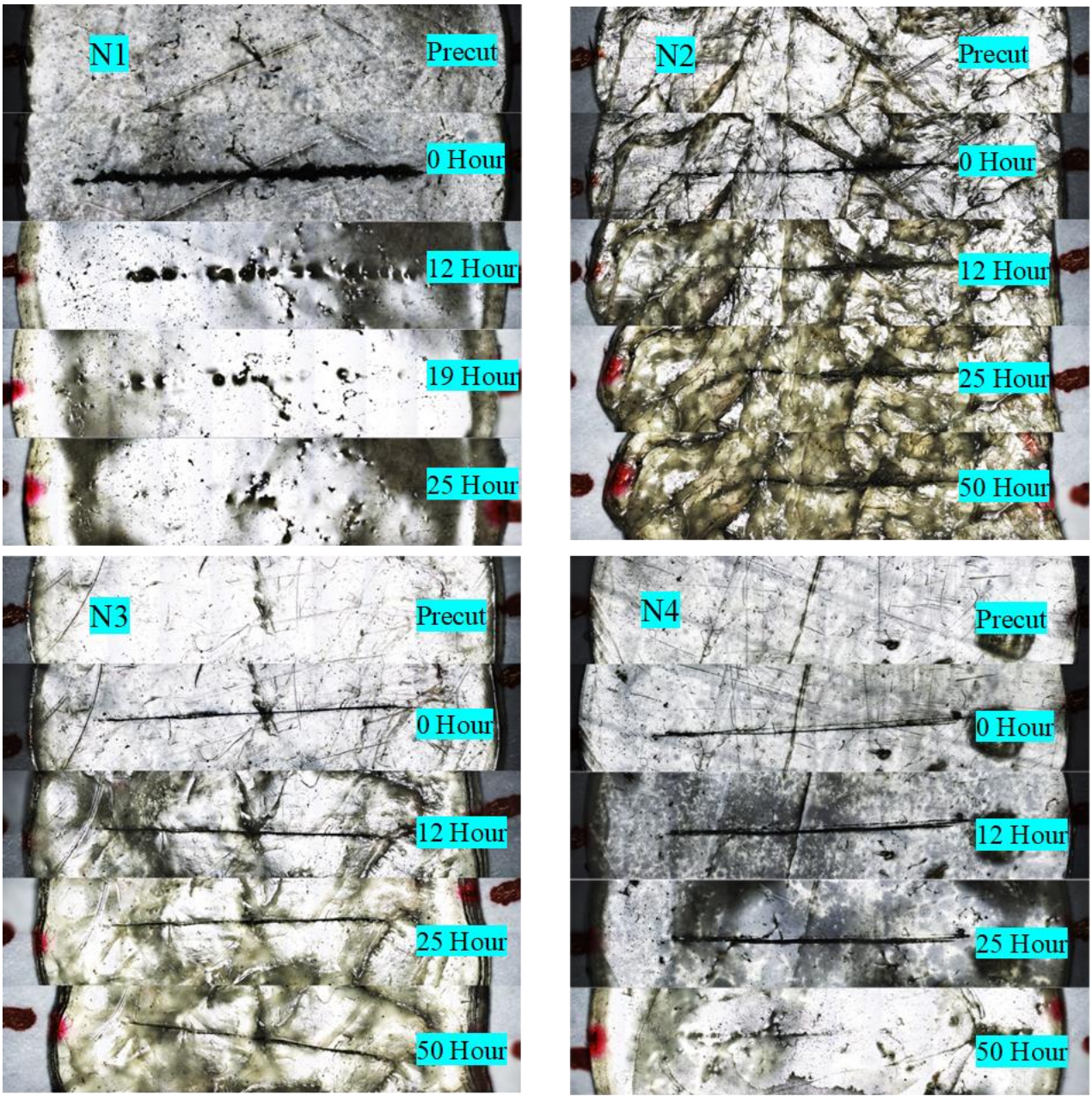

Figure B28. Scratch healing progression at 60°C, where hour 25 – 50 saw the addition of water to the location of the scratch to encourage boronic-acid ester exchange reactions.

B3.8 Tensile Data

Reprocessing of the tensile bars, by cutting into pieces and then repressing in a hot press, was completed to assess the mechanical properties through recycling. Table B7 summarizes the average data of at least three tensile bars.

Table B7. Tensile properties through reprocessing and bulk healing of the networks.

Network	Property	R×0	R×1	R×2	Bulk Healing
N1	Stress (kPa)	212.2 ± 33.1	203.2 ± 18.3	197.2 ±14.1	302.8 ± 25.6
	Strain (%)	101.0 ± 17.8	106.5 ± 9.9	102.8 ± 7.0	123.5 ± 11.3
N2	Stress (kPa)	314.5 ± 19.7	291.0 ± 29.8	338.7 ± 40.2	238.4 ± 3.1
	Strain (%)	84.3 ± 8.4	79.4 ± 5.7	89.4 ± 8.4	71.0 ± 4.3
N3	Stress (kPa)	541.2 ± 50.0	---	--	304.3 ± 43.8
	Strain (%)	61.4 ± 2.1	--	--	35.4 ± 5.5
N4	Stress (kPa)	677.1 ± 28.6	--	--	597.9 ± 10.1
	Strain (%)	138.8 ± 6.6	--	--	121.4 ± 14.6

B4 References

(1) Wang, Z.; Gu, Y.; Ma, M.; Chen, M., Strong, reconfigurable, and recyclable thermosets cross-linked by polymer–polymer dynamic interaction based on commodity thermoplastics. *Macromolecules* **2020,** *53* (3), 956-964.